Passively Mode-Locked Semiconductor Lasers for All-Optical Applications

Josué Amílcar Parra Cetina

B. Eng., M. Sc.

A dissertation submitted in partial fulfilment of the

requirements for the award of

Doctor of Philosophy (Ph.D)

to the

DCU

Dublin City University

Faculty of Engineering and Computing

School of Electronic Engineering

Research Supervisor:

Dr. Pascal Landais

January 2014

Declaration

I hereby certify that this material, which I now submit for assessment on the programme of study leading to the award of Doctor of Philosophy is entirely my own work, and that I have exercised reasonable care to ensure that the work is original, and does not to the best of my knowledge breach any law of copyright, and has not been taken from the work of others save and to the extent that such work has been cited and acknowledged within the text of my work.

Signed: _____   ID No.: 59113707   Date: _____

Dedications

This thesis is dedicated with all my love to my parents Nicolás Parra and Noemí Cetina who are my motivation, source of inspiration and strength to improve every single day. All my personal achievements are possible thanks to you.

Dedico este trabajo con todo mi amor a mis padres Nicolás Parra y Noemí Cetina. Ustedes son mi motivación, fuente de inspiración y fortaleza para mejorar cada día. Todos mis logros personales son posibles gracias a ustedes.
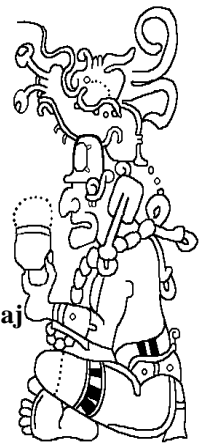
To my brothers Nicolás, Jacob, and my sister Paula, my aunties Adela and Ligia and the rest of relatives.

A mis hermanos Nicolás, Jacob, mi hermana Paula, mis tías Adela y Ligia y demás familiares.

"ZAMNÁ"

**"Cultivad las artes y las ciencias como lo habéis hecho
hasta estos tiempos. Conservad vuestra fama y
vuestro talento para las cosas bellas
y sed la admiración de los otros pueblos"**

**"Ya'abkunse'ex jats'uts ba'alo'ob yéetel ka'anal xooko'ob je'e
bix a beetmile'ex tak te' k'iino'oba'. Kalant a k'ajóolanile'ex
yéetel ba'ax a wojle'ex yo'olal ba'ax jats'utstako'ob utia'al ka'aj
a jak'óolte'ex uláak' kaajo'ob".**

Acknowledgements

Contents

List of Figures

ix

List of Tables

Abstract

The recent increase of internet traffic is creating demand for higher bandwidth in telecommunication networks. In order to satisfy this ever increasing demand for bandwidth, it is necessary to investigate new devices and technologies for all-optical signal processing that allow increasing the transmission data rate and the capacity for the current and future optical networks.

Optical time division multiplexing (OTDM) is a widely deployed technique that allows increasing the bit rate and capacity of optical networks. In OTDM networks the regeneration and the demultiplexing of the data channels are two common and important functions normally carried out. However, they require a clock signal, which is usually implemented by optoelectronics components, making a system expensive, bulky and difficult to implement. In order to provide a solution to this issue, the focus of this thesis is to investigate all-optical clock recovery by using external injection locking of passively semiconductor mode-locked lasers. In particular, quantum-dash mode-locked laser diodes (QDash-MLLDs) are studied. These lasers can generate optical pulses with durations in the order of picoseconds and femtoseconds using only DC-bias with no need for external modulation. Besides, they are attractive due to their simplicity of operation, low power consumption, fast carrier dynamics and compactness. Furthermore, they provide a narrow radio frequency beating linewidth, resulting in a small amount of phase noise and low timing jitter.

In this thesis, all-optical clock recovery of data signals at base bit rate (40 Gb/s) and high bit rates (up to 320 Gb/s) was achieved using QDash-MLLDs. The recovered clocks from the different data input signals considered in this thesis feature low values of timing jitter, which are compliant with the minimum requirements for practical applications. Furthermore, the recovered clocks at high speed are used to demultiplex signals to tributaries of 40 Gb/s, achieving error free performance. Finally, investigation of the QDash-MLLD dynamics demonstrated that the laser provides a very fast locking time (25 ns) when synchronised to data signals which enables it as a solution to optical burst/packet switched networks. All these results contribute to demonstrate that the laser is an extremely reliable, cost-effective and a green solution for all-optical signal processing.

List of Acronyms

AMP	Amplifier
AWG	Arbitrary waveform generator
B2B	Back-to-back
BER	Bit error rate
BERT	Bit error rate tester
BMOCR	Burst mode optical clock recovery
CDM	Carrier density modulation
CH	Carrier heating
CR	Clock recovery
DBR	Distributed Bragg reflector
DCF	Dispersion compensating fiber
DFB	Distributed feedback laser
DPSK	Differential quadrature phase shift keying
EAM	Electro-absorption modulator
ECL	External cavity laser
EDFA	Erbium doped amplifier
EOM	Electro-optical modulator
ESA	Electrical spectrum analyser
LD	Laser diode
FDC	Frequency down-conversion
FDIV	Frequency divider
FFT	Fast-Fourier transform
FP	Fabry-Pérot
FPF	Fabry-Pérot filter
FROG	Frequency resolved optical gating
FSR	Free spectral range
FWHM	Full width at half maximum
FWM	Four wave mixing

GEN	Generator
GS-MBE	Gas source molecular beam epitaxy
ISO	Isolator
LI	Optical power versus current
LO	Local oscillator
MAN	Metropolitan access network
MLFL	Mode-locked fiber laser
MLL	Mode-locked laser
MLLD	Mode-locked laser diode
MZM	Mach-Zehnder modulator
NOLM	Nonlinear optical loop mirror
NRZ	Non-return-to-zero
OBPF	Optical bandpass filter
OBS	Optical burst switching
OCR	Optical clock recovery
ODL	Optical delay line
OEO	Optoelectronic Oscillator
OFDM	Orthogonal frequency division multiplexing
OMUX	Optical time multiplexer
OOK	On-off keying
OPLL	Optoelectronic phase locked loop
OSA	Optical spectrum analyser
OSO	Optical sampling oscilloscope
OTDM	Optical time division multiplexing
OTN	Optical transport network
PLL	Phase locked loop
PC	Polarization controller
PD	Photo-detector
PM	Phase modulator
PML	Passively mode-locked
PPLN	Periodically poled lithium niobate

PPNR	Peak power-to-noise ratio
PPG	Pulse pattern generator
PRBS	Pseudo random binary sequence
PTB	Precision time base
QW	Quantum well
QDot	Quantum dot
QDash	Quantum dash
RBW	Resolution bandwidth
RF	Radio frequency
RIN	Relative intensity noise
RMS	Root-mean-square
RTO	Real-time oscilloscope
RZ	Return-to-zero
SCH	Separate confinement hetero-structure
SCOPE	Sampling Oscilloscope
SHB	Spectral hole burning
SHD	Self-heterodyning detection
SMF	Single mode fiber
SOA	Semiconductor optical amplifier
SNR	Signal-to-noise ratio
SSB-PSD	Single sideband phase noise spectral density
TBP	Time-bandwidth product
TMLL	Tunable mode-locked laser
TPA	Two photon absorption
TX	Transmission
VI	Voltage versus current
VOA	Variable optical attenuator
WC	Wavelength converter
WDM	Wavelength division multiplexing
XGM	Cross-gain modulation
XPM	Cross phase modulation

Chapter 1

Introduction

1.1 General introduction

In recent years, the exponential growth of the internet traffic has driven a rapid increase in the demand for higher speeds and greater bandwidth in the Telecommunication networks. Today, major service providers are devoting significant efforts towards the development of new technologies and devices to cope with the demand. With recent advances in optical technology, wavelength-division multiplexing (WDM) and optical time division multiplexing (OTDM) have been identified as two of the techniques that aim for effective network deployment [1-3]. WDM consists of the parallel transmission on a single fibre of several data streams on several wavelengths. This technique is a widely deployed transport mechanism for improving fibre bandwidth utilisation providing improvement in the transmission capacity for future optical systems and networks [2], [3]. OTDM transmits multiple data channels in the form of ultra-short pulses, which are multiplexed onto a single high-speed data stream by assigning a recurrent time slot to each of the tributaries [2-5]. This technique can provide high speed data transmission up to terabits per second (Tb/s) [5]. OTDM and WDM can operate separately or simultaneously to further increase the bandwidth capability of the optical networks [2], [6], [7]. Another approach that has emerged is to employ optical packet switching. In packet switching the information is transmitted across the network in the form of data packets [8]. With packet switching large amounts of information can be transported in a more efficient and economical way. In order to take advantage of the full potential of the optical fibre, and the multiplexing technologies already mentioned, it is important to improve the architectures and topologies of the current optical networks [6-8]. This fact has led to the concept of optical transport networks (OTN). In an OTN the signal processing should be in the all-optical domain, hence, it has been named a transparent network [1], [2], [7-9]. However, there is still a lot of research on OTN and on the individual OTDM, WDM and packet switching technologies. I will focus on OTDM and the benefits of OTDM. In order that OTDM can provide very high speed data transmission, it needs other techniques such as high repetition ultra-short pulses, high speed demultiplexing and

clock recovery. At the moment, these techniques are limited by their constituting elements making OTDM a relatively expensive transmission solution limiting its full deployment.

As a consequence, there have been great efforts to develop devices and components to employ in OTDM systems. In this regard, mode-locked lasers (MLLs) have been a topic of extensive research in many optical communication laboratories around the world [10-16]. Their ability of generating high repetition rate ultra-short pulses is of great interest and importance for ultra-high speed optical communication systems and networks. In addition, it can provide an effective component for all-optical signal processing. Specifically, mode locked semiconductor lasers can find wide applications in optical packet switching [17], optical sampling [18], clock distribution [19] and frequency comb generation [20]. With this regard, a special type of laser will be studied in the subsequent Section. This laser has the potential of being the element capable of solving various limitations to deploy OTDM in OTNs.

1.2   All-optical signal processing

1.2.1   Generation of ultra-short pulses

"An optical pulse is a flash of light" [20]. A pulse possesses different properties such as power, pulse duration, repetition rate, chirp and timing jitter. When considering devices capable of generating optical pulses, lasers seem to be the first option [20], [21]. Normally, lasers produce a continuous beam of light; however, it is possible to obtain pulses from them. There are several types of lasers, such as fibre lasers, semiconductor lasers, gas lasers, among others. Moreover, there are different techniques to generate pulses from these lasers. Generation of optical pulses with picosecond pulse width can be generated with three main methods: Q-switching [21-23], gain switching [22], [24] and mode-locking [22], [25], [26]. Depending on the application, one technique can be preferred over the other. However, mode-locking is the most reliable and is the simplest way to achieve the generation of ultra-short pulses with picosecond and femtosecond pulse duration. Additionally, the pulses produced with this technique exhibit low timing jitter. Mode locking has been demonstrated in all of the lasers listed above, but the capability of semiconductor laser diodes to provide stable optical pulses, at high repetition rates, in a compact and simple presentation makes their use highly desirable for applications in OTDM. Among some of the applications for the optical pulses produced from a semiconductor mode-locked laser are: optical sampling, clock recovery, and radio over fibre.

1.2.2 Clock recovery

Some of the most important functionalities for current OTDM systems and for future optical signal processing include clock recovery (CR), demultiplexing and regeneration. However, clock recovery is the critical component, since a clock with good quality allows achieving high performance demultiplexing and regeneration functionalities.

Clock recovery is the result of the process where a synchronised clock signal is derived from a received data signal. In digital communications, a clock must be used as the timing basis to sample the received signal. The clock should be locked in both phase and frequency with respect to the received data signal. Clocking signals can be extracted and recovered from a data signal through electrical [27], optical [10], [11], [17] or hybrid techniques [28], [29].

Current techniques for clock recovery require optoelectronic phase locked loops (OPLL) [30], [31]. A phase locked loop (PLL) is a control system in a closed-loop that generates an output signal in relation to the frequency and phase of a reference input signal. The PLL consists basically of a phase detector, a low-pass filter and a variable frequency oscillator. An example of a very simple PLL is depicted in Fig.1.1. The phase-locked loop circuit responds to the input signal by automatically adjusting the frequency of the controlled oscillator until it is matched to the frequency of the reference signal. Normally, the feedback loop increases the complexity and locking time of the system. In addition, it requires costly and power consuming high speed electronics (oscillators, photo-detectors, and amplifiers) and optical components. This is the reason why an extensive research has been conducted over the last years in order to achieve all-optical approaches for clock recovery, which can allow performing optical functions at ultra-high bit rates, in a more compact presentation and with a significant reduction in the power consumption.
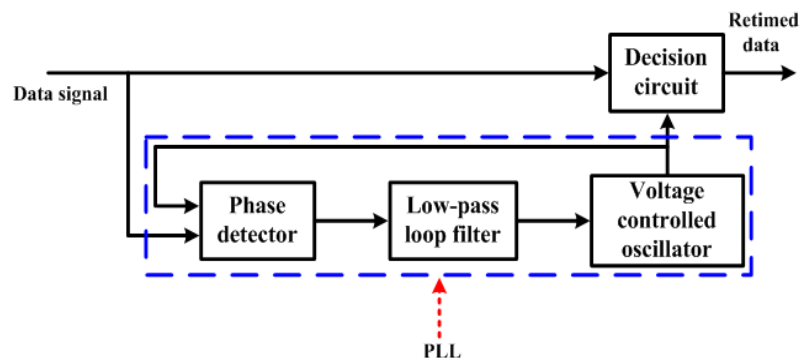
Figure 1.1: Schematic representation of a PLL.

Different techniques for all-optical clock recovery extraction have been demonstrated using self-pulsating laser diodes [32], passively mode locked (PML) semiconductor lasers [10-12], [14], [15], [17], [33] and fibre lasers using optical fibre and semiconductor nonlinearities [34], [35]. From the various techniques demonstrated, PML semiconductor lasers are significant as they typically exhibit lower phase noise and amplitude noise than self-pulsating lasers and less clock latency than fibre based devices. Clock recovery with semiconductor lasers have been demonstrated using: distributed Bragg reflector (DBR), quantum well (QW) and quantum dot/dash (QD/QDash) lasers. However, due to the 3D energy level as well as the small confinement factor the lasers based on QD/QDash exhibit a higher gain, lower threshold current, faster carrier dynamics, and narrower RF linewidth and lower timing jitter than their counterparts [11], [36]. In addition, the possibility of synchronising the mode locked laser through an external optical data signal will allow reducing the phase noise and its associated timing jitter as a consequence; this will improve the recovered clock performance [10], [11], [33], [37]. Furthermore, another advantage of the QDash-MLLDs is that they are designed to operate in the 1.5 µm spectral region, emitting an optical frequency comb spectrum which can be utilised not only for clock recovery but also for other applications such as multi-wavelength carriers for high capacity transmission and high-speed communications [38], [39].

1.3   My approach

In this thesis, Fabry-Pérot quantum dash mode locked laser diodes (QDash-MLLDs) are used to conduct investigation of all-optical signal processing with emphasis on clock recovery from OTDM and burst data signals. This QDash-MLLD is a compact and single section semiconductor laser, not including any saturable absorber. As it will be demonstrated, passively mode-locking is achieved under DC current biasing. This simple operation of the laser results in low power consumption, great stability and the ability to operate at room temperature. The laser is designed to operate in the 1.5 μm spectral region (Telecommunications bandwidth). The QDash-MLLD is capable of synchronising its frequency to pulses or data signal at harmonic or sub-harmonic frequencies of its free spectral range (FSR) providing stable optical short pulses.

The main contributions from the work carried out towards this thesis are:

- Demonstration of the synchronisation of a QDash-MLLD to optical pulses at harmonic and sub-harmonic frequencies relative to its intrinsic 40 GHz frequency giving rise to a 40 GHz signal with less than 8 Hz linewidth.

- Demonstration of the 23 nm wide tunability of the recovered clock with respect to the incoming data signal over the C-band for data signal at base bit rate 40 Gb/s with return-to-zero (RZ) and non-return-to-zero (NRZ) formats.

- Corroboration that the QDash-MLLD provides high quality clock signal when synchronised to up to 320 Gb/s data rates signal, even lacking of the 40 GHz fundamental component. This clock features less than 100 fs of timing jitter.

- Validation of the optical recovered clock from the QDash-MLLD to perform demultiplexing of signals at 320 Gb/s to tributaries of 40 Gb/s with error free performance.

- Characterisation and measurement of very fast switching-on and locking time of a QDash-MLLD in free running operation as well as the laser is synchronised to optical data, achieving 30 ns, 42 ns and 25 ns, respectively, towards application of clock recovery for packetized data.

All these results along with its small physical dimensions and low energy consumption (green aspect) give a very promising device for all-optical clock recovery and signal processing of ultra-high speed signals in future transparent networks.

1.4   Thesis overview

This dissertation consists of eight Chapters; the first Chapter comprises of this introduction and the remaining seven Chapters are structured as follows:

Chapter 2 provides a basic overview of mode locking theory, reviewing the main types of mode locking and a brief theory on the mode-locking mechanism achieved in multimode lasers via four wave mixing.

Chapter 3 presents in more detail the type of QDash-MLLD used in this work. Characterisations on the QDash-MLLD towards the demonstration of passive mode-locking are shown.

Chapter 4 demonstrates optical pulse generation from the QDash-MLLD, first in its passive mode-locking condition and immediately after, when the QDash-MLLD is synchronised to a signal at 10 GHz in order to multiplex the original 40 GHz to higher frequencies such as 160 GHz. Moreover, the capability of the QDash-MLLD to synchronise its frequency to pulses with a sub-harmonic, fundamental and harmonic frequency is demonstrated. Under this synchronisation, the QDash-MLLD retrieves stable 40 GHz pulses.

Chapter 5 deals with the performance of the QDash-MLLD as a clock recovery component for signals at 40 Gb/s for both return-to-zero and non-return-to-zero data formats. In addition, an application of the recovered clock for achieving 3R regeneration with data format conversion from NRZ to RZ is provided.

Chapter 6 presents a study on sub-harmonic all-optical clock recovery with the QDash-MLLD from OTDM data signals of up to 320 Gb/s. Furthermore, an application of the recovered clock is performed to demultiplex OTDM signals at 160 and 320 Gb/s.

Chapter 7 presents the implementation of experimental setups for measuring the QDash-MLLD dynamics for data synchronisation such as the switching-on and locking times.

Chapter 8 concludes the thesis with a brief overview of the results obtained from this work and discusses the future work to carry out with this kind of mode-locked lasers.

References

[1] S. Seung Woo, K. Bergman, P. R. Prucnal, "Transparent optical networks with time-division multiplexing," *IEEE Journal on Selected Areas in Communications*, vol. 14, no. 5, pp. 1039-1051, Jun. 1996.

[2] M. J. O'Mahony, "Optical multiplexing in fiber networks: progress in WDM and OTDM," *Communications Magazine, IEEE*. vol. 33, no. 12, pp. 82, 10.1109.

[3] Y. Lv, and J. Lin, "Future all-optical networks," *Info-tech and info-net, 2001. Proceedings. ICII 2001-Beijing. 2001 International Conferences on*, vol. 2, pp. 193-198, Nov. 2001.

[4] S. A. Hamilton, B. S. Robinson, T. E. Murphy, S. J. Savage, and E. P. Ippen, "100 Gb/s Optical Time-Division Multiplexed networks," *IEEE Journal of Lightwave Technology*, vol. 20, no. 12, pp. 2086-2100, Dec. 2012.

[5] M. Nakazawa, T. Yamamoto, and K.R. Tamura, "1.28 Tbit/s-70 km OTDM transmission using a third-and fourth-order simultaneous dispersion compensation with phase modulator," *Electronics Letters*, vol. 36, no. 24, pp. 2027-2029, Nov. 2000.

[6] A. A. Aboketaf, L. Cao, D. Adams, A. W. Elshaari, S. F. Preble, M. T. Crowley, L. F. Lester, and P. Ampadu, "Hybrid OTDM and WDM for multicore optical communication," *Green computing conference (IGCC), 2012 International*, pp. 1-5, Jun. 2012

[7] M. Mellia, E. Leonardi, M. Feletig, R. Gaudino, and F. Neri, "Exploiting OTDM technology in WDM networks," *INFOCOM 2002. Twenty-First Annual Joint Conference of the IEEE Computer and Communications Societies. Proceedings. IEEE*, vol. 3, pp. 1822-1831, 2002.

[8] V. Puglia, and O. Zadedyurina, "Optical transport networks: from all-optical to digital," *Innovations for digital inclusions, 2009. K-IDI 2009. ITU-T Kaleidoscope*, pp. 1-8, Aug/Sep. 2009.

[9] M. Bischoff, M. N. Huber, O. Jahreis, F. Derr, and F. Ulm, "Operation and maintenance for an all-optical transport network," *IEEE Communications Magazine*, vol. 34, no. 11, pp. 136-142, Nov. 1996.

[10] J. C. Cartledge, X. Tang, M. Yañez, M. Shen, A. Akrout, and G.H. Duan, "All-optical

clock recovery using a quantum-dash Fabry-Pérot laser," *in Proceedings IEEE Microwave Photonics Conference, 2010*, Paper TH3-1. pp. 201-204, Oct. 2010.

[11] F. Lelarge, B. Dagens, J. Renaudier, R. Brenot, A. Accard, F. van Dijk, D. Make, O. Le Gouezigou, J.-G. Provost, F. Poingt, J. Landreau, O. Drisse, E. Derouin, B. Rousseau, F. Pommereau, and G.-H. Duan, "Recent advances on InAs/InP quantum dash based semiconductor lasers and optical amplifiers operating at 1.55 μm," *IEEE Journal of Selected Topics in Quantum Electronics,* vol. 13, no. 1, pp. 111-124, Jan./Feb. 2007.

[12] S. Arahira, H. Takahashi, K. Nakamura, H. Yaegashi, and Y. Ogawa, "Polarization-, wavelength-, and filter-free all-optical clock recovery in a passively mode-locked laser diode with orthogonally pumped polarization-diversity configuration," *IEEE Journal of Quantum Electronics*, vol. 45, no. 5, pp. 476-487, May. 2009.

[13] B. Huettl, H. Hu, R. Ludwig, R. Kaiser, C. Schmidt-Langhorst, A.G. Steffan and C. Schubert, "Linewidth investigation of monolithically integrated 40 GHz mode-locked laser diodes for high speed RZ-DQPSK transmission," *Optical Communication, 2008. ECOC 2008. 34th European Conference on*, Paper Th.1.C7, pp. 1-2, Sep. 2008.

[14] G. Carpintero, M. G. Thompson, R. V. Penty, and I. H. White, "Low noise performance of passively mode-locked 10 GHz quantum-dot laser diode," *IEEE Photonics Technology Letters*, vol. 21, no. 6, pp. 389-391, Mar. 2009.

[15] L. Hou, M. Haji, B. Qiu, J. Akbar, A. C. Bryce, and J. H. Marsh, "10-GHz AlGaInAs /InP passively mode-locked laser with low divergence angle and timing jitter," *IEEE Photonics Technology Letters*, vol. 23, no. 15, pp. 1079-1081, Aug. 2011.

[16] K. Yvind, D. Larsson, L. J. Christiansen, C. Angelo, L. K. Oxenlowe, J. Mork, D. Birkedal, J. M. Hvam, and J. Hanberg, "Low-jitter and high-power 40 GHz all-active mode-locked lasers," *IEEE Photonics Technology Letters*, vol. 16, no. 4, pp. 975-977, Apr. 2004.

[17] J. Luo, J. Parra-Cetina, P. Landais, H.J.S. Dorren, and N. Calabretta, "40G Burst Mode Optical Clock Recovery after 52 km Transmission Enabled by a Dynamically Switched Quantum Dash Mode-Locked laser," *presented in ECOC 2013*, London, UK, paper Th.2.A.2, Sep. 2013.

[18] T. Miyazaki, H. Sotobayashi, and W. Chujo, "Optical sampling and demultiplexing of 80 Gb/s OTDM signals with optically recovered clock by injection mode-locked laser diode," *Optical Communication, 2002. ECOC 2002. 28th European Conference on.* vol. 1, pp. 1-2, Sep. 2002.

[19] H. Sotobayashi, "Ultra-wideband 40 GHz optical-combs generation and distribution through WDM optical fiber netwroks," *Frequency Control Symposium, 2007. Joint with*

the 21st European Frequency and Time Forum. IEEE International, pp. 984-985, May. 2007.

[20] R. Paschotta, *Field guide to laser pulse generation*, SPIE Press, vol. FG14, Bellingham, WA. 2008.

[21] C. Rulliere, *Femtosecond laser pulses, principles of experiments*, 2nd ed., USA: Springer, 2003.

[22] O. Svelto, *Principles of Lasers,* 4th ed., USA: Springer, 1998.

[23] Yariv, Amnon, *Quantum Electronics*, 3rd ed*.,* USA: John Wiley & Sons, 1975.

[24] P. Paulus, R. Langenhorst, and D. Jäger, "Generation and optimum control of picosecond optical pulses from gain-switched semiconductor lasers," *IEEE Journal of Quantum Electronics*, vol. 24, no. 8, pp. 1519-1523, Aug. 1988.

[25] K. Merghem, A. Akrout, A. Martinez, G. Aubin, A. Ramdane, F. Lelarge, and G. Duan, "Pulse generation at 346 GHz using a passively mode locked quantumdash- based laser at 1.55 μm," *Applied Physics Letters*, vol. 94, no. 2, pp. 021107–3, Jan. 2009.

[26] S. Latkowski, R. Maldonado-Basilio, and P. Landais, "Sub-picosecond pulse generation by 40-GHz passively mode-locked quantum-dash 1-mm-long Fabry-Prot laser diode," *Optics Express*, vol. 17, no. 21, pp. 19166–19172, Oct. 2009.

[27] K. Murata and Y. Yamane, "40 Gbit/s fully monolithic clock recovery IC using InAlAs/InGaAs/InP HEMTs," *Electronics Letters*, vol. 36, no. 19, pp. 1617–1618, 2000.

[28] M. W. Chbat, P. A. Perrier, and P. R. Prucnal, "Optical clock recovery demonstration using periodic oscillations of a hybrid electrooptic bistable system," *IEEE Photonics Technology Letters*, vol. 3, no. 1, pp. 65–67, Jan. 1991.

[29] X. S. Yao and G. Lutes, "A high-speed photonic clock and carrier recovery device," *IEEE Photonics Technology Letters*, vol. 8, pp. 688–690, May 1996.

[30] H.C.H. Mulvad, E. Tangdiongga, H.de Waardt, and H. J. S. Dorren, "40 GHz clock recovery from 640 Gbit/s OTDM signal using SOA-based phase comparator," *Electronics Letters*, vol. 44, no. 2, pp. 146-147, Jan. 2008.

[31] N. Jia, T. Li, K. Zhong, J. Sun, M. Wang, and J. Li, "Simultaneous clock enhancing and demultiplexing for 160-Gb/s OTDM signal using two bidirectionally operated electroabsorption modulators," *IEEE Photonics Technology Letters,* vol. 23, no. 21, pp. 1615-1617, Nov. 2011.

[32] X. Tang, J. C. Cartledge, A. Shen, F. V. Dijk, and G.-H. Duan, "All-optical clock recovery for 40 Gb/s MZM-generated NRZ-DPSK signals using a self-pulsating DBR

laser," *IEEE Photonics Technology Letters*, vol. 20, no. 17, pp. 1443-1445, Sep. 2008.

[33] J. Parra-Cetina, S. Latkowski, R. Maldonado-Basilio, P. Landais, "Wavelength tunability of all-optical clock recovery based on quantum dash mode-locked laser diode under injection of a 40 Gb/s NRZ data stream," *IEEE Photonics Technology Letters*, vol. 23, no. 9, pp. 531-533. May. 2011.

[34] D. M. Patrick and R. J. Manning, "20 Gb/s all-optical clock recovery using semiconductor nonlinearity," *Electronics Letters*, vol. 30, no. 2, pp. 151–152, Jan. 1994.

[35] L. E. Adams, E. S. Kintzer, and J. G. Fujimoto, "All-optical clock recovery using a modelocked figure eight laser with a semiconductor nonlinearity," *Electronics Letters*, vol. 30, no. 20, pp. 1696–1697, Sep. 1994.

[36] G.-H. Duan, A. Shen, A. Akrout, F. V. Dijk, F. Lelarge, F. Pommereau, O. LeGouezigou, J.-G. Provost, H. Gariah, F. Blache, F. Mallecot, K. Merghem, A. Martinez, and A. Ramdane, "High performance InP-based quantum dash semiconductor mode-locked lasers for optical communications," *Bell Labs Tech. Journal*, vol. 14, no. 3, pp. 63-84, Nov. 2009.

[37] F. Lelarge, F. Pommereau, F. Poingt, L. Le Gouezigou, and O. Le Gouezigou, "Active mode-locking of quantum dot Fabry-Pérot laser diode," *IEEE International Semiconductor Lasers Conference*, 1708132, pp. 153-154, 2006.

[38] T. Sakamoto, "Optical comb and pulse generation from CW light," *Lasers and Electro-Optics (CLEO) 2011 Conference on*, pp. 1-2, Paper CMBB1, May. 2011.

[39] S. Latkowski, and P. Anandarajah, "Optical frequency comb generation and its applications," *Transparent Optical Networks (ICTON 2011), 2011, 13th Conference on*, pp. 1-2, Paper Tu.B1.1, Jun. 2011.

Chapter 2

Mode-locking in semiconductor lasers

2.1 Mode-locking

Mode-locking is a technique that allows the generation of laser pulses with durations between nano and picoseconds [1-4]. Mode-locking occurs when the cavity modes are made to oscillate with comparable amplitudes and locked phases. In a laser, many modes are allowed to propagate along the resonator axis with frequency separation, known as the free spectral range (FSR) equal to $c/2L$, where L is the optical length of the cavity and c is the speed of light in the semiconductor medium. These modes usually oscillate with random phases and irregular amplitudes within the round-trip period, $\tau_{RT} = 2L/c$, inside the laser cavity. However, if these modes have the same phase $\emptyset$, they will constructively interfere at the same instant, $\tau_c = (\emptyset/2\pi)\tau_{RT}$, of the round-trip time. Therefore, the output will consist of a series of pulses and the laser is said to be ''mode-locked.'' The element to fix these relative phases is referred to as the mode locker. In mode-locked lasers, the optical modes are equally spaced and their relative phases are fixed [1-4].

To further explain this pulse formation, a series of equations considering the electric fields interacting in the laser cavity is introduced herein. For a laser with **M** odd modes with a frequency separation $\Delta\omega$, between the longitudinal modes equivalent to

$$\Delta\omega = 2\pi FSR = \pi c/L \tag{2.1}$$

the expression of the total electric field emitted by a laser is given by [1], [5]

$$E(t) = \sum_{n=-\frac{(M-1)}{2}}^{\frac{(M-1)}{2}} A_n(t) exp\{j(\omega_0 + n\Delta\omega)t + \emptyset_n(t)\} \tag{2.2}$$

where $A_n(t)$ is the amplitude fluctuation, ω_0 is the frequency of the central mode, and $\emptyset_n(t)$ is the phase of the nth mode. In order to reduce the complexity of the calculations in this approach, the amplitude fluctuation, also known as the amplitude noise, $A_n(t)$, and chromatic dispersion effects in the material composing of the active media of the laser are neglected. Moreover, the phase $\emptyset_n(t)$, is set to zero as it is considered the modes have the same phase. As a result, the total electric field is now expressed as

$$E(t) = \sum_{n=-\frac{(M-1)}{2}}^{\frac{(M-1)}{2}} exp\{j(\omega_0 + n\Delta\omega)t\} = exp(j\omega_0 t)\sum_{n=-\frac{(M-1)}{2}}^{\frac{(M-1)}{2}} exp\,(jn\Delta\omega t) \qquad (2.3)$$

Solving the summation, it is found that [4], [5]

$$E(t) = exp(j\omega_0 t)\frac{1 - exp(jM\Delta\omega t)}{1 - exp(j\Delta\omega t)} \qquad (2.4)$$

Considering that the total power is given by equation (2.5)

$$P(t) = \langle E(t)^* E(t)\rangle \qquad (2.5)$$

in turn, the new expression for the total power is [1], [2], [4], [5]

$$P(t) = \frac{sin^2\left(\frac{M\Delta\omega t}{2}\right)}{sin^2\left(\frac{\Delta\omega t}{2}\right)} \qquad (2.6)$$

As a result of this locking condition, the longitudinal modes interfere constructively and produce short pulses of light. The maximal powers of the pulses occur for values where $\left(\frac{\Delta\omega t}{2}\right)$ in the denominator in equation (2.6) becomes zero. $P(t)$ is a periodic function with period $\tau_{RT} = \frac{2\pi}{\Delta\omega} = \frac{2L}{c}$. To achieve a large power in the pulse it is needed to have a large number of modes, and all of them synchronised, i.e. with the same phase. The oscillation can be pictured as a pulse which propagates back and forth in the cavity in a time τ_{RT} [1].

The pulse width Δt_p of each of the successive pulses is approximately equal to the inverse of the frequency range (or laser bandwidth Δv) spanned by the modes being locked in phase

$$\Delta t_p \approx \frac{1}{\Delta v} \qquad (2.7)$$

whereas Δv can also be expressed as [1], [5]:

$$\Delta v = \frac{M\Delta\omega}{2\pi} \qquad (2.8)$$

Substituting equation (2.8) into equation (2.7), is obtained another representation of the pulse width

$$\Delta t_p = \frac{2\pi}{M\Delta\omega} \qquad (2.9)$$

From expressions (2.6) and (2.9), it can be seen that a large laser bandwidth or a large number of modes are required for the generation of very short pulses [1], [4], [5]. Fig. 2.1 provides an illustration of the mode-locking principle by plotting equation (2.6), for 8, 16 and 24 modes present in the laser spectrum and assuming that the modes are phase locked and that only the variation on the number of modes locked can provide a modification of the pulse width.
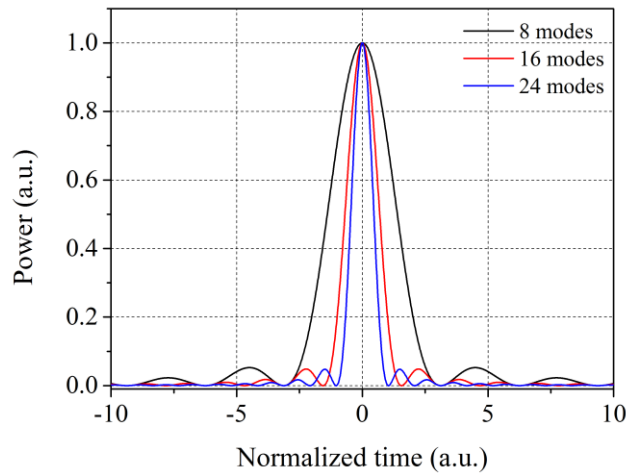
Figure 2.1: Illustration of the mode-locking principle. Reduction of the pulse duration as a function of the number of mode-locked modes for: 8 modes (black), 16 modes (red) and 24 modes (blue).

The synchronisation of the phase, or in other words the mechanism to make the phases identical, can be carried out according to several techniques including mainly: passive mode locking, active mode-locking and hybrid mode-locking [6]. These techniques will be explained in Section 2.2.

2.2   Mode-locking techniques

There are three broad categories of mode-locking mechanisms: passive, active, and hybrid. These methods of mode-locking will be described below.

2.2.1   Passive mode-locking

Passive mode locking is an approach for the generation of ultra-short optical pulses, in which the element that induces mode-locking is not driven externally but instead exploits nonlinear optical effects [2], [7]. This technique requires a section within the laser cavity to behave as a saturable absorber having an absorption that decreases with increasing incident intensity until it saturates and becomes completely transparent to the signal inside the cavity.

A laser suitable for passive mode-locking will have a gain region and a region of saturable absorption [8]. The pulse generation can be understood in the following way: when the device is forward biased, spontaneous emission of photons begins, and some stimulated emission may begin. In steady state, the loss is greater than the gain. When the generated light first reaches the saturable absorber, it experiences loss, but as the light travels through the cavity it will amplify. Therefore, some of the stimulated emission can grow to the point at which it saturates the absorption region allowing the peak of the pulse to travel through. For this brief period, the gain is greater than the loss, and a short duration pulse of light is amplified. Most of the modes within the gain region of the cavity are lasing at the same time, and therefore start with the same phase and as a result are synchronised. The absorption of the saturable absorber saturates faster than the gain, meaning that the absorber has lower saturation energy than the gain of the gain medium [8]. The recovery time of the absorber must be quicker than that of the gain section. This ensures that the loss quickly reverts back to being greater than the gain, and the light experiences loss once more [9]. In this process the leading and trailing edge of a light pulse experience loss, while its peak experiences gain. This cycle repeats itself in successive round trips in the cavity that serves to shorten the duration of the pulse and boost its peak power as it passes through the device [10].

2.2.2   Active mode-locking

Active mode-locking can be achieved by periodic external modulation of the cavity gain or loss of the round trip phase changes synchronised with resonator round-trips [1], [2], [7]. This leads to the generation of ultra-short pulses usually in the order of picoseconds. The modulation can be realised with the use of a semiconductor electro-absorption modulator, an acousto-optic

modulator or a Mach-Zehnder integrated optic modulator [11] placed in the cavity and driven by an external signal. With active mode-locking, it is necessary to synchronise the modulating signal with the round trip time of the resonator (mode spacing frequency) or a factor or multiple integer of it, in order to achieve stable operation. Precise tuning can be achieved by accurate and stable laser setup alignment or by a feedback circuit adjusting the modulation frequency or cavity length accordingly. Only during the peak of the external signal pulse, will the optical gain of the amplifier be high enough to overcome the losses in the cavity. During this short period of positive net gain, an optical pulse is generated. Again some of the modes selected by the cavity start to lase at the same instant and therefore, they possess the same phase.

2.2.3 Hybrid mode-locking

When the active and passive mode-locking are present simultaneously in the same laser system, we find the third method of mode-locking called *hybrid mode-locking.* In a hybrid mode-locked laser, the generation of the optical pulses are in the same way as in a passively mode-locked laser, while the pulses are synchronised with an electrical signal like in the actively mode-locked method [6], [7].

2.2.4 Passive mode-locking by FWM in Fabry-Pérot semiconductor lasers

The most common element associated with passively mode-locked lasers is the saturable absorber; however, in its absence, the passive mode-locking can occur due to nonlinear interactions between longitudinal modes that induce dynamic modulation of both the gain and the refractive index in the active region of the semiconductor laser diode [12-14]. The dynamics are originated from the sensitivity of the carrier density to the modulation of the optical power at the frequency of the mode beatings [15].

Such behaviour is strongly improved when the active region in a laser diode consists of quantum structures (dot, dash, well), allowing control of material properties giving rise to better optical confinement and smaller active cross section dimensions [16], where the interactions between optical fields intensities inside the active region and mutual coupling are increased.

The optical field of the k_{th} longitudinal mode generated in a laser cavity can also be expressed as a monochromatic wave given by equation

$$E_k^{(c)} = UA_k(t)\exp\left(-j\left(\omega_k t - \phi_k(t)\right)\right) \qquad (2.10)$$

where the superscript c over E indicates that E is a complex wave-function describing the monochromatic wave, U is the spatial mode distribution in the linear polarisation (it is assumed equal to one for the rest of the calculation), A_k is the slowly time varying amplitude, ω_k is the locked angular frequency and ϕ_k is the instantaneous phase fluctuation [15]. In the case of a laser with M longitudinal modes, a mode beating occurs leading to a quadratic temporal average of the total electric intensity with the following expression [16]:

$$\langle |E_T|^2 \rangle = \sum_{k=1}^{M} \langle |E_k|^2 \rangle + \sum_{k=1}^{M} \sum_{j \neq k} 2 \langle E_k E_j \cos\left(\Omega_{jk} t + \left(\phi_j(t) - \phi_k(t)\right)\right) \rangle \qquad (2.11)$$

where Ω_{jk} is defined as $\left(\omega_j - \omega_k\right)$ beating between any two modes.

The spatial dependency of the electromagnetic fields is neglected in equations (2.10) and (2.11), and for the remainder of the analysis. The longitudinal modes of the cavity are beating in the medium and producing a signal at the frequency $\left(\omega_j - \omega_k\right)/2\pi$, which modulates the active material through third order nonlinear effects, resulting in the creation of modulation sidebands around the optical modes. The beating is believed, according to our approach, to be sustained by four wave mixing (FWM) processes [12], [17], [18].

Interactions between the optical modes inside a semiconductor laser cavity through FWM are schematically expressed in Fig. 2.2. For the sake of simplicity, the beating between modes E_1 and E_2 is considered and in this example can be assumed as the origin of mode-locking. This beating results in a modulation of the gain with the frequency corresponding to the difference frequency between contributing optical modes $v = \left(\omega_2 - \omega_1\right)/2\pi$. Such modulation generates equidistant (in the spectral domain) side-bands S_1, S_3 and S_2, S_4 around the modes E_1 and E_2 respectively. These sidebands can be expressed as follows [16]:

$$S_1 = \alpha_1 \cdot E_1 \cdot E_1 \cdot E^*_2 = \alpha_1 \cdot E_1{}^2 \cdot E^*_2 \qquad (2.12)$$

$$S_2 = \alpha_2 \cdot E_1 \cdot E^*_1 \cdot E^*_2 \qquad (2.13)$$

$$S_3 = \alpha_3 \cdot E_2 \cdot E^*_1 \cdot E^*_2 \qquad (2.14)$$

$$S_4 = \alpha_4 \cdot E^*_1 \cdot E_2 \cdot E_2 = \alpha_4 \cdot E_1{}^* \cdot E_2{}^2 \qquad (2.15)$$

where α_k are the coupling efficiency factors, and E^*_k are the complex conjugates of the respective fields E_k. Sideband S_4 whose amplitude and phase are related to both modes E_1 and E_2, result in pulling the mode E_3 from the Fabry-Pérot (FP) resonant position and correlates the phase of the mode E_3 with two other modes (in Fig. 2.2, the FP resonant modes are represented with a dotted line, by taking into account the dispersive nature of the semiconductor). Similar processes result from beating modes E_2 and E_3 and transfer the phase information to the mode E_1; this snap view of the process was for the case of three modes, but it can be further extended to a larger number of optical modes.
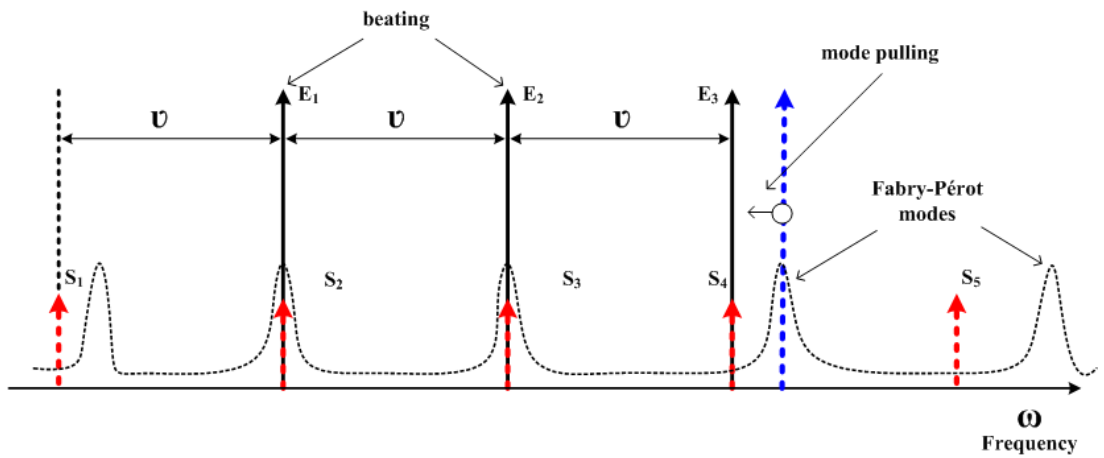
Figure 2.2: Schematic description of mutual injection regime through modulation sidebands from FWM. E_1, E_2 and E_3 represent the lasing modes and S_1 to S_5 are the sidebands resulting from FWM.

The sidebands created by the FWM process can act as optical injection signals for modes leading to a mutual injection-locking phenomenon. This phenomenon reaches equilibrium when all mode-spacing frequencies are locked to the same value with appropriate power distribution among modes. This phenomenon is supported by the material gain dynamics of the laser, which provides the mechanism for a phase information exchange between optical fields, and allows for their phase fluctuations (phase noise) and synchronisation [15], [16].

The assumption that the phase of each mode is uncorrelated with contributing modes implies that the second term in the right hand side of equation (2.11) is equal to zero; as a consequence the linewidth of the generated beat signal is equal to the sum of the linewidths of the optical modes. However, if the modes are phase correlated, this term is non-zero and the linewidth of the beat signal should be smaller than the sum of the linewidths of the optical modes [19].This gives rise to the following criterion for identify mode locking phenomenon:

$$\Delta \upsilon_{RF} << \sum_i \Delta \upsilon_i \qquad (2.16)$$

where $\Delta \upsilon_{RF}$ is the linewidth at the RF frequency and $\Delta \upsilon_i$ the linewidth of the i_{th} optical mode [20], [21].

As was previously explained for the case of a semiconductor laser, the correlation of the phases of the optical longitudinal modes can occur through the four wave mixing process (FWM) resulting from material nonlinearities [15], [16], and resulting in passive mode locking. There are five main effects that can result with four wave mixing in semiconductor devices: carrier density modulation (CDM), carrier heating (CH), spectral hole burning (SHB), two photon absorption (TPA) and the Kerr effect [22]. Dominance of some of these effects over the others is related to the separation frequency between optical modes. With the free spectral range between modes in the order of below 100 GHz, the CDM effect is dominant and so the others maybe neglected. For frequencies beyond 100 GHz up to 2.5 THz, CH plays the main role, and above 2.5 THz, the main effect is the SHB [15], [16].

2.3   Summary

In this Chapter an overview of mode locking in semiconductor lasers was presented. Mode locking is achieved when the electrical fields corresponding to each of the longitudinal modes present in the laser cavity are made to oscillate in each round trip with the same frequency and phase in such a way that they interfere constructively. This interference gives rise to a phase correlation between the modes and as a consequence optical pulses are generated with short durations, high repetition rate and low timing jitter. The duration of the pulses is inversely proportional to the number of modes correlated. There are several techniques to achieve mode-locking in semiconductor lasers in their different structures. Most of the techniques require extra elements either inside or outside the laser cavity making the fabrication or implementation process more complex and expensive. The possibility to have laser structures where the passive mode locking mechanism is supported by nonlinearities in the active region that create a mutual injection locking to obtain a stable operation and only requiring to be DC-biased and controlled in their temperature is of great interest. Recently, modern passive mode-locked single section Fabry-Pérot semiconductor devices with quantum structures that produce multiple modes in a broad gain spectrum are able to provide short pulses with potential applications for telecommunications. These types of devices will be studied throughout this thesis.

In addition, in Section 2.2.4 some theory on the mode-locking mechanism achieved in multimode lasers via four wave mixing was briefly presented. In Chapter 3, some experimental

evidence of passive mode-locking in Fabry-Pérot Quantum dash lasers will corroborate the possibility of mode-locking by FWM.

References

[1]   O. Svelto, *Principles of lasers*, 4th ed., ISBN:0-306-45748-2, pp: 330-343, USA: Plenum Press, 1998.

[2]   A. Yariv, *Quantum electronics*, 3rd ed., USA: John Wiley & Sons, Inc., 1988.

[3]   K. Thyagarajan, and A.K. Ghatak, *Lasers theory and applications*, New York: Plenum Press, 1981.

[4]   B.E.A. Saleh and M.C. Teich, *Fundamentals of Photonics*, USA: *John Wiley & Sons, Inc.*, 1991.

[5]   P. Landais, *Lecture note: Pulsed regime in semiconductor lasers*, Dublin City University, Ireland 2011.

[6]   J. Javaloyes, and S. Balle, "Mode-locking in semiconductor Fabry-Pérot lasers," *IEEE Journal of Quantum Electronics*, vol. 46, no. 7, pp. 1023-1030, Jul. 2010.

[7]   G. M. Roger, P. Koumans and Raymond van Roijen, "Theory for passive mode-locking in semiconductor laser structures including the effects of self-phase modulation, dispersion, and pulse collisions," *IEEE Journal of quantum Electronics*, vol. 32, no. 3, pp. 478-492, Mar. 1996

[8]   D. J. Derickson, R. J. Helkey, A. Mar, J. R. Karin, J. *G.* Wasserbauer, and J. E. Bowers, "Short pulse generation using multisegment mode-locked semiconductor lasers," *IEEE Journal of Quantum Electronics*, vol. 28, no. 10, pp. 2186-2201, Oct. 1992.

[9]   W. S. C. Chang, *Principles of lasers and optics*, USA: Cambridge University Press, 2005.

[10]   J. Wang, *Fundamental Principles of Lasers and Ultrafast Optics*, Notes by Jyhpyng Wang, 1999-2000.

[11]   L. Schares, R. Paschotta, L. Occhi, and G. Guekos, "40-GHz mode-locked fiber ring laser using a Mach-Zehnder interferometer with integrated SOAs," *IEEE Journal of Lightwave Technology*, vol. 22, no. 3, pp. 859-873, Mar. 2004.

[12]   L. F. Tiemeijer, P. I. Kuindersma, P. J.A. Thijs, and G. L.J. Rikken, "Passive FM locking in a InGaAsP semiconductor lasers," *IEEE Journal of quantum electronics*, vol. 25, no. 6, pp. 1385-1392, Jun. 1989.

[13]   K. A. Shore, "Theory of self-locking FM operation in semiconductor lasers," *IEE*

Proceedings Journal, vol. 138, no. 2, pp. 91-96, Apr. 1991.

[14] W.M. Yee, K.A. Shore, "Multimode analysis of self locked FM operation in laser diodes," *IEE Proceedings Journal,* vol. 140, no. 1, pp. 21-25, Feb. 1993.

[15] J. Renaudier, G.-H. Duan, P. Landais, and P. Gallion*,* "Phase correlation and linewidth reduction of 40 GHz self-pulsation in distributed Bragg reflector semiconductor lasers," *IEEE Journal of Quantum Electronics,* vol. 43, no. 2, pp. 147-156, Feb. 2007.

[16] S. Latkowski, "*Radio frequency and terahertz signals generated by passively mode-locked semiconductor lasers,"* Thesis, 2010.

[17] S. Latkowski, F. Surre, R. Maldonado-Basilio, and P. Landais, "Investigation on the origin of terahertz waves generated by dc-biased multimode semiconductor lasers at room temperature," *Applied Physics Letters*, vol. 93, no. 24, pp. 241110-03, Dec. 2008.

[18] H. Kasuya, M. Mori, R. Goto, T. Goto, and K. Yamane, "All optical mode locking of Fabry-Perot laser diode via mutual injection locking between two longitudinal modes," *Applied Physics Letters*, vol. 75, no. 1, pp. 13-15, Jul. 1999.

[19] S. Latkowski, F. Surre, E. Degirmenci, and P. Landais, "Passively phase locked multimode semiconductor laser: from milimetre to terahertz wave generation," *in Lasers and Electro-optics, 2008 and 2008 Conference on Quantum Electronics and Science. CLEO/QELS 2008. Conference on*, pp. 1-2, 2008.

[20] S. Latkowski, F. Surre, and P. Landais, "Passively mode-locked semiconductor lasers and their applications," *Transparent Optical Networks, 2008. ICTON 2008*, Tu.D2.3 pp.110-113, Jun. 2008.

[21] R. Maldonado-Basilio, S. Latkowski, and P. Landais, "Linewidth study of 40-GHz passively mode-locked multimode semiconductor lasers," *in Lasers and Electro-optics, 2009 and the European Quantum Electronics Conference. CLEO Europe-EQEC 2009. European Conference on.* pp. 1, Jun. 2009.

[22] G.P. Agrawal and N.K. Dutta, *Long wavelength semiconductor lasers*, United States: Van Nostrand Reinhold Co. Inc., New York, NY, 1986.

Chapter 3

Passively mode-locked quantum dash Fabry-Pérot laser diode

3.1 Introduction

The development of new devices for optical signal processing in current and future telecommunication networks is of crucial importance [1], [2]. In order to achieve a practical implementation of such devices, there are many factors to consider, such as: capability to work at high bit rates in the C-Band (1530-1565 nm), low power consumption, small foot print. In this regard, the use of semiconductor devices is a good option.

In this Chapter, the quantum dash Fabry-Pérot laser diodes (QDash FP-LDs) utilised in this research are introduced and their free running optical and electrical characterisations are performed. This Chapter is organised as follows: in Section 3.2, the QDash Fabry-Pérot laser diode is described; in Section 3.3, a set of characterisations are performed. On one hand, we have the voltage versus bias current and optical power versus bias current characterisations, the optical linewidths for each of the longitudinal modes emitted by the QDash FP-LD are also investigated. Furthermore, the RF linewidth generated by the beating of the longitudinal modes is analysed. Moreover, an identification of passive mode-locking mechanism in this kind of lasers is performed and the hypothesis claimed in Chapter 2 supported by equation 2.16 is experimentally verified.

3.2 Device description

The QDash-based heterostructure is grown by gas source molecular beam epitaxy (GS-MBE) on a S-doped InP substrate. The active core consists of six layers of InAs QDash embedded in 40 nm-thick InGaAsP barriers [2]. The entire active structure is surrounded by two 80 nm-thick separate confinement hetero-structure (SCH) layers. Both barriers and SCHs are undoped. Both facets are cleaved, forming a 1mm-long FP cavity. It is a single section laser, without phase or

saturable absorption sections [3]. Typical dimensions along the growth axis and width of the QDash to achieve emission at 1.55 μm, are 2 nm and 20 nm respectively. The density of dashes per layer is 2×10^{10} cm^{-2}. The device is designed and manufactured by Alcatel-Lucent III-V Lab, France. Fig. 3.1 shows a cross-sectional transmission electron microscopy image of a stack of 3 layers of dashes-in-a-barrier structures in the laser active layer [4].
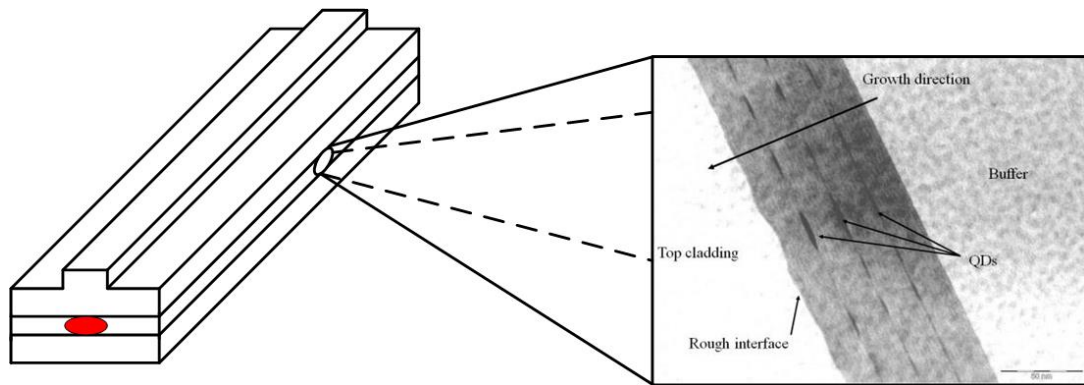
Figure 3.1: QDash Fabry-Pérot semiconductor laser structure with a photograph of the cross-sectional transmission electron microscopy image of a stack of 3 layers of dashes-in-a-barrier structures. The dashes are elongated in the direction transverse to the beam propagation inside the laser cavity [4], [5].

3.3   Steady state characterisations

The quantum dash mode-locked laser under investigation is a pre-cut wafer-bar, mounted and wire-bounded to the electrodes on a ceramic sub-mount. This device was characterized in its two presentations: packaged in a butterfly case or not, showing similar features. In the case of the unpackaged device, the whole sample is placed on a probe station and connected to two individual DC probes for bias and ground connections, as shown in Fig. 3.2(a). A similar laser was packaged by Achray Photonics and placed on a mounting board, as shown in Fig. 3.2(b). The temperature is controlled and stabilised at 25 ºC unless otherwise stated. I investigated the behaviour of the tested laser under DC-bias conditions in the optical and electrical domains as a function of injected current.

(a)	(b)
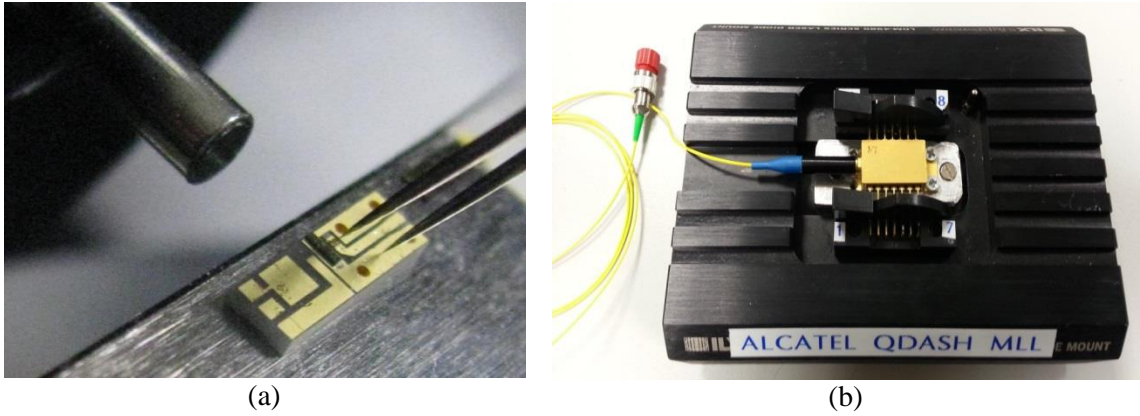
Figure 3.2: Picture of the QDash-FP-LD: (a) chip mounted on a probe station, (b) in a butterfly package and mounted on a testing module board.

3.3.1 Voltage versus bias current and optical power versus bias current characterisations

In order to study the QDash FP-LD device, a basic electrical and optical characterisation setup was developed, where mainly the voltage versus current (VI), and optical power versus current (LI) characteristic curves are of interest. As shown in Fig. 3.3, the experimental setup and procedure is basic. It consists of the measurement of the voltage across the active layer and the emitted optical power as a function of the driving bias supplied on the device under test. The bias current applied to the laser is automatically controlled and varied from 0 mA to 400 mA in steps of 1 mA. The optical power is measured with both an optical power meter and an optical spectrum analyser (OSA-1, Yokogawa AQ 6370).
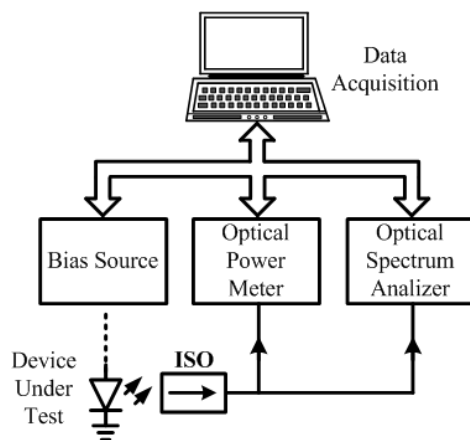
Figure 3.3: Experimental setup for the characterisation of the power collected vs. bias current, and optical power spectrum vs. bias current (--) electrical cable (-) optical cable, (||) data interface cable.

Fig. 3.4 depicts the LI and VI characteristics for the QDash FP lasers in its two presentations: packaged (black trace) and unpackaged (blue trace). The LI curves show the measured threshold current which is at I_{TH} =18 mA. It was recorded in two ways: by increasing and decreasing the bias current. Both curves are overlapping each other; this demonstrates that there is no unbiased part of the lasers functioning as a saturable absorber. In addition, a maximum optical power of 5.7 mW at the output of the packaged laser is collected from a pigtail single mode fibre, after passing through an optical isolator to avoid back reflections. In the case of the unpackaged laser, a maximum optical power of 3.7 mW is collected by a 0.5 NA lensed fibre followed by an isolator when operating at 400 mA. From Fig. 3.4, it can be verified that the packaged device exhibits better coupling when compared to its unpackaged version. From the manufacturers, it is known that the coupling losses for the packaged laser are approximately 3.5 dB. Considering that datum, the coupling efficiencies are 44 % and 29 % for the packaged and unpackaged versions, respectively. The VI curves correspond to the electrical characteristics of the semiconductor components utilised, and dynamic impedance across the active section is calculated from these curves, obtaining 1.7 Ω and 5.93 Ω for the packaged and unpackaged QDash FP-LDs, respectively. The difference in the dynamic impedance obtained for the two lasers can be attributed to parasitic impedances from the connections utilised between the lasers and the biased source.

Another parameter that can be calculated from the VI curve is the external differential quantum efficiency, obtaining efficiencies of 8 % and 5 % for the packaged and unpackaged laser, respectively. This value depends on the material used in the design of the laser, as well as on the cavity length [6].
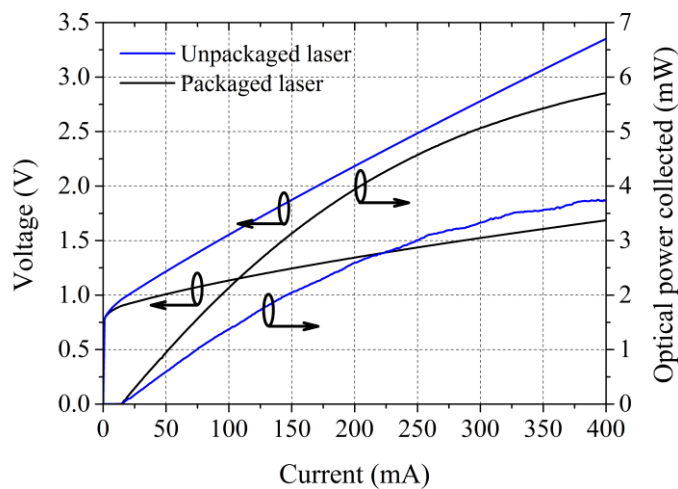
Figure 3.4:   The VI and LI curves obtained from the QDash-FP-LD in its packaged and unpackaged presentations.

3.3.2 Optical spectrum analysis

3.3.2.1 Multimode analysis

From the previous characterisations it was obtained that for all currents exceeding the threshold value, the optical spectra emitted by the QDash FP lasers feature a multimode behaviour with a nearly flat envelope. Increasing the bias current leads to an increment in the number of optical modes present in the 3 dB bandwidth as well as a slight displacement of the optical spectrum envelope towards shorter wavelengths. The rise in the number of longitudinal modes with the increment in the DC-bias applied to the device spans from the threshold current to approximately 100 mA, after which the number of emitted longitudinal modes present in the optical spectrum remains to circa 40 in the 3 dB bandwidth. An example of the optical spectra recorded with the device at 350 mA and temperature controlled at 25 ℃ is presented in Fig. 3.5. The optical spectrum is centered at 1524 nm with a 3 dB bandwidth spanning 12 nm and containing approximately 40 optical modes. The longitudinal optical modes in the spectrum are separated by 0.31 nm free spectral range (FSR), corresponding to an approximate frequency of 40 GHz. Furthermore, from Fig. 3.5, it is possible to estimate the peak power-to-noise ratio on the longitudinal modes within the 3 dB bandwidth, when taking as the reference 10 dB below the maximum peak power of the optical modes to the noise power level. It is of around 40 dB, demonstrating the associated low level of noise. This result along with the wide optical spectrum suggests the feasibility of the QDash FP laser to generate optical pulses with 40 GHz repetition. In this regard, Chapter 4 will demonstrate the optical pulse formation.
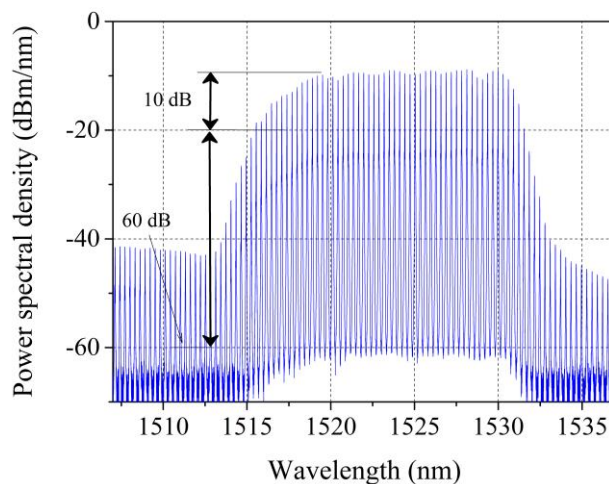
Figure 3.5: Optical spectrum emitted by the QDash FP-LD recorded for a bias condition of 350 mA, and temperature controlled at 25 ℃.

3.3.2.2　Optical linewidth measurement

An optical linewidth measurement setup based on a self-heterodyning detection (SHD) approach is utilised in order to assess the optical linewidth corresponding to each mode in the optical spectrum emitted by the QDash FP-LD [7]. The setup is shown in Fig. 3.6. For this characterisation, the use of an optical spectrum analyser (OSA) is not practical owing to its resolution, which does not allow measurements below 0.01 nm. The SHD technique is used as detailed in the next paragraph.

This measurement is performed on the QDash FP-LD chip placed on a probe station but similar results are expected from a packaged laser. The optical power of the QDash PF-LD is collected with a lensed fibre and coupled to an isolator (ISO) for suppressing back reflections from other elements of the setup which could disturb operation of the investigated laser. An Alnair BVF-200 tunable optical bandpass filter (OBPF), set to 0.2 nm bandwidth, allows every individual optical mode to be selected with a minimum adjacent-mode suppression of 25 dB. This OBPF does not affect the features of the modes measured, such as their individual phases. A semiconductor optical amplifier (SOA, SOA-XN-OEC-1550-CIP) operating in linear regime is used to boost the optical modes after the OBPF, allowing sufficient optical power to be provided to the SHD. In the SHD, the original optical signal from an optical mode is split into two paths. On the optical signal on one path, a HP E4437B signal generator (GEN) with a frequency of 2 GHz and the phase modulator (PM, EOspace PM-OK5-10-PFU) produce a phase modulation which generates harmonics with frequency separation corresponding to 2 GHz. The 12 km of single mode fibre (SMF) introduce a time delay and bring the signal in this branch beyond the coherence length (inversely proportional to the signal linewidth) and enables to achieve the minimum measurable linewidth of 17 kHz. The resulting signal, obtained from the frequency beating of the delayed signal and the first sideband of the modulated signal, is detected with a 10 GHz photo-detector (PD, Lab Buddy-PP DSC-R401HG) and an electrical spectrum analyser (ESA-1, Anritsu MS2661C) is used to assess the beat-tone from the SHD. The experiment consists in tuning the OBPF from its shortest wavelength achievable (~1520 nm) to the longest wavelength (~1532 nm) falling into the 3 dB bandwidth of the laser spectrum for four different bias conditions applied to the QDash FP-LD.
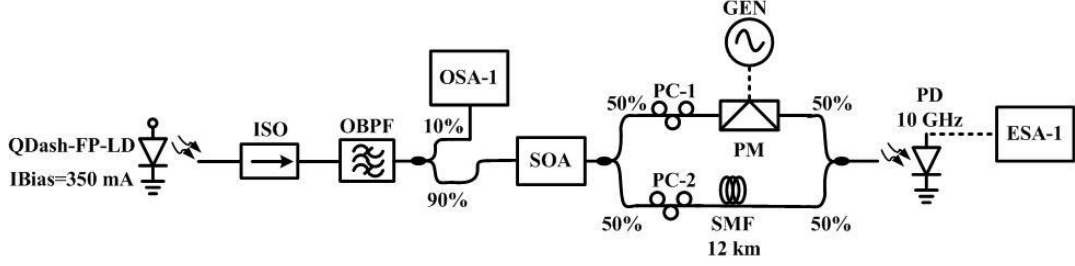
Figure 3.6: Self-heterodyning setup for optical linewidth measurement: QDash-FP-LD: quantum dash Fabry-Pérot laser diode; ISO: optical isolator; OBPF: optical band pass filter; OSA: optical spectrum analyser; SOA: semiconductor optical amplifier; PC: polarisation controller; GEN: signal generator; PM: phase modulator; SMF: single mode fibre; PD: photo-detector; ESA: electrical spectrum analyser (see Appendix A for equipment specifications).

The full width at half maximum (FWHM) linewidth of each optical mode is obtained by width measurements of the Lorentzian lineshape signal visualised with the ESA-1 at 10 dB drop from the peak value denoted with Δv_{10dB} by use of the equation [8]:

$$\Delta v_{FWHM} = \frac{\Delta v_{10dB}}{2\sqrt{10}} \tag{3.1}$$

The optical linewidth associated to each longitudinal mode as a function of the bias current is shown in Fig. 3.7. A decreasing trend in the optical linewidth is observed as a function of the mode wavelength at a given bias current. The linewidths of the longitudinal modes vary from 10 MHz at 1532 nm to 45 MHz at 1520 nm [7]. These optical linewidths values are in the same range as for a distributed feedback laser (DFB) [9], [10], with the advantage over the DFB lasers of having not a single mode but multiple modes. Further analysing the trend in these results, it might be seen as a consequence of the intrinsic four wave mixing that affects each of the longitudinal modes. The modes that are closer to the center of the gain envelop are more affected by the cavity gain. This increases their power and they function as a pump; meanwhile the modes on the right hand side with slightly minor power act as probes; this fact results in a more efficient up-conversion in the conjugate signal affecting the coherency of the modes on the right hand side [11-13]. This phenomenon also affects the noise of the individual modes on the right hand side resulting in a reduction of their linewidth. The change in the magnitude of the mode linewidth from 10 to 45 MHz (associated to the slope and position of the trace) related to the different bias currents might be due to a combination of events. These events directly involve the temperature, the gain and the carrier density in the laser cavity which affect the laser performance. For instance, an increase in the bias current increases the temperature in the QDash FP-LD, making the active layer of the device hotter. The increase in the temperature causes more carriers to be injected into the conduction band resulting in the creation of more

spontaneous emission, thus giving rise to an increment in the noise and a widening in the mode linewidth. These measurements on the linewidth of the optical modes will be analysed in more detail later in this Chapter, when comparing them with the RF linewidth of the beat-tone signal produced by the full optical spectrum emitted by the QDash-Fabry-Pérot laser and directed to a fast PD, in order to determine if there is a mode-locking mechanism engaged [11], [14].
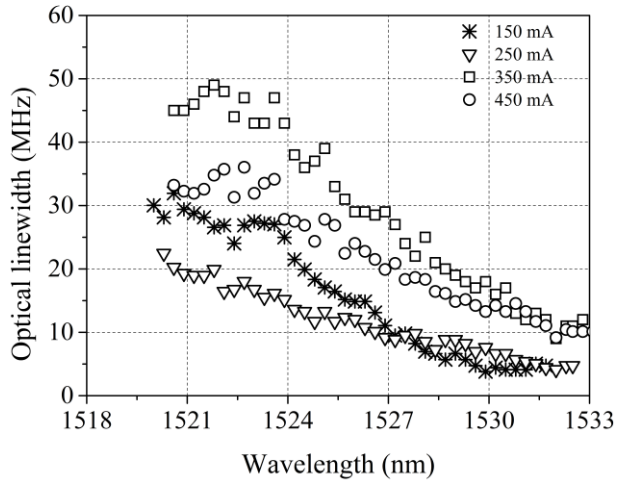
Figure 3.7: Optical mode linewidth measurements as a function of the wavelength at different bias currents.

3.3.3   RF spectrum analysis

3.3.3.1   RF beating linewidth measurement

The QDash laser emits a multimode spectrum for a wide range of bias currents above threshold, as was mentioned in Section 3.3.2. Above 100 mA, there are around 40 optical modes in the optical spectrum produced by the device in a 3 dB bandwidth window. The free spectral range between modes is approximately 40 GHz. The experimental setup depicted in Fig. 3.8 is used to investigate whether there is a beat signal generated at this frequency in the RF domain. The signal produced by the beating of all the modes on a fast 50 GHz photo-detector (PD, u^{2}t XPDV2020R) is analysed using a 40 GHz electrical spectrum analyser (ESA-2, Anritsu MS2668C) with resolution and video bandwidths set at 30 kHz.
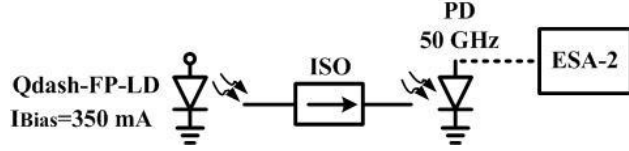
Figure 3.8: Experimental setup for RF mode-beating linewidth investigation.

The mode-beating signal measured from the QDash FP-LD is depicted in Fig. 3.9 for a bias current of I_{Bias}= 350 mA and temperature controlled at 25 ℃. At this bias condition, a peak at 39.7 GHz is recorded. The measured data points are fitted with a Lorentzian shape (red trace), and the FWHM linewidth of 25 kHz is estimated from the width of the fitted curve at 10 dB drop from the maximum value following equation 3.1 [7], [15], [16]. Furthermore, this result in a Q-factor of 1588000, which is calculated with the following equation:

$$Q = \frac{f}{\Delta f_{FWHM}}$$
(3.2)

where f is the central frequency and Δf the bandwidth of the resonator. This high Q-factor value indicates that the device is a very good resonator, capable of generating optical pulses with high stability and with good efficiency.
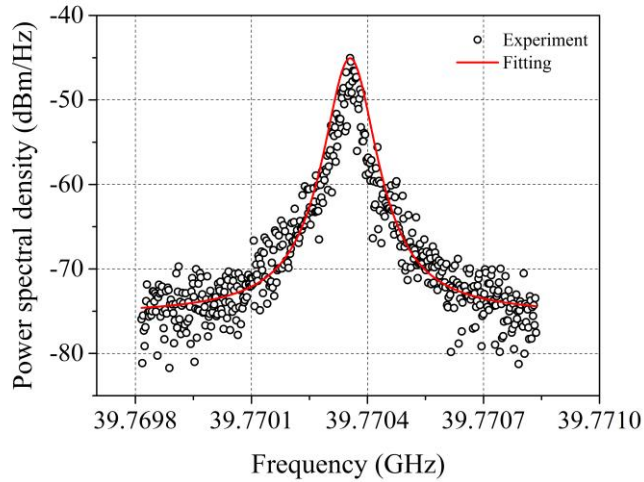
Figure 3.9: Mode-beating signal measured at the output of the QDash FP-LD at 350 mA. Measured data marked with open circles (o) and its Lorentzian fitting with solid red line.

The RF beating linewidth value is about three orders of magnitude lower than the sum of the optical linewidths associated to the optical modes produced by the laser and that contribute to that beating signal. This difference can be attributed to the high correlation between the modes, which results in a reduction of the noise of the beating signal, which is corroborated with the Q-factor calculated above. This is a signature of mode-locking [14-16].

In order to complement this explanation and to support the phase correlation of the optical modes which derives from mode-locking, a setup is implemented, which is shown in Fig. 3.10. It is a setup similar to the one already shown in Fig. 3.8, but with the addition of an OBPF (Alnair Labs BVF-200) set to 0.4 nm. The filter allows selecting out a pair of adjacent optical modes and it is tuned within the range of wavelengths from 1520 to 1532 nm, and their beating signal is retrieved by a PD (u^2t XPDV2020R) and ESA-2 (Anritsu MS2668C) for RF analysis.
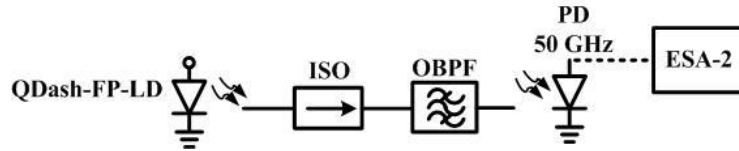
Figure 3.10: Experimental setup for RF mode-beating linewidth investigation.

The mode-beating linewidth is obtained by a Lorentzian fitting of the photocurrent measurements. A fairly constant profile of the mode-beating FWHM linewidth is observed. Indeed, it fluctuates from a minimum value of 10 kHz to a maximum of 25 kHz regardless of the bias supplied to the QDash FP-LD (above threshold), as the example shown in Fig. 3.11(a) for a bias current of 350 mA. Since phase noise is the origin of spectral linewidth, from these results it is proven that the relative phases of adjacent modes have similar characteristics, and as a consequence all the longitudinal modes are strongly phase correlated, due to the passive mode-locking mechanism [2]. Fig. 3.11(b) depicts the superposition of the optical spectrum emitted by the QDash FP-LD along with the results already illustrated in Fig. 3.11(a). From Fig. 3.11(b), it is possible to identify a quasi-sinusoidal behaviour in the retrieved points regarding the mode-beating FWHM linewidth measurements, coinciding with a similar shape of the optical spectrum and revealing a main composition of 6 regions of emission. These 6 regions can be attributed to the 6 layers of InAs Dash that comprise the active core, which might be the initiators of the multimode emission and the passive mode-locking condition in this kind of laser. The initially formed modes provoke nonlinear interactions in the active medium that give rise to FWM, leading to a mutual injection locking, which results in the passive mode-locking condition in the QDash FP-LD.
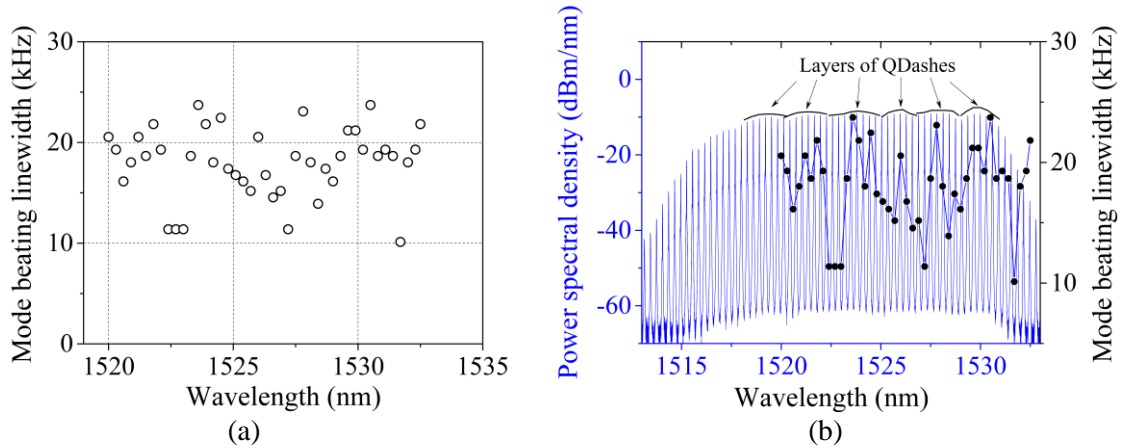
Figure 3.11: (a) Mode-beating linewidth associated with each pair of optical modes as a function of the OBPF central wavelength. (b) Comparison of the optical spectrum with the mode-beating linewidth associated with each pair of optical modes in a span from 1520 to 1532 nm.

From the results obtained throughout this Chapter such as the wide multimode optical spectrum, the narrow RF mode-beating linewidth and the demonstration of the mode-locking mechanism in these QDash Fabry-Pérot semiconductor lasers, it is expected that this device should generate optical pulses with low timing jitter. Moreover, it is envisaged that it should exhibit excellent synchronisation by external optical injection [2]. These statements are based on the results obtained in this Chapter along with the fact that this kind of laser is required to be only DC-biased, with low power consumption and with a small footprint, this would enable it as a solution for developing applications in the field of optical fibre communications.

3.4 Summary

In this Chapter, a QDash Fabry-Pérot semiconductor laser was introduced in its two presentations available in the optics labs at Dublin City University and on which this entire thesis work is based. Regardless of the presentation (packaged or unpackaged), these lasers have the same characteristics in their optical and electrical spectrum, only varying in their optical power collected by a lensed fibre or a pigtail patchcord. Moreover, the QDash laser generates a multimode optical spectrum with 12 nm bandwidth within the 3dB power range, suggesting the possibility of obtaining optical pulses from it. In addition, the optical linewidths of the longitudinal modes were measured, retrieving a value on the order of megahertz. Furthermore, the analysis of the mode-beating linewidth of the RF spectrum produced by the optical modes of the laser revealed a value of ~25 kHz when driving the laser at 350 mA, for instance. The difference of about three orders of magnitude between the RF beating linewidth and the optical

mode linewidths results helped to demonstrate the passive mode-locking mechanism in the QDash Fabry-Pérot semiconductor laser. This passive mode-locking mechanism was confirmed through the analysis of the RF mode-beating linewidth of the RF signal generated by pairs of adjacent optical modes, where their relatively similar values indicate a strong phase correlation among the modes. In addition, the high Q-factor value indicates that the QDash Fabry-Pérot laser is a good resonator capable of producing very stable pulses. In Chapter 4, an extension of the investigation of this quantum dash mode-locked laser diode (QDash-MLLD) will be performed, focusing on the demonstration of its applications for optical signal processing in subsequent Chapters.

References

[1] J. J. Coleman, J. D. Young, and A. Garg, "Semiconductor quantum dot lasers: a tutorial," *IEEE Journal of Lightwave Technology*, vol. 29, no. 4, pp. 499-510, Feb. 2011.

[2] F. Lelarge, B. Dagens, J. Renaudier, R. Brenot, A. Accard, F. van Dijk, D. Make, O. Le Gouezigou, J.-G. Provost, F. Poingt, J. Landreau, O. Drisse, E. Derouin, B. Rousseau, F. Pommereau, and G.-H. Duan, "Recent advances on InAs/InP quantum dash based semiconductor lasers and optical amplifiers operating at 1.55 μm," *IEEE Journal of Selected Topics Quantum Electronics,* vol. 13, no. 1, pp. 111-124, Jan./Feb. 2007.

[3] A. Shen, J. G. Provost, A. Akrout, B. Rousseau, F. Lelarge, O. Le Gouezigou, F. Pommereau, F. Poingt, L. Legouezigou J. Landreau, G.-H. Duan, et al., "Low confinement factor quantum dash mode-locked Fabry-Perot laser diode for tunable pulse generation," *in Optical Fiber Communication/National fiber Optic Engineers Conference, 2008. OFC/NFOEC 2008. Conference on,* p. 13, 2008.

[4] K. Merghem, R. Rosales, A. Martinez, G. Patriarche, A. Ramdane, N. Chimot, F. van Dijk, Y. Moustapha-Rabault, F. Poingt, and F. Lelarge, "Improvement of model gain of InAs/InP quantum-dash lasers," *in 23rd International, Conference on Indium Phosphide and Related materials, (IPRM 2011)*, pp. 1-4, May 2011.

[5] S. Latkowski, "Radio frequency and terahertz signals generated by passively mode-locked semiconductor lasers," *Dublin City University*, *Thesis*, 2010.

[6] K. S. Mobarhan. *Test and characterization of laser diodes: determination of principal parameters*, pp.1-8, Newport Application note.

[7] R. Maldonado-Basilio, J. Parra-Cetina, S. Latkowski, and P. Landais, "Timing jitter, optical, and mode-beating linewidths analysis on subpicosecond optical pulses generated by a quantum-dash passively mode-locked semiconductor laser," *Optics Letters*, vol. 35, no. 8, pp. 1184-1186, Apr. 2010.

[8] D. Derickson, J. Vobis, L. Stokes, P. Hernday, V. McOmber, D.M. Barney, W. V. Sorin, J. Beller, C.M. Miller, S.W. Hinch, and C. Hentschel, *Fiber Optic Test and Measurement*, Nova Jersey: Prentice Hall PTR, 1998.

[9] K. Shi, R. Watts, D. Reid, T. N. Huynh, C. Bowning, P. Anandarajah, F. Smyth, and L. Barry, "Dynamic linewidth measurements method via an optical quadrature front end," *IEEE Photonics Technologies Letters*, vol. 23, no. 21, pp. 1591-1593, Nov. 2011.

[10] T.N. Huynh, F. Smyth, L. Nguyen, and L. Barry, "Effects of phase noise of monolithic tunable laser on coherent communication systems," *Optics Express*, vol. 20, no. 26, pp. B244-B249, Dec. 2012.

[11] J. Renaudier, G. H. Duan, P. Landais, and P. Gallion, "Phase correlation and linewidth reduction of 40 GHz self-pulsation in distributed bragg reflector semiconductor lasers," *IEEE Journal of Quantum Electronics*, vol. 43, no. 2, pp. 147-156, Feb. 2007.

[12] N. Kumar Das, Y. Yamayoshi, and H. Kawaguchi,"Analysis of basic four-wave mixing characteristics in a semiconductor optical amplifier by the finite-difference beam propagation method," *IEEE Journal of quantum electronics*, vol. 36, no. 10. pp. 1184-192, Oct. 2000.

[13] O. Svelto, *Principles of lasers*, 4th ed., ISBN:0-306-45748-2, pp: 330-343, USA: Plenum Press,1998.

[14] S. Latkowski, F. Surre, E. Degirmenci, and P. Landais, "Passively phase locked multimode semiconductor laser: From milimetre to terahertz wave generation," *Lasers and Electro-optics, 2008 and 2008 Conference on Quantum Electronics and Laser Science. CLEO/QELS 2008. Conference on*, pp. 1-2, 2008.

[15] R. Maldonado-Basilio, S. Latkowski, F. Surre, P. Landais, "Linewidth analysis of 40-GHz passively mode-locked multimode semiconductor lasers," *Optics communications*, vol. 283, no. 2, pp. 299-303, Jan. 2010.

[16] R. Maldonado-Basilio, S. Latkowski, and P. Landais, "Linewidth study of 40-GHz passively mode-locked multimode semiconductor lasers," *Lasers and Electro-optics, 2008 and the European Quantum Electronics Conference on. CLEO/EQEC 2009.*pp. 1-2, Jun. 2009.

Chapter 4

Pulse generation by a quantum-dash mode-locked laser diode

4.1 Introduction

For current telecommunications networks and future high-speed optical communications systems, the possibility to generate high quality pulses in terms of repetition rate, short pulse duration and low timing jitter from compact devices such as semiconductor lasers is very important. There are several techniques to generate pulses from semiconductor lasers, among which are: Q-switching, gain-switching and mode-locking. Recently, quantum dot/dash semiconductor lasers have attracted significant interest over their counter parts named, i.e. QWell, due to a smaller phase noise and lower timing jitter in the pulses that they can produce [1-4]. This chapter is presented as follows: in Section 4.2 an overview on the techniques for the generation of pulses is addressed. In Section 4.3, a short review about one of the techniques used nowadays to fully characterise short pulses and that is used in this Chapter to carry out pulse analysis is given. In Section 4.4, the demonstration of pulse generation from a passively mode-locked quantum-dash laser diode (QDash-MLLD) is presented. Section 4.5 deals with an application of the QDash-MLLD as a pulse generator at frequencies of up to 160 GHz with the aid of a time multiplexing system. In Section 4.6, the first step approach towards a clock recovery system is presented. It consists of the synchronisation of the quantum-dash to pulses at sub-harmonic and harmonic frequencies. Finally, a summary of the main results in the Chapter is provided.

4.2   Pulse generation techniques

4.2.1   Q-switching

This technique consists of the modulation of the intracavity losses of the laser [5]. The modulation is achieved by inserting an element inside the resonator, which creates saturable absorption regions [5]. These regions of absorption increase the losses of the cavity (Q-factor is degraded) and as a consequence the laser action is inhibited. Meanwhile the population inversion is pumped far above the threshold population so that the gain can be built up to a very high value. Then, suddenly the losses are drastically reduced. The laser exhibits a gain that greatly exceeds losses; the stored energy is released in the form of a short and intense light pulse. As a result, a train of short pulses is produced due to the quick periodic change in the Q-factor of the cavity (from low to high) [5]-[7].   Among the elements that can be used to control (switch) the cavity losses (cavity Q) are: saturable absorber, electro-optic crystals and acousto-optical switches [6], [7].   These elements are generally grouped into two categories, active and passive Q-switches. In active Q-switching, some external active operation must be applied to this device. On the other hand, in passive Q-switching, the switching operation is automatically produced by the optical nonlinearity of the element employed (usually the saturable absorber).   With this technique it is possible to achieve high power pulses, but at expenses of obtaining the pulses with low repetition rate and relatively wide pulse width.

4.2.2   Gain-switching

In this technique, the pulses are generated in analogous manner to Q-switching, but as the name suggests the gain is modulated instead of the losses.   Unlike Q-switching, gain-switching does not require the insertion of elements in its cavity [8-10], but it requires external elements to modulate the laser gain. These elements are a RF signal source and a DC-bias current source coupled by a bias-T. Gain-switching is produced by injecting very rapidly a large number of carriers into the active region of the device. This produces an increase of the population inversion and of the gain above the threshold leading to the formation of photons (light signal) that will reduce the gain to below the threshold, deriving in the reduction of the photon density, quenching the light signal [6], [8], [11], [12].   With this technique many longitudinal modes are created with a well-defined spectral envelope. The pulse repetition rates achievable are limited usually to the gain bandwidth of the laser, which can be extended by strong optical injection, resulting in pulses at repetition rates up to several gigahertz with pulse durations between nano and picoseconds, with low timing jitter, which can be useful for telecommunication applications

[13]. In addition, one important advantage when compared to Q-switching is that gain-switching is wavelength tunable [14].

4.2.3   Mode-locking

An overview of the mode-locking theory has been presented in Chapters 1 and 2 along with its different variations. Mode-locked diode lasers can generate pulses shorter than both gain-switched and Q-switched lasers. In the case of semiconductor mode-locked lasers, the pulse repetition rate is determined by the optical length of the laser cavity. Pulses with durations in the order of femtoseconds at high repetition rates can be reached [15-19]. Depending on the application, one technique can be preferred over the other one, for instance Q-switching can produce pulses with more energy than gain-switching or mode-locking, but gain-switching provides more tunability. Mode-locking is simple to implement and can provide pulses with low phase noise and timing jitter. These aspects will be demonstrated later in this Chapter.

4.3   Pulse measurement techniques

One of the methods used to characterise a short pulse is by directly employing electronic techniques for temporal pulse-width measurements. This method consists of fast photodiodes and high bandwidth (electrical sampling) oscilloscopes. However, they are limited to pulses in the picosecond regime and normally they require a high quality clock to trigger the oscilloscope. These limitations make this method unsuitable for recording a pulse temporal profile [20]. The use of spectrograms can provide information of the intensity pulse purely in the frequency domain, but information of the phase is lost [21]. In order to fully characterise ultra-short pulses, optical correlation techniques that operate in the time-frequency domain are necessary. One of the most reliable techniques to analyse short pulses is the frequency resolved optical gating [20-26], better known as FROG.

4.3.1   Frequency resolved optical gating (FROG)

The FROG technique is built on an auto-correlator, and it is used to fully characterise the ultrashort pulses allowing the determination of the intensity and phase versus time or frequency [18-26]. An auto-correlator can only retrieve information of the amplitude or intensity versus

delay time of the second harmonic signal generated. Consequently, it can estimate the duration of pulses produced by a laser assuming an initial pulse shape. The FROG technique follows the same principle as the auto-correlator, but for the detection of the second harmonic signal, uses a spectrometer instead of a slow detector.

In this technique, as in the case of the auto-correlation, the signal to analyse *E(t)* is split into two, one of the replicas is time delayed *E(t- τ),* and they are combined (*E_sig (t,τ)*) in a second harmonic generation (SHG) crystal. In this crystal one of the replicas gates the other signal and the time delay is varied (see Fig. 4.1). The signal-pulse electric field obtained after crossing the SHG crystal has the form

$$E_{sig}(t,\tau) \propto |E(t)E(t-\tau)|^2 \tag{4.1}$$

This signal is then resolved by a spectrometer, to yield the FROG trace or spectrogram of the form

$$I_{FROG}(\omega,\tau) \propto \left| \int_{-\infty}^{\infty} E_{sig}(t,\tau)\, exp(-i\omega t)dt \right|^2 \tag{4.2}$$
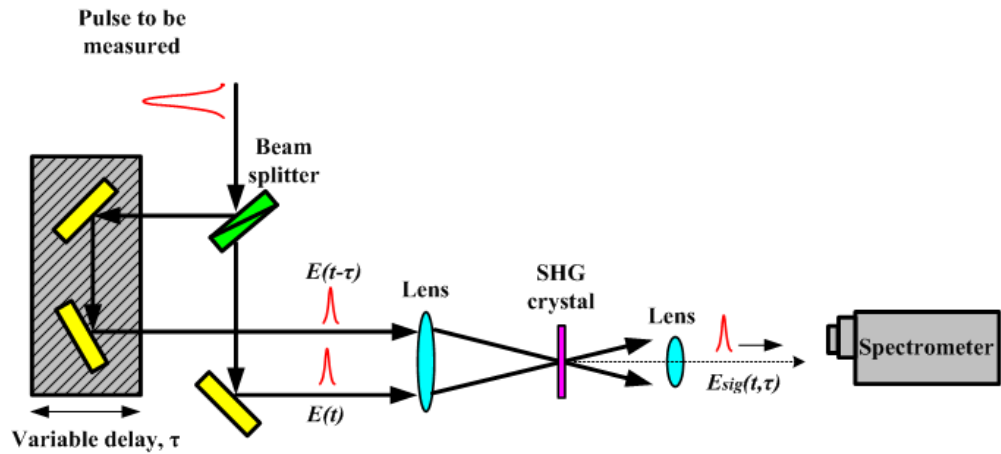
Figure 4.1: Schematic of the SHG FROG apparatus [27].

This measurement can be done on a single shot or many shots. At this stage, the FROG system has no information about *E(t)*, the recorded spectrogram is used as an input of an iterative algorithm which process and retrieves the full information of the electric field such as intensity

and phase of the pulse to analyse. *E(t)* is the solution that gives the lowest error between the measured spectrogram and that given by the algorithm calculation.

4.4   Pulse generation from passively mode-locked quantum dash laser diode

The experimental analyses performed on the QDash-MLLD in Chapter 3 indicate that the laser is passively mode-locked. In addition, due to its spectral optical and electrical features such as: multimode behaviour with more than 40 longitudinal modes in the 3 dB bandwidth contributing to 12 nm in a nearly flat spectrum, along with a narrow RF beating signal of < 50 kHz derived from the beating of the optical modes on a photo-detector, it is expected that the laser generates short optical pulses. Further investigations on pulse formation in this laser were carried out and are presented in the next subsection of this Chapter. They are based on the FROG technique explained above.

4.4.1   Investigation of pulses at the output of the QDash-MLLD

4.4.1.1   Experimental setup

The experimental setup to investigate the optical pulse generation based on a QDash-MLLD is depicted in Fig. 4.2. The measurements shown in this Chapter are performed on the QDash-MLLD in its unpackaged presentation, which is placed on a probe station, but similar results are expected for a packaged laser. The optical power of the QDash-MLLD is collected with a lensed fibre and coupled to an isolator (ISO) for suppressing back reflections from other elements of the setup which could disturb the operation of the investigated laser. This signal is amplified through (EDFA-1) and it can be either sent directly for analysis or, before that, be passed by an optical band-pass filter (OBPF-1, Santec OTF-950) centered at a wavelength of 1530 nm. The signal is split by a 50/50 optical coupler, where half of the power is amplified (EDFA-2) and optimized in polarisation (PC-1) then directed to the pulse analyser, frequency resolved optical gating (FROG, Southern Photonics HR 150). The EDFA-2 and PC-1 are components imposed by the FROG system. The other half of the power of the optical signal is photo-detected (PD, u^{2}t XPDV2020R), amplified with a low noise broadband RF amplifier (RF Amp) and frequency divided (FDIV, Centellax Div/4 TD40MCA) from 40 GHz to 10 GHz in order to use this 10 GHz signal as the electrical trigger for the optical sampling oscilloscope (OSO-Picosolve,

PSO-101) offering a 0.83 ps temporal resolution. The signal emitted by the QDash-MLLD is then visualised with the OSO-Picosolve and further analysed with the FROG. Neither technique relies on the synchronisation of the QDash laser to an external source. This means that the measurements presented have been carried out in free running and have not been distorted by an external signal applied to the device.
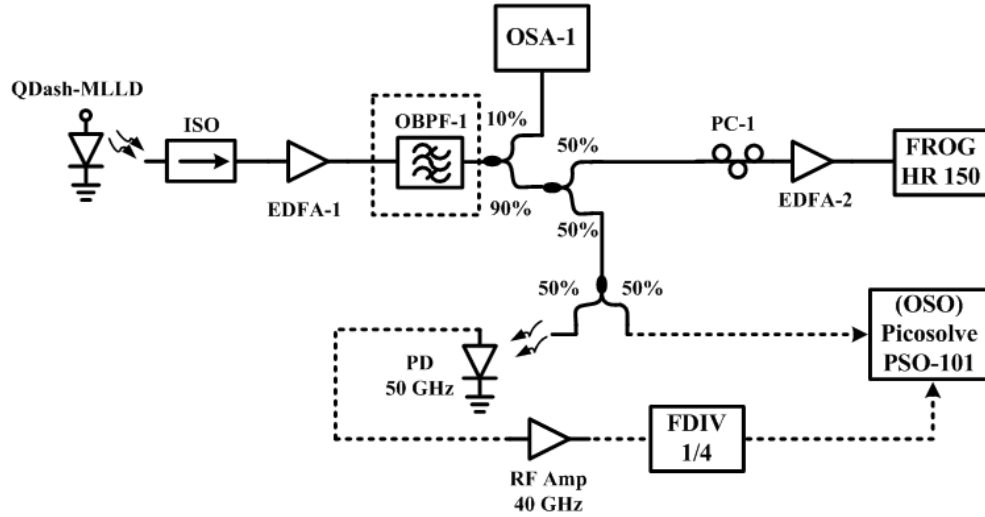
Figure 4.2: Experimental setup for the analysis of the output of the QDash-MLDD under DC-bias condition. Temperature is stabilised at 25 °C. QDash-MLLD: quantum dash mode-locked laser diode; ISO: optical isolator; EDFA: erbium-doped fibre amplifier; OBPF: optical band pass filter; OSA: optical spectrum analyser; PC: polarisation controller; PD: photo-detector; FDIV: frequency divider; FROG: frequency resolved optical gating; OSO-Picosolve: optical sampling oscilloscope (See appendix A for equipment specifications).

4.4.1.2   Analysis

Firstly, the signal transmitted by the QDash-MLLD without any filtering stage is analysed. Fig. 4.3(a) shows the eye diagram of the output of the QDash-MLLD obtained with the OSO-Picosolve, when the device is DC-biased at 350 mA and controlled in temperature at 25 °C. Pulses are retrieved with a repetition rate of 39.8 GHz. It is not possible to have precise quantitative measurements from this temporal trace due to two main factors: the temporal resolution of the OSO-Picosolve is close to the expected pulse duration (below 1 ps); and its sensitivity to the quality of the trigger, as it is not at 40 GHz, but one quarter of it (10 GHz) [15]. However, it can be observed that the rising edge of the pulses is shorter than the trailing edge. Also, the trailing edge might present some features. The peak power is of 6 mW.

Further investigation has been carried out with the FROG system. Fig. 4.3(b) presents the results. The black trace shows the temporal intensity versus time delay in picoseconds for the

characterised pulses featuring a pulse width of 2.6 ps, comparable to that measured with the limitation of the optical sampling oscilloscope. In addition, a feature can be observed beside the main pulse which looks like a secondary pulse, which can be attributed to the chirping of the pulses generated by the QDash-MLLD. The blue trace presents the chirp of the pulse generated. It confirms the positive chirped pulse at the QDash-MLLD output.
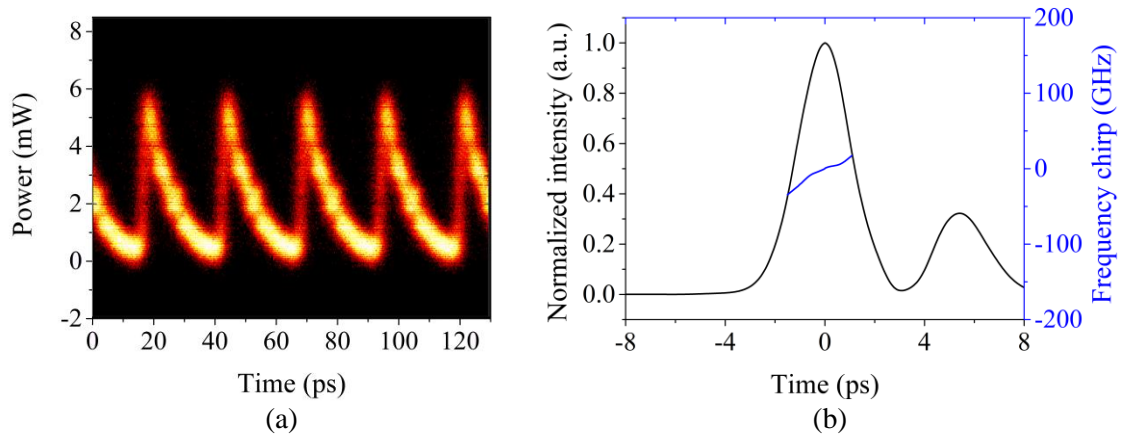
Figure 4.3: Pulse traces at the output of the QDash-MLLD retrieved with: (a) optical sampling oscilloscope; (b) frequency resolved optical gating.

Secondly, the analysis of the pulses at the output of the QDash-MLLD is carried out after filtering of the optical spectrum with a 1 nm bandwidth filter. A trace of the pulse retrieved with the FROG system is shown in Fig. 4.4. A pulse duration of 6 ps is measured and the positive chirp is still present. The positive slope associated with the pulses emitted by the QDash-MLLD results in an interesting feature since it allows the introduction of a simple compression scheme based on group velocity dispersion in a standard single-mode fibre. This fact will be exploited in the following Section for pulse compression in order to achieve shorter pulse generation. This result is taken from a more extensive analysis on the dependence of the pulse duration with respect to the bandwidth of the filters performed in the Radio and Optical Communications Laboratory research group at Dublin City University [15], [27]. From those results it was demonstrated that the pulse duration varies inversely proportional to the spectral bandwidth.
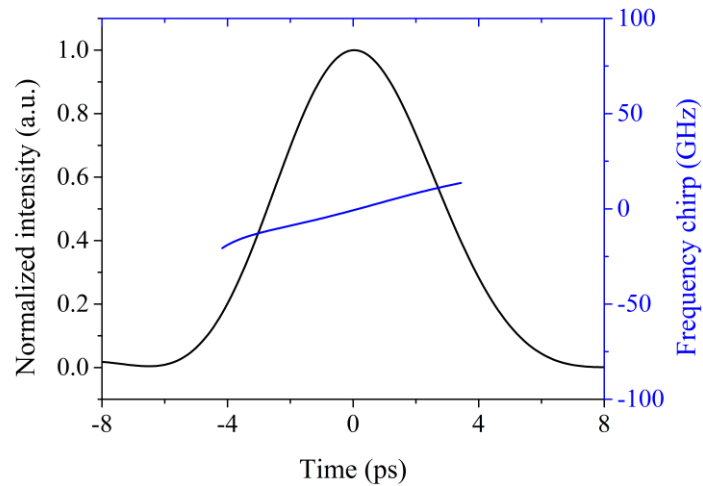
Figure 4.4: Optical pulses generated from the QDash-MLLD and resolved with the FROG system after optical spectrum filtering with 1 nm bandwidth.

4.4.2 Generation of pulses at the output of the QDash-MLLD with a compression scheme

4.4.2.1   Experimental setup

Following the results obtained in previous Section, where the pulses generated at the output of the QDash-MLLD exhibited a positive chirp, it is worth investigating the changes in their pulse duration by adding a passive element, in this case, a single-mode fibre (SMF) [27],[28]. The standard SMF operates in anomalous dispersion regime for wavelengths around 1530 nm. This property allows compensating such positive chirp exhibited by the pulses when combined with a proper fibre length.

In order to investigate the pulse compression, 450 m of SMF was added to the setup shown in Fig. 4.2 to obtain the configuration depicted in Fig. 4.5. The 450 m of SMF used in this experiment was the only fibre available in the Radio and Optical Communications Laboratory at Dublin City University to almost flatten the chirp shape.
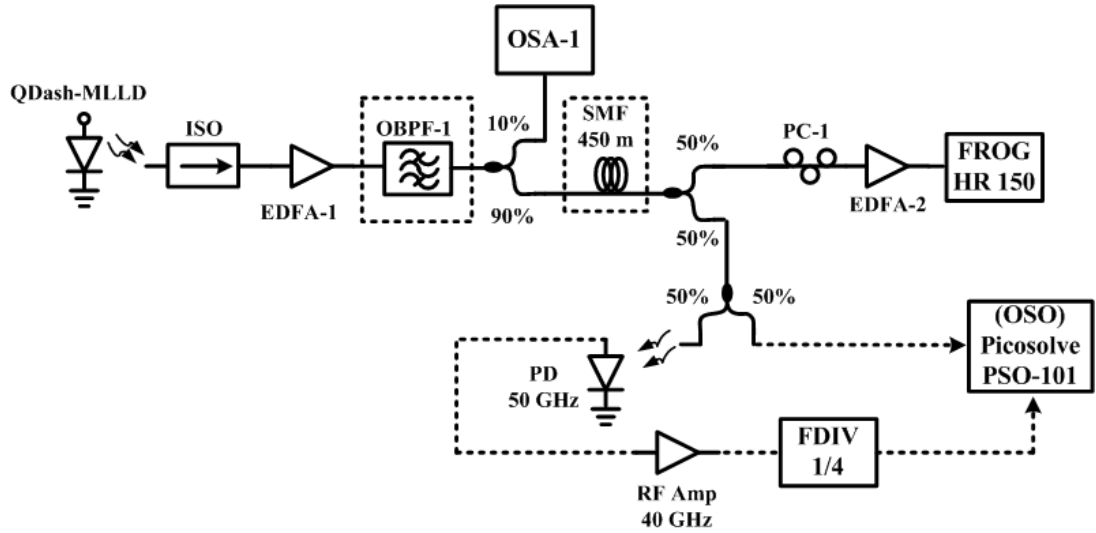
Figure 4.5: Experimental setup for the analysis of the output of the QDash-MLDD under DC-bias conditions. Temperature is stabilised at 25 °C. The 450 m of SMF is introduced for chirp compensation.

4.4.2.2 Analysis

The pulses are first visualised with the optical sampling oscilloscope (OSO-Picosolve); the corresponding trace is shown in Fig. 4.6(a). However, owing to the two drawbacks mentioned in previous Section regarding the OSO-Picosolve, the trace does not allow obtaining more accurate details on the pulse characteristics, but it provides a view of such pulses. The pulses present a reduction in their pulse width and an increase in the peak power from 6 mW to 18 mW, while remaining at a frequency of 39.8 GHz. Fig. 4.6(b) shows the FROG traces of intensity and chirp. It is confirmed the reduction in the pulse width when compared to Fig. 4.3(b), the pulse width is now approximately 720 fs. The chirp trace reveals that the length of SMF utilised is still not the optimum but the pulse has been compressed.
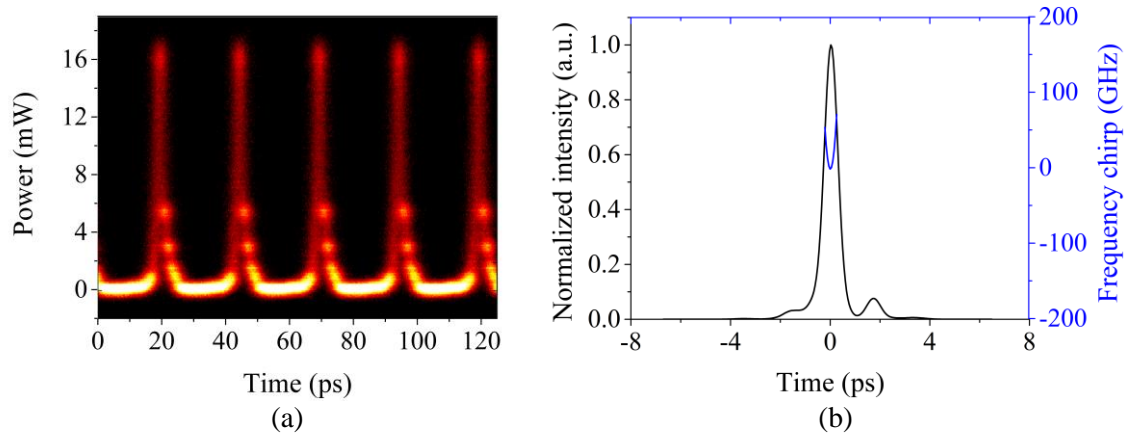
Figure 4.6: Pulse traces at the output of the QDash-MLLD after the introduction of 450 m of SMF and retrieved with: (a) optical sampling oscilloscope; (b) frequency resolved optical gating.

Fig. 4.7 depicts the FROG traces of intensity and chirp versus time delay for the pulses generated by the QDash-MLLD when the optical spectrum is filtered with a 1 nm filter bandwidth and the inclusion of 450 m of SMF. The intensity versus time trace reveals the expected reduction in the pulse width compared with the trace shown in Fig. 4.4, but it is wider than the trace shown in Fig. 4.6(b) which was obtained without any filtering stage. However, the chirp is now negative but not fully flat, confirming that the length of the SMF utilised is not optimal. Chirp changes on the pulses associated to optical spectral filtering of the QDash-MLLD when compared to the non-filtering case can be expected depending on the number of modes filtered out and the way in which they are transmitted through the filter. The length of 450 m SMF was picked as is the shortest length of fibre available in the Radio and Optical Communications Laboratory research group at Dublin City University. A proper length of optical fibre would retrieve a flat chirp trace, indicating no chirping in the pulses generated.
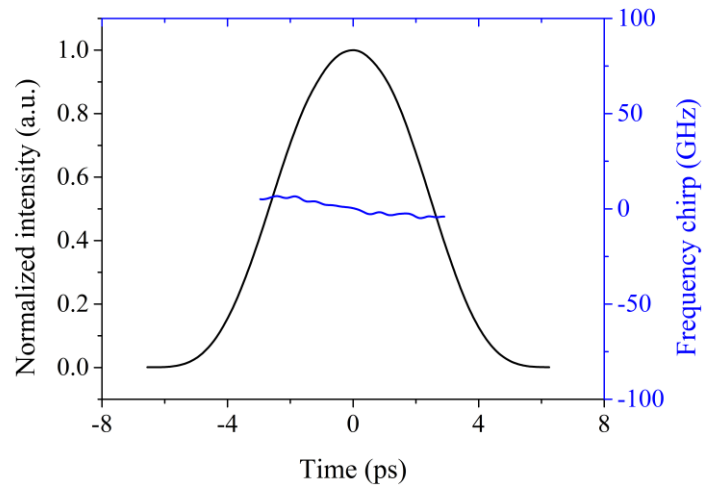
Figure 4.7: Optical pulses generated from the QDash-MLLD and resolved with the FROG system after optical spectrum filtering with 1 nm bandwidth and the introduction of 450 m of SMF.

A more detail analysis on the dependence of the pulse duration with respect to the bandwidth of the filters with or without inclusion of 450 m of SMF was performed in the Radio and Optical Communications Laboratory research group at Dublin City University and can be consulted in the following references [15],[27]. From those results it was demonstrated that the pulse duration varies inversely proportional to the spectral bandwidth and that the introduction of the piece of fibre helped to compensate for the initial positive chirp of the pulses emitted by the passively QDash-MLLD, as a consequence achieving the generation of shorter pulses.

4.4.2.3   Analysis of the timing jitter in free running

Furthermore, the width of the optical pulses produced by the passively QDash-MLLD, as well as the associated timing jitter (both of them retrieved from the FROG system), are shown in Fig. 4.8 as a function of the DC-bias current applied to the device, with no filtering of the optical spectrum but including the 450 m of SMF. For this experiment, the QDash-MLLD does not require any optical or electrical signal applied to it. In other words, the QDash-MLLD operates in free running and the timing jitter measured with this technique does not require any trigger signal that would affect the measurements. In the case of the timing jitter, it is calculated by considering the intensity auto- and cross-correlation traces obtained from the FROG system according to the equation

$$\tau_j = (\tau_p / \tau_{ac})\sqrt{\tau^2_{cc} - \tau^2_{ac}} \qquad (4.3)$$

where τ_{ac} and τ_{cc} are the full-width at half maximum (FWHM) of the auto- and cross-correlation pulses, respectively. As can be observed in Fig. 4.8, the pulse width (τ_p) and associated timing jitter (τ_j) present a decreasing trend with the DC-bias. The slight increments of timing jitter for bias currents between 300 and 350 mA can be associated to the large differences in phase noise among the optical modes which are visualised from the optical mode linewidth measurements presented in Chapter 3, Fig. 3.7. The magnitude of such differences in the optical mode linewidth is proportional to the slopes of the traces; a bigger slope for a bias current of 350 mA is present when compared to the optical linewidth measurements for the other bias currents.

The most widely used method for measuring the timing jitter is by the frequency domain technique, which is based in the utilisation of the Von der Linde method [29], which consists of integrating the single sideband phase noise spectral density around the frequency carrier measured on an RF spectrum analyser over a range of frequencies. Usually, this can be directly done by using spectrum analysers capable of performing the integration of the single side band phase noise by only capturing the RF beating signal from the optical signal to analyse. For this experiment we did not rely on such apparatus, but instead implemented a time domain approach for measuring the timing jitter, which is quantitatively comparable to the frequency domain technique. Its advantage is that it requires neither an extremely fast photo-detector nor a so-called timing jitter analyser. For instance, the τ_j associated with the widest measured pulse (τ_p =1.6 ps, obtained at 150 mA) is above 350 fs, associated to the shortest pulse (τ_p=720 fs, obtained in the range from 300 to 450 mA) is ~150 fs. This low value of timing jitter confirms the QDash-MLLD as a source of stable optical pulses. Furthermore, as it has been mentioned in this and the previous Chapter, if the QDash-MLLD is synchronised by an external optical signal, it would provide a quality clock signal. Notice that even though the 25 kHz mode-beating linewidth of the QDash-MLLD is inferior with respect to the narrowest linewidth obtained in free running conditions from a 4-mm-long two-section passively mode-locked QD device at 10 GHz with saturable absorber section [30], its performance is comparable in terms of the timing jitter (minimum of 150 fs with respect to 147 fs reported in [30]). The timing jitter evaluated in the referred reference was made by using the Von der Linde method, integrating the single sideband phase noise spectral density around the 10 GHz carrier measured on an RF spectrum analyser over the 4 MHz to 80 MHz frequency range. The setup is comparable to the one shown in previous Section, since the optical output of the QDash laser is coupled via a single-mode lensed fibre to an angled connector and directed to the RF spectrum analyser [30]. On the other hand, considering a collected power of 4 mW at the QDash-MLLD output with

τ_p = 2.2 ps at 40 GHz, a peak power of 40 mW is estimated, while for compressed pulses with τ_p= 720 fs, the peak power is ~140 mW.
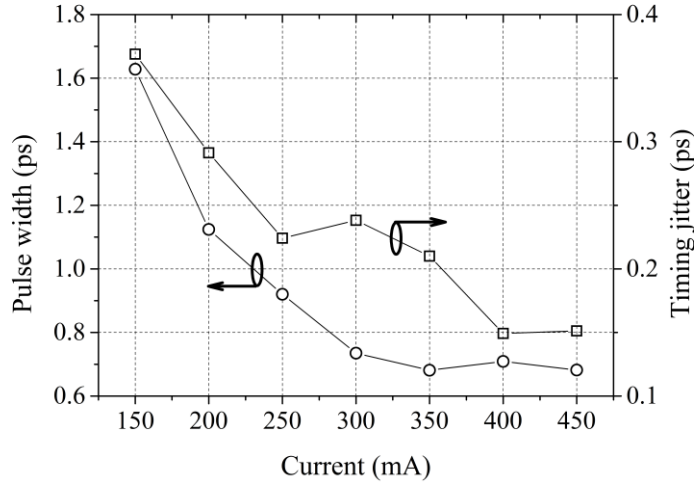
Figure 4.8: Pulse width (○) and timing jitter (□) associated to the optically generated pulses in terms of the DC-bias current supplied to the QDash-MLLD.

4.5 Multiplexing of pulses from a quantum dash mode-locked laser

In the previous Section, the generation of pulses from the passively mode-locked QDash laser diode was investigated. It was found that it is possible to obtain short pulses in the order of femtoseconds (below 800 fs). This fact along with the mode-locking theory provided in Chapters 1 and 2, encourage the investigation of pulse generation when the device is synchronised to a train of optical pulses with or without data. As a first approach, in this Section the synchronisation of the QDash-MLLD to a train of pulses at 10 GHz generated by a mode-locked laser source is studied. This synchronisation will allow the generation of very stable 40 GHz pulses at the QDash-MLLD output which can be used as a pulse source not only at that frequency but at higher frequencies after using a time multiplexing technique.

4.5.1 Experimental setup to generate pulses at high frequency from a synchronised QDash-MLLD

The setup to examine the generation of pulses at a rate up to 160 GHz from a synchronised QDash-MLLD is depicted in Fig. 4.9. It consists of a u^2t tunable mode-locked laser (TMLL) with central wavelength at 1552 nm and actively mode-locked with a 10 GHz clock signal from a RF generator (Yokogawa AP9945). This signal also triggers the OSO-Picosolve (PSO-101). Fig. 4.10 shows the optical spectrum and temporal (eye diagram) traces of the TMLL output signal taken with an optical spectrum analyser (OSA, Apex AP2443B) set at resolution bandwidth (RBW) of 20 MHz and an optical sampling oscilloscope (OSO-Picosolve) with resolution of 0.83 ps, respectively. The pulses at the output of the TMLL are passed through an isolator (ISO) to avoid back reflections, amplified with an Erbium doped amplifier (EDFA-1) and injected into the QDash-MLLD by using a circulator with an optical power of 3 dBm. The QDash-MLLD is DC-biased at 110 mA and stabilised in temperature to 25 °C.
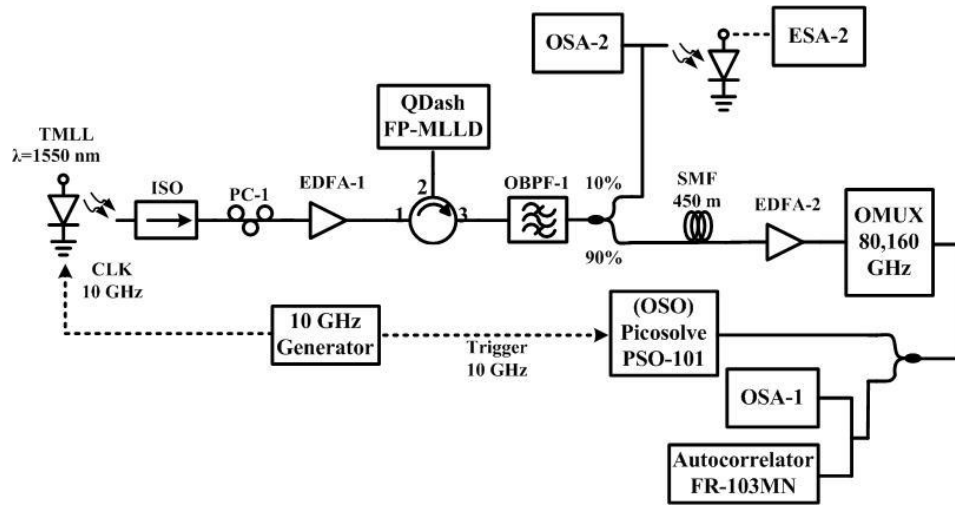
Figure 4.9: Experimental setup to generate pulses at up to 160 GHz: TMLL: tunable mode-locked laser; ISO: optical isolator; EDFA: erbium-doped fibre amplifier; QDash-FP-MLLD: quantum dash Fabry-Pérot laser diode; OBPF: optical band pass filter; OSA: optical spectrum analyser; ESA: electrical spectrum analyser; PC: polarisation controller; SMF: single-mode fibre; OMUX: optical multiplexer; FROG: frequency resolved optical gating; OSO-Picosolve: optical sampling oscilloscope (See appendix A for equipment specifications).
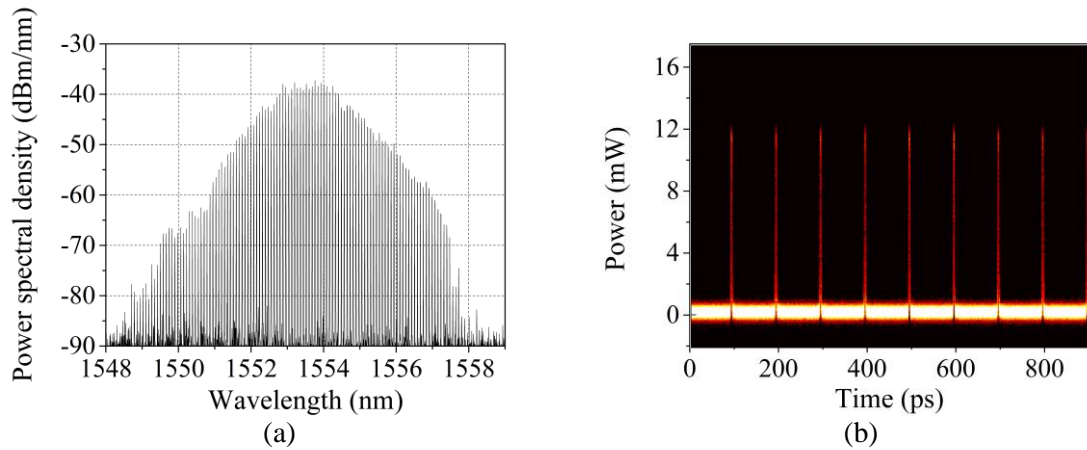
Figure 4.10: u²t tunable mode-locked laser emitting at 10 GHz: (a) optical spectrum taken with RBW of 20 MHz (b) temporal trace with resolution of 0.83 ps.

At the output of the QDash-MLLD, a 6 nm optical band-pass filter (OBPF-1, Alnair Labs BVF-200) centered at 1530 nm, is utilised to suppress both the spontaneous emission from EDFA-1 and the synchronising injected signal. At the output of the OBPF-1, 10% of the power is used for analysis and monitoring of the synchronised signal. Fig. 4.11 presents the optical spectrum and eye diagram of the synchronised QDash-MLLD taken with resolutions of 0.02 nm (OSA-1, Yokogawa AQ 6370) and 0.83 ps, respectively. The optical spectrum trace (Fig. 4.11(a)) shows a nearly flat shape with 20 longitudinal modes separated by approximately 0.33 nm, equivalent to ~40 GHz, which is confirmed by the eye diagram in Fig. 4.11(b) where the pulses have a temporal separation of 25 ps and which features an optical signal-to-noise-ratio (SNR) of 15 dB. The variation in the amplitude of the temporal traces visualised with the optical sampling oscilloscope is due to the trigger signal of 10 GHz from the pulse generator which is not the ideal 40 GHz for the detected signal.
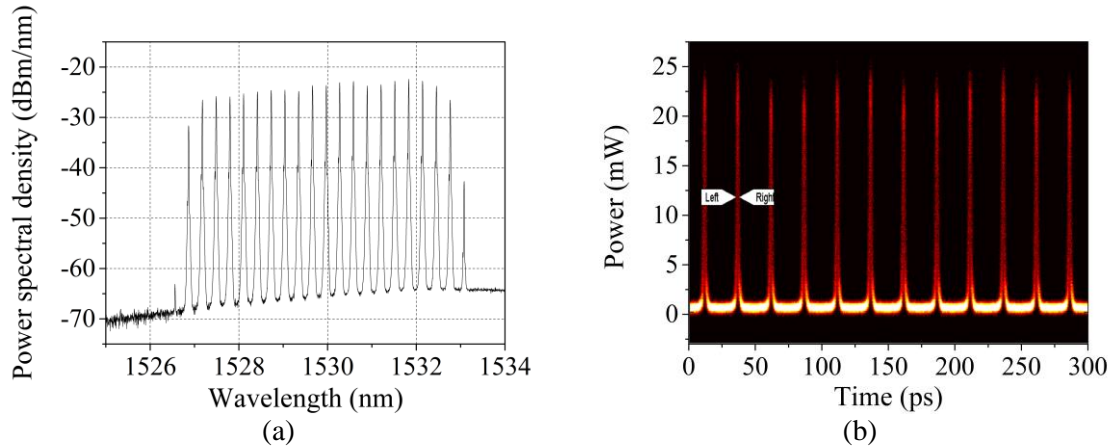
Figure 4.11: Synchronised QDash-MLLD emitting at 40 GHz: (a) optical spectrum taken with RBW of 0.02 nm (b) temporal trace with resolution of 0.83 ps.

The remaining 90% of the optical power emitted by the QDash-MLLD is sent to the 450 m of SMF for pulse compression. It is amplified and passed into a two-stage optical time multiplexer (OMUX, Calmar Optcom BRM-T-16), which allows for the generation of pulses at repetition rates of 80 and 160 GHz. The pulses are visualised with the OSO-Picosolve, the OSA (Yokogawa AQ 6370) and an auto-correlator (Femtochrome Research FR-103MN).

4.5.2 Analysis

Fig. 4.12(a) presents the optical spectrum of the filtered QDash-MLLD after the first multiplexing stage measured within a span of 9 nm and resolution of 0.02 nm. Clearly, the main longitudinal modes have a peak power-to-noise ratio of 10 dB and a separation of 0.66 nm, corresponding to approximately 80 GHz. Ideally, a better time multiplexing process should retrieve a peak-power-to-noise ratio of at least 30 dB. Using the OSO-Picosolve it is possible to visualise and to record the time domain trace of the pulses provided by the QDash-MLLD. The eye diagram shown in Fig. 4.12(b) confirms the frequency of the pulses provided by the QDash-MLLD as the pulse separation is 12.5 ps, and features a SNR of 8 dB. Owing to the low temporal resolution of the OSO-Picosolve (0.83 ps), the trigger of 10 GHz from the generator and the low peak-power-to-noise ratio on the multiplexed pulses, it is not possible to obtain any further information on these pulses from Fig. 4.12(b). However, after averaging the optical pulses retrieved from the OSO-Picosolve and calculating their Fast Fourier Transform, it is verified that the pulses present a fundamental frequency component at the expected 80 GHz, as depicted in Fig. 4.12(c).
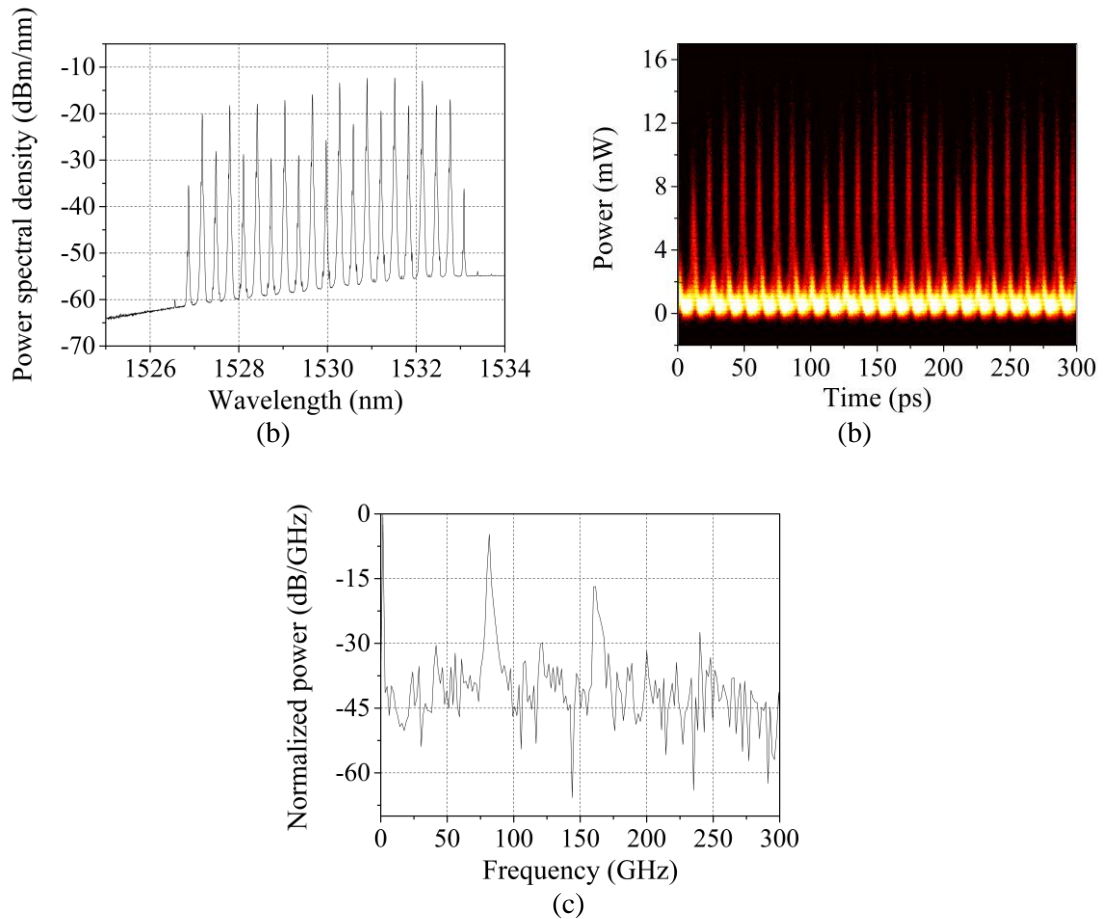
Figure 4.12: Generated pulses at 80 GHz, after the first time multiplexing stage: (a) optical spectrum taken with RBW of 0.02 nm, (b) temporal trace with resolution of 0.83 ps, (c) RF spectrum.

A similar analysis is performed on the pulses generated after a second time multiplexing stage. In this case, the generated pulses are at a frequency of 160 GHz, which can be corroborated from Fig. 4.13. The optical spectrum (shown in Fig. 4.13(a)) of the resulting signal is measured within a span of 9 nm and resolution of 0.02 nm. From this trace can be distinguished five main longitudinal modes with a peak power-to-noise ratio of 10 dB and a separation of 1.32 nm, corresponding to approximately 160 GHz. Using the OSO-Picosolve, it is still possible to visualise and to record the time-domain trace of the pulses provided by the QDash-MLLD. The eye diagram shown in Fig. 4.13(b) provides a view of the multiplexed pulses with a separation of 6.25 ps which feature a signal-to-noise-ratio of 6 dB. The increase in the power of these pulses when compared to Fig. 4.12(b) is only due to an increment in the input power at the optical input port of the OSO-Picosolve. After calculating the Fast Fourier Transform of the pulses displayed on the OSO-Picosolve, it is confirmed that the pulse train presents a main frequency component at the expected 160 GHz, as shown in Fig. 4.13(c).
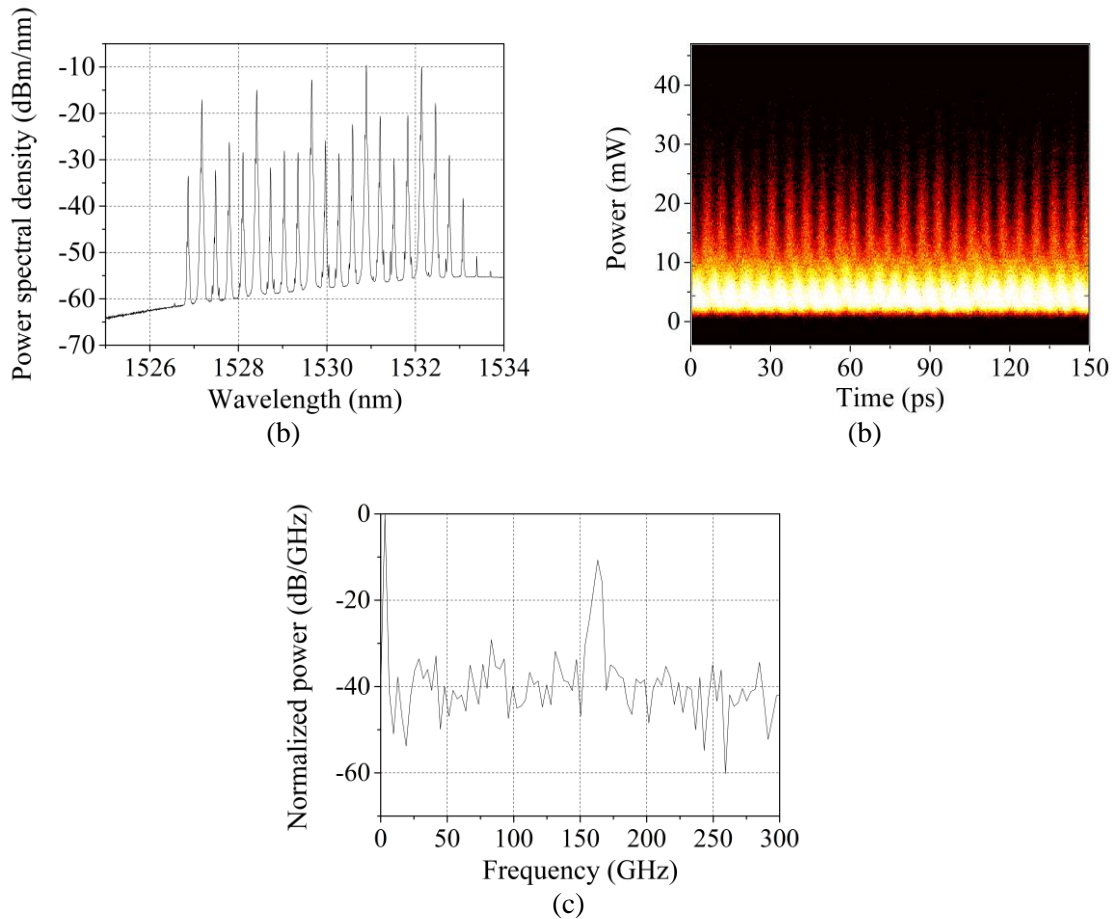
Figure 4.13: Generated pulses at 160 GHz, after the second time multiplexing stage: (a) optical spectrum taken with RBW of 0.02 nm, (b) temporal trace with resolution of 0.83 ps, (c) RF spectrum.

Unfortunately, for the experiments corresponding to subsection 4.5.1, it was not possible to analyse the pulses with the FROG system, but a conventional auto-correlator was used, retrieving only the pulse width values. The time domain multiplexed pulses exhibit a FWHM of 1.8 ps irrespective of the pulse repetition rate after a passive compression scheme based on the reduction of the pulses' chirp by the chromatic dispersion in a standard single-mode fibre [15], [31].

The sub-picosecond pulse generation at up to 160 GHz from a QDash-MLLD and multiplexing stage shows evidence for the potential of using this device for applications in OTDM systems. It should be possible to obtain pulses with this kind of device at higher frequencies, determined by the cavity length of the laser [16], [17] as well as by manipulating the optical longitudinal mode separation with a wave shaper [32].

4.6 Multi-pulse synchronisation of quantum dash mode-locked laser

The demonstration of the synchronisation of the QDash-MLLD to a train of pulses at 10 GHz shown in Section 4.5 indicates the possibility of achieving synchronisation not only to pulses at higher frequencies but also to data signals. These can give rise to an application of the device to perform all-optical clock recovery of OTDM signals at high speed [33]. Therefore, in this Section, synchronisation of the QDash-MLLD to pulses from 10 up to 160 GHz is investigated.

4.6.1 Experimental setup

The experimental setup to assess the performance of the QDash-MLLD under synchronization with pulses at high frequency is illustrated in Fig. 4.14. Again the u^{2}t TMLL at a central wavelength of 1550 nm, driven by an electrical clock from a pattern generator (PPG, Yokogawa AP9945), is used to generate a train of optical pulses at a 10 GHz repetition rate. The 10 GHz pulses are amplified and directed to the OMUX (Calmar Optcom BRM-T-16) where pulse sequences at 20, 40, 80, and 160 GHz are obtained. An optical bandpass filter (OBPF-1) set at ~1550 nm with 6 nm bandwidth suppresses part of the amplified spontaneous emission of the amplification modules (EDFA-1 and EDFA-2). Pulses at various repetition rates are then injected into the QDash-MLLD through an optical circulator.
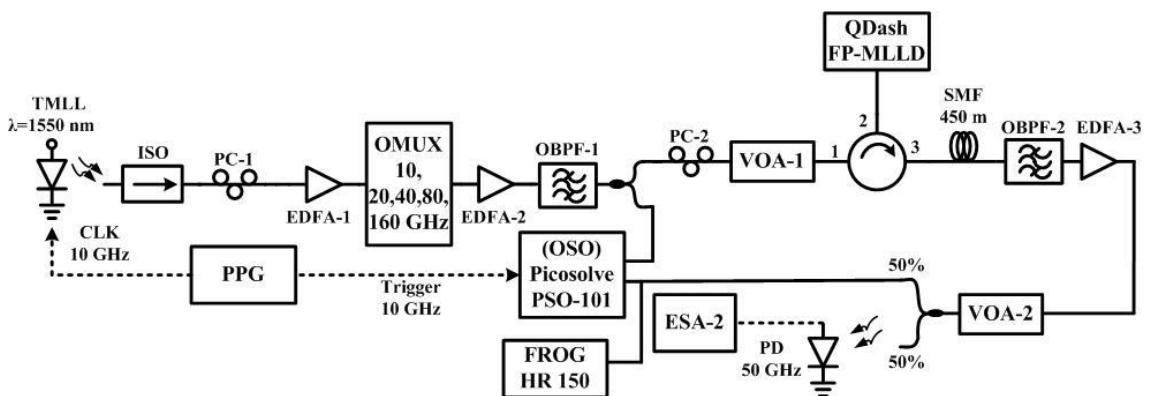
Figure 4.14: Experimental setup for sub-harmonic and harmonic pulse synchronisation: TMLL: tunable mode-locked laser; ISO: optical isolator; PC: polarisation controller; EDFA: erbium-doped fibre amplifier; OMUX: optical multiplexer; OBPF: optical band pass filter; VOA: variable optical attenuator; QDash-FP-MLLD: quantum dash Fabry-Pérot laser diode; PPG: pulse pattern generator; ESA: electrical spectrum analyser; PD: photo-detector; SMF: single-mode fibre; FROG: frequency resolved optical gating; OSO-Picosolve: optical sampling oscilloscope (See appendix A for equipment specifications).

54

Eye diagrams of the generated multiplexed pulses to be injected into the QDash-MLLD at frequencies of 10 GHz, 20 GHz, 40 GHz, 80 GHz and 160 GHz are shown in Figs. 4.15(a)-4.15(e), respectively. The pulses are resolved by the optical sampling scope (note that injected signals in Figs. 4.15(d) (for 80 GHz) and 4.15(e) (for 160 GHz) appear less discrete due to the 0.83 ps resolution of the OSO-Picosolve). The spectral components of the generated pulses at 20, 40, 80, and 160 GHz have been minimized below their corresponding fundamental frequency by optimizing the operational conditions of the OMUX in terms of delay and optical power balance between the time domain multiplexed pulses. Intensity (black trace) and chirp (blue trace) of the multiplexed pulses at frequencies of 10, 20, 40, 80, and 160 GHz are also resolved by the FROG system (Southern Photonics HR 150), as it is shown in Figs. 4.15(f)-4.15(j). The pulses feature a FHWM pulse width of 1.6 ps, independent of the pulse frequency. In addition, from the same figures, it is possible to see that they present negative chirp. The complex phase (chirp in the frequency domain) dependence of the input signals is due to the presence of a saturable absorber in the TMLL cavity [34].
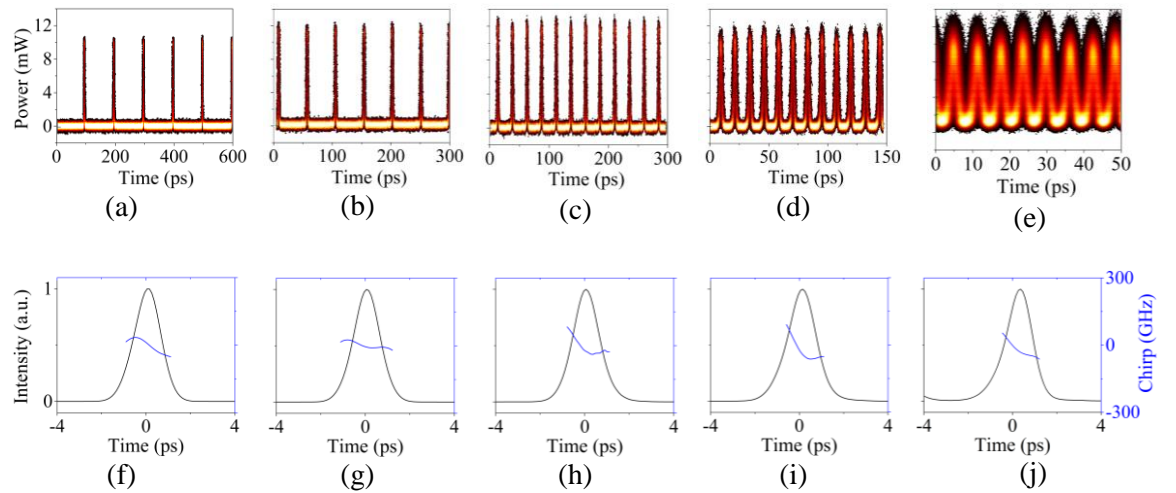
Figure 4.15: Pulses generated at 10, 20, 40, 80, and 160 GHz: (a)–(e) Eye diagrams, resolved by the optical sampling scope; and (f)–(j) intensity versus time and chirp versus time delay traces, resolved by the FROG system.

4.6.2 Analysis of the pulses generated by the QDash-MLLD after synchronisation

The synchronisation of the QDash-MLLD resulting from the injection of the pulses at 10, 20, 40, 80 and 160 GHz is found to be sustained for injected optical powers between +6 and +10 dBm, measured by the variable optical attenuator (VOA-1), along with a fine tuning of their

state of polarisation. The QDash-MLLD is operated at 90 mA and stabilised in temperature at 25 °C. Synchronised recovered optical pulses from the QDash-MLLD are isolated from injected signals by the OBPF-2 set at ~1530 nm with a 6 nm bandwidth. The pulses are passively compressed by a 450 m single-mode fibre [34]. The synchronisation is firstly analysed with the ESA-2 (Anritsu MS2668C), previously carrying out the photo-detection (u^2t XPDV2020R) of the optical signal. Fig. 4.16 depicts the RF spectra of the QDash-MLLD in free running and in synchronisation by pulses at 40 GHz, taken with a span of 40 MHz and resolution of 10 MHz. A shift in the central frequency and a significant increase in the FWHM are observed on the 40 GHz beat-tone signal when there is no external signal applied (free running), passing from ~ 30 kHz (free running) to less than 10 Hz under synchronisation, irrespective of the frequency of the pulse injected into the laser as long as its harmonic frequency coincides with 40 GHz.
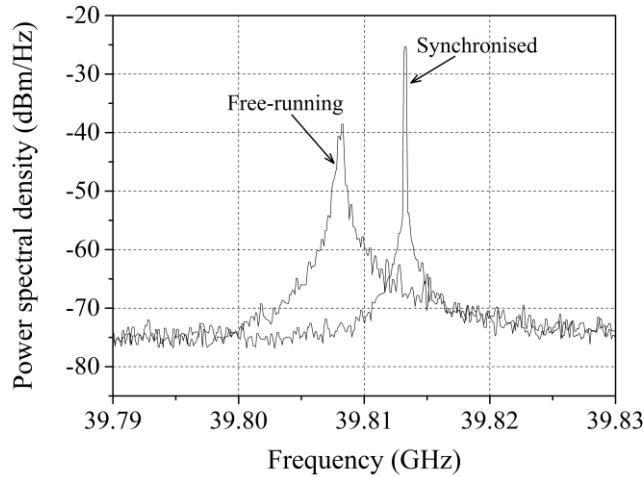
Figure 4.16: Comparison of the RF spectra of the QDash-MLLD in free running and synchronisation.

Moreover, the optical sampling oscilloscope (OSO-Picosolve) featuring a resolution of ~0.83 ps is used as a visual aid to monitor the QDash-MLLD operation under external optical synchronisation. No eye diagrams are retrieved from the OSO in the absence of external locking of the QDash-MLLD because the trigger signal from PPG is not synchronised with the free-running frequency of the laser. Fig. 4.17(a) shows the eye diagram of the recovered pulses from the QDash-MLLD under pulse synchronisation. This trace allows verifying the pulse generation with a pulse separation of ~ 25 ps corresponding to ~ 40 GHz. In addition, the Fast Fourier Transform of such a trace results in a characteristic Sinc-like shape, featuring a fundamental component at 40 GHz, as shown in Fig. 4.17(b). The power spectral density of components at 10 and 20 GHz is negligible, more than 40 dB below the main component, which implies that

injected frequencies at 10 and 20 GHz do not create any amplitude modulation in the active locking process achieved by the injection of pulses at 10 and 20 GHz [34].

(a)   (b)
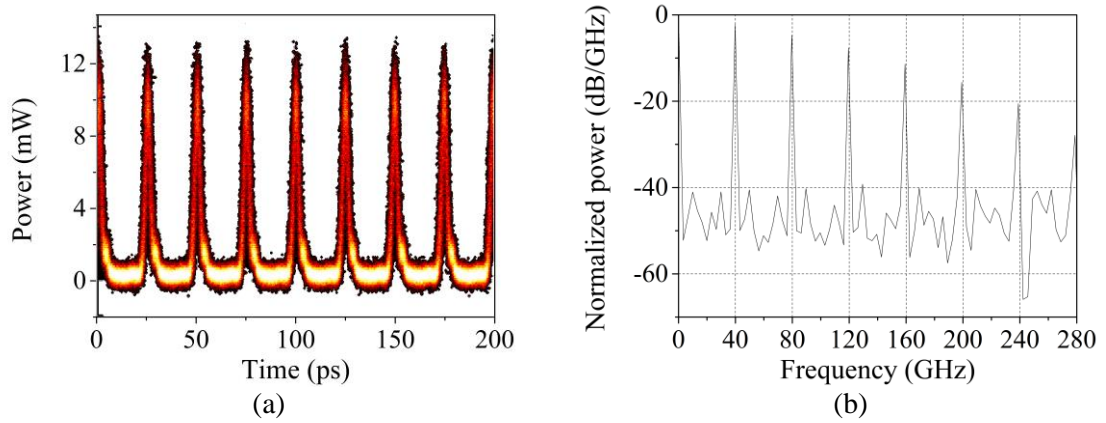
Figure 4.17: Recovered clock pulses at ~ 40 GHz, resolved by the optical sampling oscilloscope: (a) eye diagram; (b) frequency components after Fast Fourier Transform calculation.

Similarly to the input pulses, an analysis of the recovered optical pulses is performed with the FROG system [22]. Shown in the temporal traces in Figs. 4.18(a)-4.18(e) are recovered clock pulses at 40 GHz after synchronisation from pulses at 10, 20, 40, 80 and 160 GHz, respectively. They exhibit a FWHM of ~1.8 ps and nearly linear chirp regardless of their repetition rate. Time domain characteristics of the recovered clock pulses remain unchanged despite the shape and phase (or chirp) variations of the input pulses, (see Figs. 4.15(f)-4.15(j)). In addition, a maximum timing jitter of 0.4 ps is estimated for recovered clock pulses by implementing the method described in Subsection 4.4.2.3 [35].

(a)   (b)   (c)   (d)   (e)
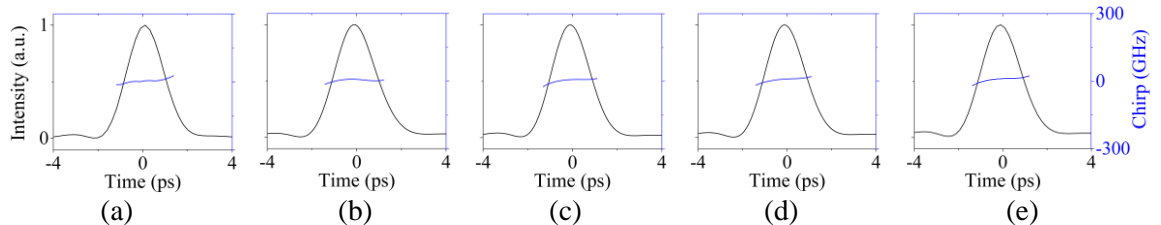
Figure 4.18: Intensity versus time delay and chirp versus time delay traces, resolved by the FROG system, of recovered clock pulses from injection of pulses at: (a) 10 GHz, (b) 20 GHz, (c) 40 GHz, (d) 80 GHz (e) 160 GHz.

The optical injection at sub-harmonic and fundamental frequencies to achieve synchronisation of the QDash-MLLD laser can be explained with help of Fig. 4.19. Since the input signals as well as the intrinsic output signal generated by the QDash-MLLD are trains of pulses and not perfect sinusoidal functions, they present a part of their fundamental frequency, some components at higher harmonic and sub-harmonic frequencies, as depicted in Fig. 4.19, for input train of pulses at 10, 20 and 160 GHz (in color) and 40 GHz from the QDash-MLLD (in black). In the case of input signals at lower frequency than the fundamental frequency of the QDash-MLLD (40 GHz), their higher harmonic components interact with the fundamental component of the QDash-MLLD, as shown in the figure for input signals at 10 and 20 GHz. When the input signal has a higher frequency than the fundamental frequency of the QDash-MLLD, the interaction occurs between the fundamental component of this input signal and a higher harmonic frequency component of the QDash-MLLD (inherent from the presence of the other longitudinal modes originated in the laser cavity) as illustrated in Fig. 4.19 for the case of an input signal at 160 GHz. The interactions of those frequency components between the input and QDash-MLLD signals achieve the synchronisation. As a consequence, the phase correlation of the longitudinal modes of the laser is improved, resulting in an enhancement in the stability of the pulses generated by the QDash-MLLD as reflected in their low timing jitter.
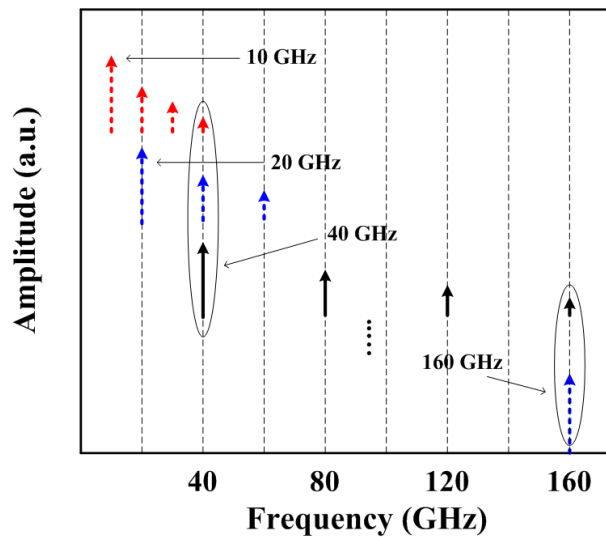
Figure 4.19: Schematic representation of the QDash-MLLD synchronisation by higher and sub-harmonic frequency components from the input signals.

The demonstration of the synchronisation of the QDash-MLLD with a resultant generation of optical narrow pulses with low values of timing jitter is a first step towards the demonstration of all-optical clock recovery from data signals. Such a study will be presented in Chapters 5 and 6.

4.7   Summary

In this chapter a study on the generation of optical pulses by a QDash-MLLD has been performed. Firstly, an overview of the pulse generation and measurement techniques was presented in Sections 4.2 and 4.3. In Section 4.4 the generation of pulses from the passively QDash-MLLD with a positive chirp was demonstrated. This positive chirp on the pulses is exploited to achieve pulse compression by using anomalous dispersion of SMF. In theory, the proper length of SMF should cancel out the chirp of the MLLD. It is possible to achieve pulses as short as 720 fs and featuring a low timing jitter of less than 200 fs even though the laser is DC-biased with no modulation applied. Following this study, in Section 4.5 the use of the QDash-MLLD as a pulse generator at frequencies of up to 160 GHz with the aid of a time multiplexing system has been demonstrated. The obtained pulses feature a FWHM of 1.8 ps irrespective of the repetition rate, after being passively compressed with 450 m of SMF.

Finally in Section 4.6, the demonstration of the synchronisation of the QDash-MLLD from pulses at 10, 20, 40, 80 and 160 GHz was carried out. As a result of the synchronization, the recovered optical pulses exhibit a FWHM of ~1.8 ps and nearly linear chirp regardless of the repetition rate of the injected pulses and with low values of timing jitter (0.4 ps). The linewidth of the RF synchronised signal is less than the resolution of the ESA. The MLLD can be understood as an oscillator with a Q-factor of 5 billion. The synchronisation of the QDash-MLLD can give rise to a real application of the device to perform all-optical clock recovery of OTDM signals at high speed, as will be demonstrated in Chapters 5 and 6.

References

[1]   K. Merghem, A. Akrout, A. Martinez, F. Lelarge, B. Rousseau, F. Poingt, L. Legouezigou, O. Legouezigou, A. Accard, F. Pommereau, G.-H. Duan, G. Aubin, A. Ramdane, "Subpicosecond pulse generation at 245 GHz using a quantum-dash passive mode-loked laser emitting at 1.53 μm," *Lasers and Electro-optics, 2008 and 2008 Conference on Quantum Electronics and Laser Science. CLEO/QELS 2008. Conference on*, paper CThP2, pp. 1-2, May 2008.

[2]   F. Lelarge, B. Dagens, J. Renaudier, R. Brenot, A. Accard, F. van Dijk, D. Make, O. Le Gouezigou, J.-G. Provost, F. Poingt, J. Landreau, O. Drisse, E. Derouin, B. Rousseau, F. Pommereau, and G.-H. Duan, "Recent advances on InAs/InP quantum dash based semiconductor lasers and optical amplifiers operating at 1.55 m," *IEEE Journal of Selected Topics Quantum Electronics*, vol. 13, no. 1, pp. 111–124, Jan./Feb. 2007.

[3]   A. Shen, J.-G. Provost, A. Akrout, B. Rousseau, F. Lelarge, O. Legouezigou, F. Pommereau, F. Poingt, L. Legouezigou, G.-H. Duan, and A. Ramdane, "Low confinement factor quantum dash (QD) mode-locked Fabry-Perot (FP) laser diode for tunable pulse generation," *in Optical Fiber Communication/National fiber Optic Engineers Conference, 2008. OFC/NFOEC 2008. Conference on,* pp. 1-3, Feb. 2008.

[4]   A. Akrout, K. Merghem, J.P. Tourrenc, A. Martinez, A. Shen, F. Lelarge, G.-H. Duan, and A. Ramdane, "Generation of 10 GHz optical pulses with very low timing jitter using one section passively mode locked quantum dash based lasers operating at 1.55 μm," *in Optical Fiber Communication/National fiber Optic Engineers Conference, 2009. OFC/NFOEC 2009. Conference on,* Paper JThA30, pp. 1-3, Mar. 2009.

[5]   C. Rulliere, *Femtosecond laser pulses, principles of experiments*, 2nd ed., USA: Springer, 2003.

[6]   O. Svelto, *Principles of lasers*, 4th ed., ISBN:0-306-45748-2, pp: 330-343, USA: Plenum Press,1998.

[7]   Yariv, Amnon, *Quantum Electronics,* 3rd ed*.,* USA: John Wiley & Sons, 1975.

[8]   R. A. Griffin, D.A. Jackson, and D.D. Sampson, "Coherence and noise properties of gain-switched Fabry-Perot semiconductor lasers," *IEEE Journal of Selected topics in Quantum Electronics*, vol. 1, no. 2, pp. 569-576, Jun. 1995.

[9]   H. Ito, H. Yokoyama, S. Murata, and H. Inaba, "Generation of picosecond optical pulses with highly RF modulated AlGaAs DH laser," *IEEE Journal of Quantum Electronics,* vol. QE-17, no. 5 pp. 663-670, May 1981.

[10]   P. Paulus, R. Langenhorst, and D. Jäger, "Generation and optimum control of picosecond optical pulses from gain-switched semiconductor lasers," *IEEE Journal of Quantum Electronics*, vol. 24, no. 8, pp. 1519-1523, Aug. 1988.

[11]   G.J. Aspin, and J.E. Carroll, "Gain-switched pulse generation with semiconductor lasers," *IEE Proceedings, Solid-State and Electron Devices*, vol. 129, no. 6, pp. 283-290, Dec. 1982.

[12]   R.W. Waynant, M. N. Ediger, *Electro-optics Handbook*, 2nd ed., p. 9.4, USA: Mc-Graw Hill, 2000.

[13]   L.P. Barry, P. Anandarajah, and A. Kaszubowska, "Optical pulse generation at frequencies up to 20 GHz using external-injection seeding of a gain-switched commercial Fabry-Perot laser," *IEEE Photonics Technology Letters*, vol. 13, no. 9, pp. 1014-1016, Sep. 2001.

[14]   L. P. Barry, P. Anandarajah, and A. Kaszubowska, "High frequency, wavelength-tunable pulse generation using a gain-swicthed commercial Fabry-perot laser with strong external-injection," *Lasers and Electro-Optics Society, 2000, LEOS 2000. 13th Annual Meeting, IEEE.*, vol. 2, pp. 587-588, paper WV5.

[15]   S. Latkowski, R. Maldonado-Basilio, and P. Landais, "Sub-picosecond pulse generation by 40-GHz passively mode-locked quantum-dash 1-mm-long Fabry-Prot laser diode," *Optics Express*, vol. 17, no. 21, pp. 19166–19172, Oct. 2009.

[16]   K. Merghem, A. Akrout, A. Martinez, G. Aubin, A. Ramdane, F. Lelarge, and G. Duan, "Pulse generation at 346 GHz using a passively mode locked quantumdash- based laser at 1.55 μm," *Applied Physics Letters*, vol. 94, pp. 021107–3, Jan. 2009.

[17]   M. Xia, C.H. Kwok, M.G. Thompson, R. V. Penty, I.H. White, F.van Dijk, A.F. Lelarge, and G.-H. Duan, "270 GHz, 580 fs optical pulse generation from a single-section quantum-dash Fabry-Perot laser using frequency multiplication," *Lasers and Electro-optics, 2009 and 2009 Conference on Quantum Electronics and Laser Science. CLEO/QELS 2009. Conference on*, Paper JThE15, PP. 1-2, Jun. 2009.

[18]   Y.-C. Xin, D.J. Kane, and L.F. Lester, "Frequency-resolved optical gating characterisation of passively modelocked quantum-dot laser," *Electronics Letters*, vol. 44, no. 21, pp. 1255-1257, Oct. 2008

[19]   S. Latkowski, R. Maldonado-Basilio, and P. Landais, "Short pulse generation with 40 GHz passively-mode locked Q-dash Fabry-Perot laser," *in Transparent Optical Networks,*

2009. ICTON 2009. 11ᵗʰ International Conference on. pp. 1-4. Jul. 2009.

[20]   F. Träger, *Handbook of lasers and optics*, USA, New York: Springer, 2007.

[21]   H. Iijima, R. Hajima, E.J. Minehara, R. Nagai, and N. Nishimori, "Development of frequency-resolved optical gating for measurement of correlation between time and frequency of chirped FEL," *Proceedings of FEL 2006*, Bessy, Berlin, Germany. Paper TUPPH002, pp. 308-311.

[22]   R. Trebino, K.W. DeLong, D.N. Fittinghoff, J.N. Sweetser, M.A. Krumbügel, B.A. Richman, and D.J. Kane, "Measuring ultrashort laser pulses in the time-frequency domain using frequency-resolved optical gating," *Review Scientific Instruments*, vol. 68, no. 9, Sep. 1997, pp. 3277-3295, Reviewed article.

[23]   K.W. DeLong, R. Trebino, J. Hunter, and W.E. White, "Frequency-resolved optical gating with the use of second-harmonic generation," *Journal of the Optical Society of America B*, vol. 11, no.11, pp. 2206-2215, Nov. 1994.

[24]   R. Trebino, and D.J. Kane, "Using phase retrieval to measure the intensity and phase of ultrashort pulses: frequency-resolved optical gating," *Journal of the Optical Society of America A.*, vol. 10, no. 5, pp. 1101-1111, May 1993

[25]   L. Xu, E. Zeek and R. Trebino, "Measuring very complex ultrashort pulses using Frequency resolved optical gating (FROG)," *Lasers and Electro-optics, 2008 and 2008 Conference on Quantum Electronics and Laser Science. CLEO/QELS 2008. Conference on*, Paper CThK2, pp. 1-2, May 2008.

[26]   D.J. Kane, and R. Trebino, "Single-shot measurement of the intensity and phase of an arbitrary ultrashort pulse by using frequency-resolved optical gating," *Optics Letters*, vol. 18, no. 10, pp. 823-825, May 15.

[27]   S. Latkowski, "*Radio frequency and terahertz signals generated by passively mode-locked semiconductor lasers*," Dublin City University, Thesis, 2010

[28]   G. P. Agrawal, *Nonlinear fiber optics,* Academic Press, 2007.

[29]   D. von der Linde, "Characterization of the noise in continuously operating mode-locked lasers," *Applied Physics B*, vol. 39, pp. 201-217, Apr. 1986.

[30]   G. Carpintero, M. G. Thompson, R. V. Penty, and I. H. White, "Sub-kHz RF Electrical linewidth from a 10 GHz passively mode-locked quantum-dot laser diode," *in Conference on Lasers and Electro-Optics/ International Quantum Electronics Conference, OSA Technical Digest (CD) (Optical Society of America, 2009)*, paper CMK2, pp. 1-2, Jun. 2009.

[31] R. Maldonado-Basilio, S. Latkowski, and P. Landais, "320 GHz time-domain multiplexed pulses from quantum-dash mode-locked semiconductor laser diodes," *Lasers and Electro-Optics Europe (CLEO EUROPE/EQEC 2011), Conference on, and12th European Quantum Electronics Conference*, p.1, May. 2011.

[32] M. Costa e Silva, A. Lagrost, L. Bramerie, M. Gay, P. Besnard, M. Joindot, J. C. Simon, A. Shen, and G. H. Duan, "Up to 427 GHz all optical frequency down-conversion clock recovery based on quantum-dash Fabry-Pérot mode-locked laser," *IEEE Journal of Ligthwave Technology,* vol. 29, no. 4, pp. 609–615, Feb. 2011.

[33] J. C. Cartledge, X. Tang, M. Yañez, A. Shen, A. Akrout, and G.-H. Duan, "All-optical clock recovery using a quantum-dash Fabry-Perot laser," *in Proceedings of IEEE Microwave Photonics Conference (MWP 2010) IEEE Topical Meeting on*, Paper TH3-1, pp. 201-204, Oct. 2010.

[34] R. Maldonado-Basilio, S. Latkowski, S. Philippe, and P. Landais, "Experimental investigation of harmonic and subharmonic synchronisation of 40 GHz mode-locked quantum-dash laser diodes," *Optics Letters*, pp. 1569- 1571, vol. 36, no. 9, May 2011.

[35] R. Maldonado-Basilio, J. Parra-Cetina, S. Latkowski, and P. Landais, "Timing jitter, optical, and mode-beating linewidths analysis on subpicosecond optical pulses generated by a quantum-dash passively modelocked semiconductor laser," *Optics Letters*, vol. 35, no. 8, pp. 1184-1186, Apr. 2010.

Chapter 5

All-optical clock recovery at 40 GHz from 40 Gb/s data streams

5.1 Introduction

As presented in Chapter 1, the possibility of developing all-optical functions for signal processing for future transparent networks is one of the main aims of many research laboratories in optical communications nowadays. Clock recovery is a key requirement for such all-optical signal processing at high speed. In a clock signal, the timing jitter is the most important parameter [1-4]. In addition, these all-optical networks are expected to support a variety of data formats and wavelengths in the C-band [5], [6]. Currently, the two standard data formats that are widely used are the return-to-zero (RZ) and non-return-to-zero (NRZ) formats. On one hand, NRZ presents a good option when looking for bandwidth efficiency, on the other hand RZ presents more tolerance to polarisation mode dispersion, inter-symbol interference and nonlinear effects. In an optical network, NRZ data format is commonly used in local area networks and RZ is employed where high data bit-rate is managed such as in between the nodes of the optical networks. The extraction of a clock signal from NRZ data is a difficult process due to the lack of a clock component in its spectrum [7-9]. Normally, to accomplish the all-optical clock recovery function from the NRZ data format a two-stage signal processing procedure is necessary [10-13].

There is a wide variety of methods to perform all-optical clock recovery [1], [2], [4-8], [11-17]. However, among the various techniques, the ones based on mode-locked semiconductor laser diodes (MLLD) have attracted significant attention because of their stable operation, cost effectiveness, low energy consumption and small size, holding possibilities for monolithic integration [18-21]. Among the different approaches of clock recovery with MLLDs, those based on quantum dot/dash (QDot/QDash) lasers have demonstrated good performance in terms of frequency stability and low timing jitter [21] because of their narrow spectral linewidth and small associated phase noise [21-23].

The assessment of clock-recovery operations based on mode-locked laser diodes can be performed either by re-modulating the recovered clock with the original data stream and then implementing bit error rate measurements, or by analysing the linewidth of the radio frequency (RF) beat-tone signals generated within the MLLD and then retrieving the root-mean-square (rms) timing jitter. In summary, the possibility to have a device capable of retrieving a quality all-optical clock signal insensitive to the data format is of great interest [24]. In this context, this Chapter presents the synchronisation of two QDash-MLLDs with the same features. One of the lasers is unpackaged which will be named QDash-MLLD-1 and another one is in a butterfly package which will be named as QDash-MLLD-2, subject to the injection of 40 Gb/s NRZ and RZ on-off keying (OOK) incoming data, respectively. The performance of the recovered clock is demonstrated over a large wavelength detuning between the data and recovered clock over the C-band. Furthermore, an application of the recovered clock from NRZ data signal is used to achieve re-timing, re-shaping and re-amplification (3-R) regeneration with data format conversion from NRZ to RZ.

5.2   All-optical clock recovery at 40 GHz based on a QDash-MLLD from 40 Gb/s NRZ data stream

5.2.1   Experimental setup

The experimental setup to investigate the clock recovery functionality based on a QDash-MLLD operating under injection of an optical NRZ-OOK data stream is illustrated in Fig. 5.1. It consists of three main parts: transmitter, clock recovery and detection stage. In the transmitter, a commercially available pulse pattern generator (PPG, Centellax TG1P4A) is utilised for producing a $(2^{31}-1)$ long pseudo random binary sequence (PRBS) in NRZ format at 40 Gb/s. The PRBS signal is applied onto an optical carrier obtained from a CW laser source (HP 8168F), whose wavelengths will be tuned from 1533 to 1556 nm, through a Mach-Zehnder modulator (MZM) and then amplified with an Erbium-doped fibre amplifier (EDFA-1). An optical band-pass filter (OBPF-1) centered at the data carrier wavelength suppresses part of the amplified spontaneous emission of EDFA-1. Data stream optical power (90 %) is injected into the QDash-MLLD-1 via an optical circulator and a lensed fibre whilst the remaining power is directed to the detection stage.

The incoming data signal is preconditioned with a polarisation controller (PC-2) and a variable optical attenuator (VOA-2). Electrical and optical spectra of the data injected to the QDash-MLLD (or equivalently at the output of OBPF-1) are illustrated in Figs. 5.2(a) and

5.2(b), respectively. Radio frequency spectrum is obtained after optical to electrical conversion and subtracting the accumulative noise added throughout the detection stage. It features components at 20 and 40 GHz inherent to the operation of the utilised PPG. However, they do not affect the quality of the NRZ wave forms, as illustrated in the optical spectrum depicted in Fig. 5.2(b). The QDash-MLLD is DC-biased at 102 mA and temperature stabilised at 25 ºC.
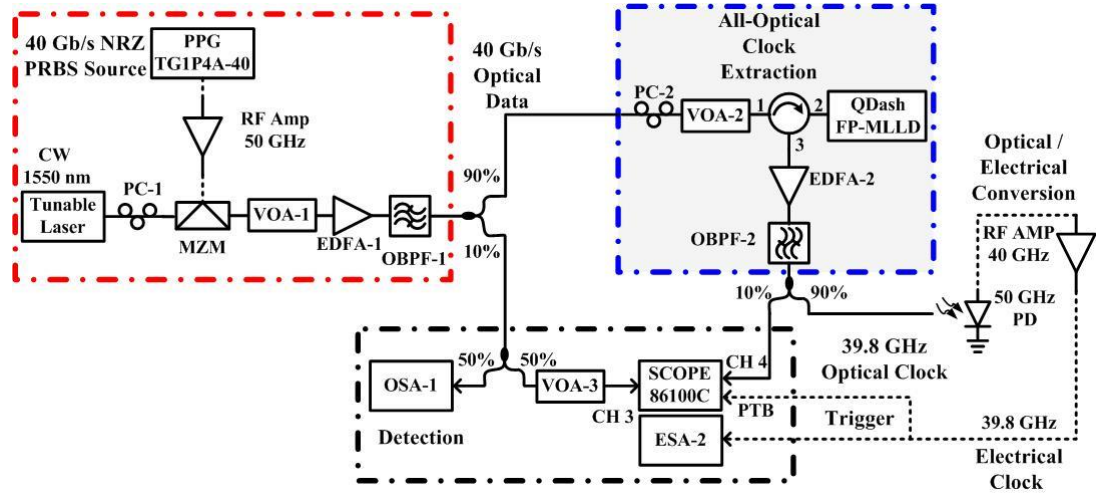
Figure 5.1: Experimental setup for the demonstration of all-optical clock recovery, based on a QDash-MLLD-1 subjected to an optical injection with a 40 Gb/s NRZ (2^{31}-1) long data stream: MZM: Mach-Zehnder modulator; PC: polarisation controller; EDFA: erbium-doped fibre amplifier; RF Amp: RF amplifier; OBPF: optical band pass filter; VOA: variable optical attenuator; QDash-FP-MLLD: quantum dash Fabry-Pérot mode-locked laser diode; PPG: pulse pattern generator; OSA: optical spectrum analyser; ESA: electrical spectrum analyser; PD: photo-detector; SCOPE: electrical sampling oscilloscope (See appendix A for equipment specifications).
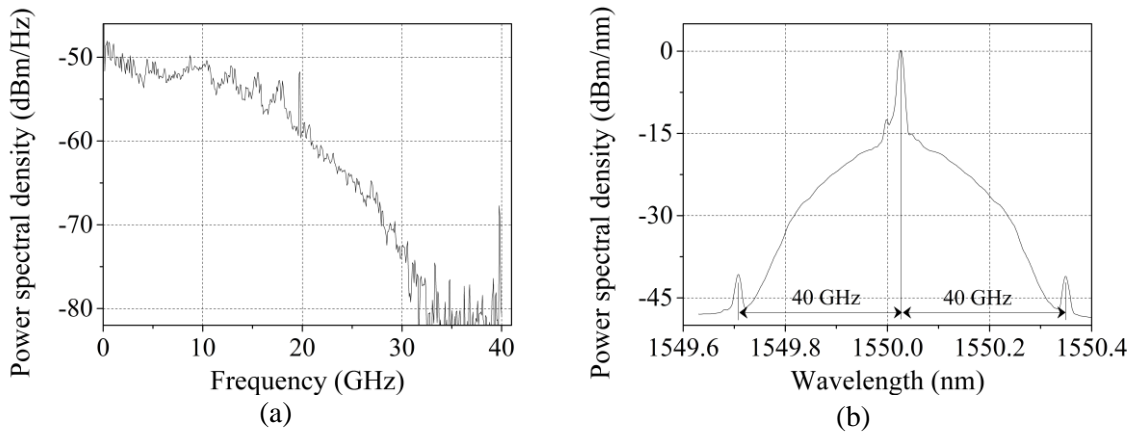
Figure 5.2: (a) Electrical and (b) optical spectra of the data signal injected into the QDash-MLLD.

The optical signal from the laser output at third port of the circulator is amplified with EDFA-2. The optical spectrum at the output of the locked QDash-MLLD is shown in Fig. 5.3(a), retrieved with an optical spectrum analyser (OSA-1, Yokogawa AQ 6370) set at a resolution of 0.02 nm. The figure shows the MLLD's emission centered at 1525 nm and the spectrum at 1550 nm due to the reflection of the injected optical signal at the input facet of the MLLD. The recovered optical clock is filtered out through OBPF-2. Such a filter has a Gaussian profile and is set with a central wavelength of 1530 nm (the minimum tunable wavelength achievable in this device) and a 3 dB bandwidth of 2 nm, which is utilised to spectrally isolate the recovered clock at the QDash-MLLD output from the reflected injected data stream. Fig. 5.3(b) illustrates this optical spectrum of the recovered clock. Inset depicts the time trace of the recovered clock retrieved by an equivalent-time electrical sampling oscilloscope (SCOPE, Agilent 86100C).
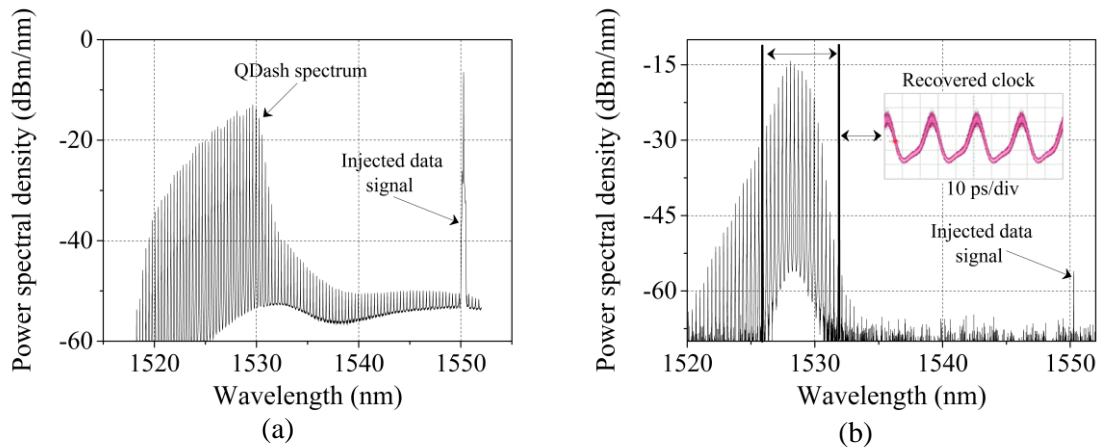
Figure 5.3: Optical spectra: (a) output of QDash-MLLD, before OBPF-2, (b) output of QDash-MLLD, after OBPF-2.

The optical clock is then converted to the electrical domain by using a 50 GHz photo-detector (PD, XPDV2020R) and a 40 GHz RF amplifier (RF-AMP). The electrical clock directed to the detection stage is analysed with an electrical spectrum analyser (ESA-2, Anritsu MS2668C) and used as a trigger signal for an electrical sampling oscilloscope (SCOPE, Agilent 86100C) with 40 GHz precision time base (PTB, Agilent 86107A). Fig. 5.4, depicts a comparison of the RF spectra of the beat-tone at the QDash-MLLD output when the laser is in free running (no injection of an optical signal) and in synchronisation (under injection of the NRZ-OOK data signal at a wavelength of 1550 nm). In Fig. 5.4 the reduction in the RF spectrum is visible when synchronisation is achieved. Further analysis is performed on this RF signal in the next

Section, as the RF beating linewidth is an important parameter to determine the quality of the clock signal [25].
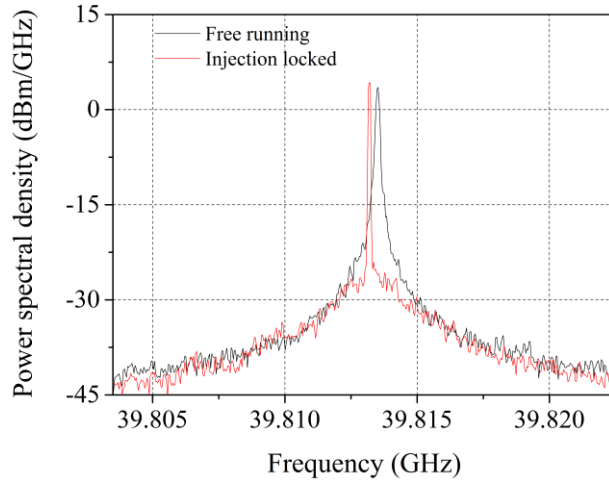
Figure 5.4: Comparison of the RF electrical spectra of beat-tones measured at the output of the QDash-MLLD, free running and injection locked. ESA is set at 20 MHz span and 30 kHz resolution bandwidth.

5.2.2 Analysis of results

The experiment is carried out by injecting a 40 Gb/s NRZ-OOK PRBS with pattern length of 2^{31}-1 signal into the QDash-MLLD at various carrier wavelengths whilst maintaining the same average power impinged onto the laser (kept at 12.7 dBm when measured at the second port of the circulator). Owing to the coupling efficiency measured as a ratio between the total emitted power and the power collected by the lensed fibre used in the system (for the same bias current and temperature conditions), injection coupling losses of at least 6.44 dB can be assumed. A fine tuning of the state of polarisation and average power of the injected data signal, as well as on the DC-bias current supplied to the QDash-MLLD allows for an optimized locking of the laser to the incoming data. As previously stated, the performance of the clock recovery operation, or in other words the locking/synchronisation of the QDash-MLLD under the injection of a 40 Gb/s NRZ data stream, is assessed by analysing the radio frequency beat-tone signals obtained at the laser output. For this analysis, the RF peak power-to-noise ratio (RF-PPNR) is defined as the difference in power in dBs between the peak power of the RF spectrum and the beginning of the pedestal of its noise level, measured directly from the ESA. The RF spectra of the ~ 40 GHz beat-tones are depicted in Figs 5.5(a) and 5.5(b) for injected data

streams whose carrier wavelengths are set at 1535 and 1550 nm, respectively. In these measurements, the ESA is set to a 20 MHz span and 30 kHz resolution bandwidth (RBW). As illustrated in Figs. 5.5(a) and 5.5(b), the noise contribution on the beat-tone signals changes with the wavelength of the injected data. As a consequence, the RF-PPNR varies with the carrier wavelength, changing from 40 to 31 dB for carriers at 1535 and 1550 nm, respectively. The reduction of the RF-PPNR with the increment of the wavelength of the input signal is due to the reduced interaction between the injected signal and the optical gain spectrum of the QDash-MLLD.
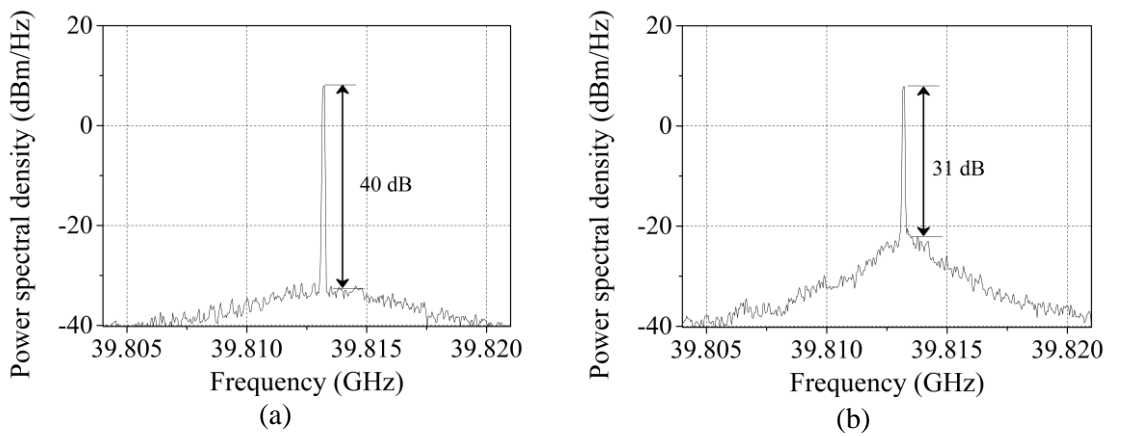
Figure 5.5: RF electrical spectra of beat tones measured at the output of the QDash-MLLD subject to the injection of data signals whose carrier wavelength are set to (a) 1535 nm and, (b) 1550 nm. The ESA is set to a 20 MHz span and 30 kHz RBW.

A complete set of experimental RF-PPNR measurements is shown in Fig. 5.6 for carrier wavelengths ranging from 1533 to 1556 nm. The term $\Delta\lambda$ is defined as the wavelength separation (in nm) of the carrier of the input signal and the optical spectrum of the QDash-MLLD at 1530 nm. At this point, it is important to stress that the synchronisation of the QDash-MLLD with NRZ data has been performed in spite of the lack of strong clock tones on the injected signals. Furthermore, a linewidth of ~ 8 Hz is measured when setting the ESA at a 600 Hz span and 10 Hz resolution bandwidth (maximum resolution achievable with the ESA utilised), regardless of the carrier wavelengths. This value of 8 Hz was obtained by measuring the linewidth at 10 dB down from the peak power of the RF beating signal retrieved with the ESA. The reduction of the beat-tone linewidth in comparison to that obtained when the QDash-MLLD is operating in passive mode-locking conditions is a signature of the good quality of the external locking process and therefore of the clock recovery operation [22], [25].

The Q-factor as defined in equation (3.2) is now equivalent to ~ 5 billion. This demonstrates the high quality of the laser as an RF resonator.
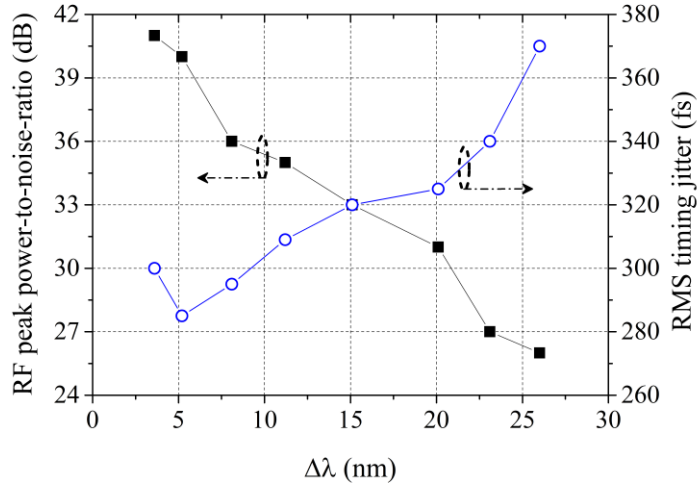
Figure 5.6: RF peak power-to-noise ratio of the ~ 40 GHz beat tones (solid squares) and timing jitter, measured directly with the scope (open circles), of the recovered clock signals in terms of the wavelength detuning between carrier and clock signals.

In regard to the characteristics of the recovered clock pulses, on average they feature a temporal width of 1.6 ps and a time-bandwidth product (TBP) of 0.61, irrespective of the wavelength detuning. This TBP value indicates that the clock pulses are not transformed limited and that they are chirped. As was mentioned in Chapter 4, this chirp can allow using a piece of SMF to compress the pulses. Considering a collected power of 1.6 mW and a repetition rate of 40 GHz, the recovered clock pulses exhibit a peak power of 25 mW. In addition, root mean square (rms) timing jitter ranging from 260 to 370 fs is measured with the time precision module of the electrical sampling oscilloscope. As depicted in Fig. 5.6, an increasing trend in the rms timing jitter is observed with the wavelength detuning resulting from a reduction in the RF-PPNR and an increment in the phase noise. These values of timing jitter on the recovered clock signals are lower (< 400 fs) when compared to the RMS timing jitter of the injected data signals which in average are 1.5 ps. The results obtained here on the evaluation of the wavelength tunability of the synchronised signal in terms of RF-PPNR and linewidth of the 40 GHz beat-tones as well as in the timing jitter demonstrate the good quality of the recovered optical clock pulses at the QDash-MLLD output [26]. Owing to these results, it can be concluded that the device is suitable to build up more all-optical functions, such as 2R or 3R regeneration or data format conversion from NRZ to RZ. This will be demonstrated in the next Section.

5.3 All-optical 3R regeneration and modulation format conversion from NRZ to RZ at 40 Gb/s

As regarded previously, clock recovery is an important element for developing all-optical functions. It can also give rise to the implementation of some other all-optical applications such as regeneration, from 2R (re-shaping and re-amplification) to 3R (re-timing, re-shaping and re-amplification) regeneration or even data format conversion. 2R and 3R data regeneration operations are key functions in the development of communication networks at high bit rate. In a 3R regenerator, a clock signal should be first recovered from the transmitted data signal, and then launched into the regenerator along with the original data to allow the signal to be reshaped, retimed and re-amplified. In addition, the recovered clock from a NRZ data signal can be used to realize all-optical data format conversion from NRZ to RZ in order to increase the network management flexibility in future transparent networks. In order to achieve data format conversion from NRZ to RZ, it is required first to recover a clock from NRZ data and then to perform an AND logic operation between the clock and the incoming NRZ data signals.

In this Section, the recovered clock pulses from NRZ data are utilised in the attempt to implement 3R regeneration. Furthermore, with the same scheme utilised for the 3R regeneration is also implemented a NRZ-to-RZ format conversion.

5.3.1 Experimental setup

The setup implemented for this study is depicted in Fig. 5.7, which is an extension of the setup shown in Fig. 5.1, in previous Section. The new blocks are displayed inside a blue-dashed box consisting of a semiconductor optical amplifier SOA (CIP SOA-XN-OEC-1550), an EDFA and an OBPF (Santec OTF-950) to achieve regeneration and data format conversion from NRZ to RZ. Firstly, the clock signal is extracted from a 40 Gb/s (2^{31}-1) long NRZ PRBS data signal using the QDash-MLLD-1. Then the recovered clock is processed along with data signal inside a semiconductor optical amplifier (SOA), carrying out the AND function followed by a filtering stage to finalise the implementation of the 3R (re-timing, re-shaping and re-amplification) regeneration.
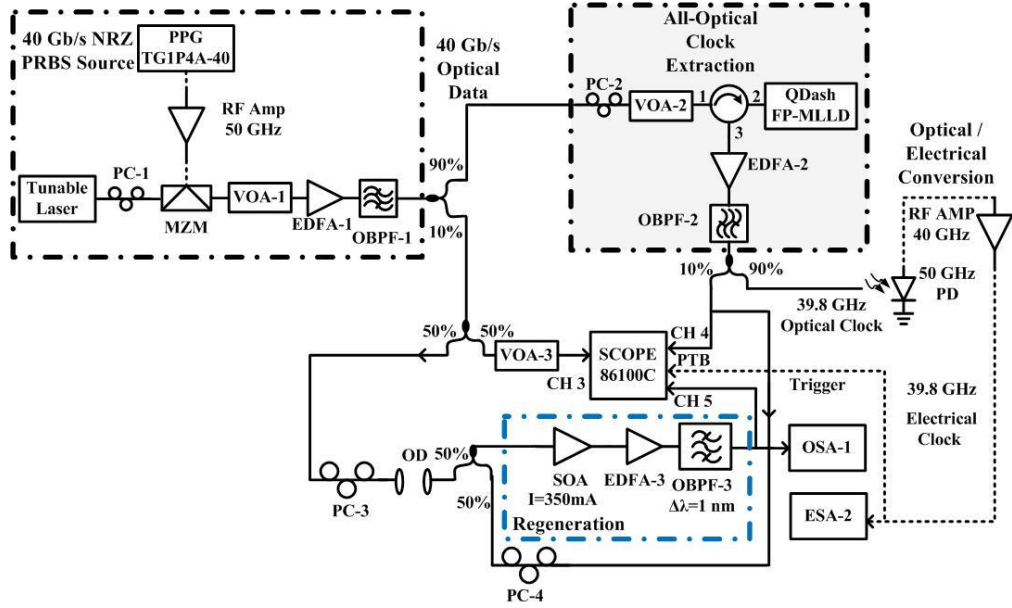
Figure 5.7: Experimental setup for the demonstration of all-optical 3R regeneration with NRZ-to-RZ data format conversion based on a SOA.

5.3.2 Analysis of results

The optical spectra and eye diagrams of the 40 Gb/s NRZ PRBS input signal at 1553.5 nm injected into the QDash-MLLD-1 for clock extraction and the corresponding recovered clock are shown in Figs. 5.8(a) and 5.8(b), respectively. The eye diagram of the input signal presents a 9 dB extinction ratio, and a signal-to-noise ratio (SNR) of 5.4 dB equivalent to a bit error rate of 3.5E-8. The features on this signal are due to the performance of the modulator utilised. Furthermore, owing to the features of the utilised equipment for generating the PRBS binary sequence, such a signal presents a minimum RMS timing jitter equal to 1.57 ps at 1553.5 nm. However, after its injection into the QDash-MLLD laser, the extracted clock presents a significant reduction of the timing jitter (0.73 ps) in comparison to that of the injected signal. As depicted in Fig. 5.9, this important feature is observed throughout the whole interval of the analysed data signal wavelengths, which ranges from 1533 to 1553.5 nm [27]. These values of timing jitter are measured with the electrical sampling oscilloscope (SCOPE, Agilent 86100C). The reduction of the timing jitter by the QDash-MLLD subject to optical injection in clock recovery has been demonstrated by analysis of the second-order filtering transfer function on these kinds of semiconductor lasers [21], [28]. In order to record these reported measurements, the optical sampling scope is triggered by the extracted clock (optical signal) after its distribution and conversion to an electrical signal.
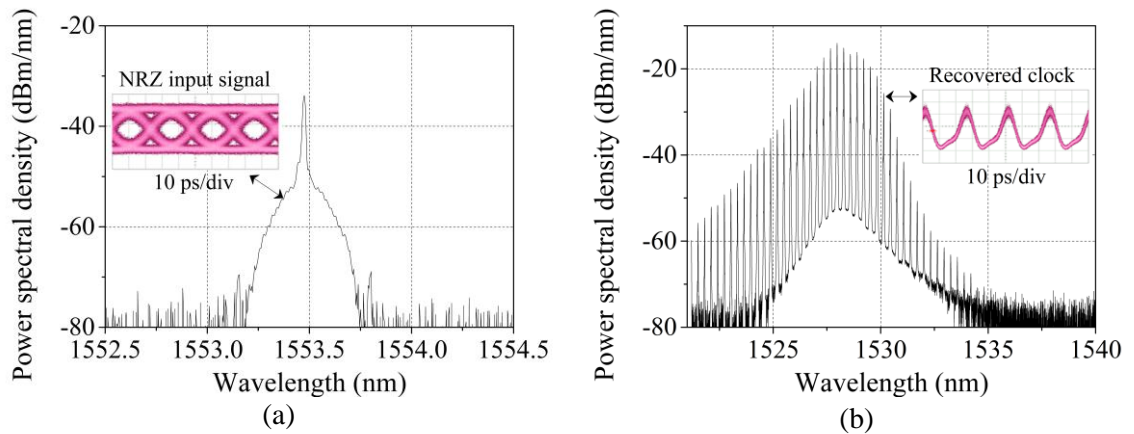
Figure 5.8: Optical spectra of the signals at the input of the regenerator block: (a) NRZ data signal at the SOA input, (b) recovered clock. Insets: corresponding eye diagrams, with horizontal and vertical scales at 10 ps/div and 500 µW/div, respectively.
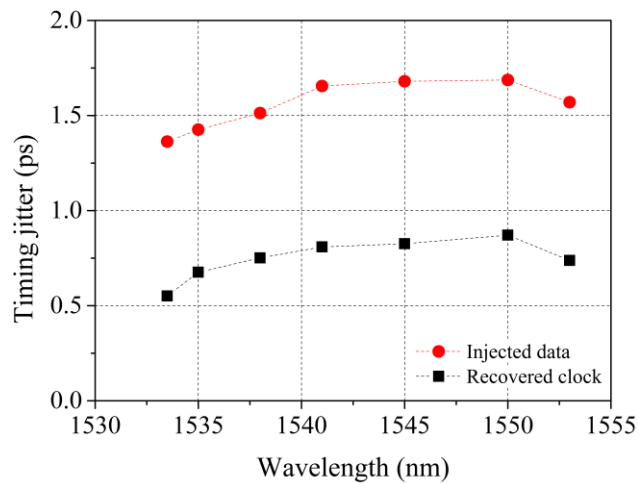
Figure 5.9: Timing jitter evolution of the recovered clock in comparison to that of the input data signal.

The recovered clock is amplified by using an EDFA and then passed through a 2 nm optical band-pass filter to reduce the excess of noise associated with the amplified spontaneous emission. The regenerating function is achieved by using cross-gain modulation (XGM) inside the SOA through the interaction of the extracted optical clock and data signal (already shown in Figs. 5.8(a) and 5.8(b)). The extracted clock power is larger than that of the data signal, functioning as the pump. This high power leads to the saturation of the amplifier during its high state. In order to retrieve the regenerated data signal, an optical square-shape band-pass filter with a 1 nm bandwidth is utilised at the SOA output. The quality of the regenerated data signal

is analysed through its eye diagram recorded after the optical band-pass filter. Figs. 5.10(a) and 5.10(b) illustrate the optical spectrum and eye diagram of the regenerated signal, respectively, when the filter is set at 1553.5 nm central wavelength. As depicted in Fig. 5.10(b) for a data signal at 1553.5 nm, a format conversion from NRZ to RZ is accomplished additionally after the regeneration stage. Moreover, a minimum SNR of 4.9 dB in the recovered signal is obtained for an input SNR of 5.4 dB. In the reported eye diagram of Fig. 5.10(b), the sampling scope is also triggered by the extracted clock (optical signal) after its conversion to an electrical signal. The detection stage formed mainly by a PD (XPDV2020R) and two RF amplifiers (not depicted in Fig. 5.7) when converting the optical recovered clock to electrical, is the main source of degradation in the output clock signal. However, it resembles a realistic scenario where the clock pulses are extracted from the incoming data signal at the receiver [29].
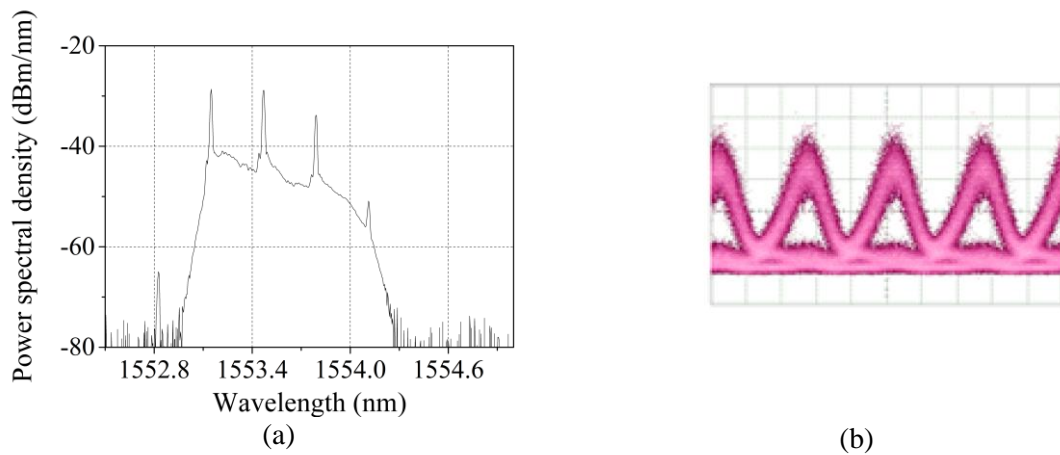
Figure 5.10: (a) Optical spectrum of the RZ data signal at the SOA output after passing through the band-pass filter, (b) eye diagram of the regenerated and data converted RZ PRBS data signal at a wavelength of 1553.5 nm. Horizontal and vertical scales are 10 ps/div and 500 μW/div, respectively.

A complete set of experimental results is presented in Fig. 5.11 for a carrier wavelength of data signal ranging from 1533 to 1553.5 nm. Note that the SNR of the regenerated signal follows a similar trend to that of the extracted clock (see Fig. 5.9) even though a corresponding degradation is observed [29]. This SNR degradation affects the performance of the 3R regenerator, in special as the re-shaping function displays a poor quality. A larger SNR degradation occurs as the data signal wavelength approaches the optical spectrum of the recovered clock. The deterioration in the SNR of the data converted signal is due to the interaction of four wave mixing (FWM) and XGM phenomena inside the SOA. FWM gets stronger as the two signals interacting inside the SOA approach one another for less than 5 nm;

this affects and reduces the XGM phenomenon from which the regenerated and converted signal is obtained.
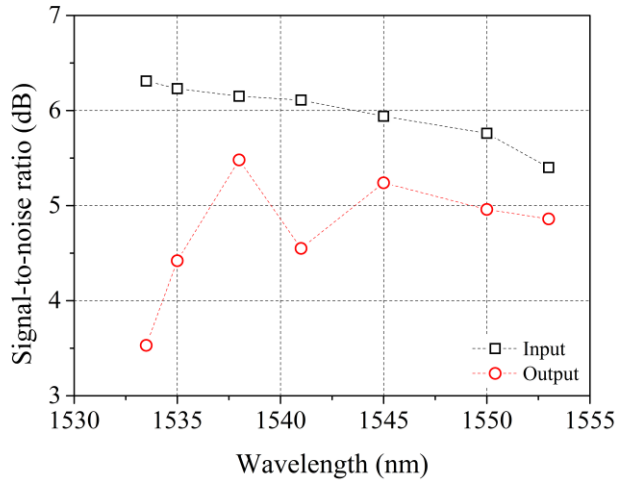
Figure 5.11: Signal to noise ratio of the data signal at the input and output of the 3R regenerator as a function of the carrier wavelength.

In this Section two all-optical functions were demonstrated, in one single experiment, using the recovered clock from an incoming NRZ data signal. They were 3R regeneration (re-timing, re-amplification and re-shaping, the latter one with poor quality) and data format conversion from NRZ to RZ. As has been already mentioned at the beginning of this Chapter, in order to demonstrate that the QDash-MLLD is a good candidate to develop real applications for all-optical signal processing such as clock recovery, it is important to demonstrate that the clock recovery functionality is insensitive to the data format. In this sense, the next Chapter will deal with the study of the all-optical clock recovery from a RZ data signal at 40 Gb/s.

5.4 All-optical clock recovery at 40 GHz based on a QDash-MLLD from 40 Gb/s RZ data stream

5.4.1 Experimental setup

In this Section, the investigation on the clock recovery functionality based on a QDash-MLLD operating under injection of an optical data stream RZ-OOK at 40 Gb/s is carried out. Fig. 5.12 illustrates the clock recovery experimental setup. It consists of two major blocks: an OTDM RZ-OOK transmitter and the clock recovery system based on the QDash-MLLD-2. In the

OTDM RZ-OOK transmitter, a 40 GHz short pulse featuring 1.3 ps pulse width, from a mode-locked fibre laser (MLFL, Calmar Optcom PSL-40-TT) is modulated by a 40 Gb/s 2^7-1 or 2^{31}-1 long pseudo random binary sequence (PRBS), to produce the 40 Gb/s RZ-OOK signal. The 2^{31}-1 long PRBS will only be used when analysing and comparing the clock recovery dependence to pattern length in Section 5.4.2.3. Fig. 5.13(a) shows its optical spectrum recorded by an OSA (OSA-3, Agilent 86142B) with a resolution of 0.06 nm and the eye diagram of this optical data signal, which is characterised by a 18.95 dB extinction ratio. The centre wavelength of the 40 Gb/s is located at 1547 nm, and its spectral width is limited to 1.5 nm by an optical bandpass filter (not depicted in Fig. 5.12). The signal is split with 30% of the power sent to the detection stage for BER measurements, while the remaining 70% is sent to the all-optical clock recovery block. First, the optical signal is amplified with an Erbium-doped fibre amplifier (EDFA-1). An optical band-pass filter (OBPF-1) centered at 1547 nm and bandwidth of 5 nm suppresses part of the amplified spontaneous emission from EDFA-1. This optical data stream signal is injected into the QDash-MLLD-2 via an optical circulator. A polarisation controller (PC-1) is required to optimize the state of polarisation of the injected signal. The optical power of the injected signal is in the range of -3 dBm to +4 dBm controlled by a variable optical attenuator (VOA-1). The QDash-MLLD-2 is DC-biased at 120 mA and temperature stabilised at 25 ºC. The optical spectrum at the output of the locked QDash-MLLD is shown in Fig. 5.13(b). The figure shows the QDash-MLLD emission centered at 1527 nm and the spectrum at 1547 nm due to the reflection of the injected optical signal at the input facet of the QDash-MLLD.
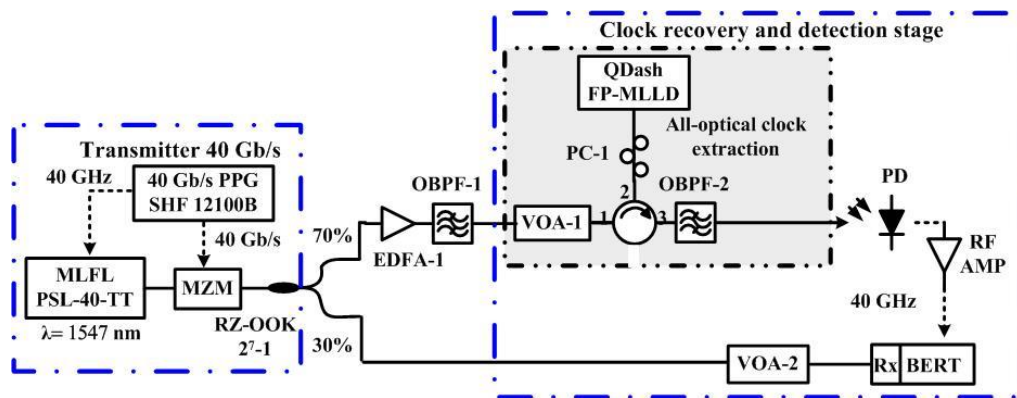
Figure 5.12: Experimental setup of the all-optical clock recovery from 40 Gb/s RZ-OOK: MZM: Mach-Zehnder modulator; MLFL: mode-locked fibre laser; PC: polarisation controller; EDFA: erbium-doped fibre amplifier; RF Amp: RF amplifier; OBPF: optical band pass filter; VOA: variable optical attenuator; QDash-FP-MLLD: quantum dash Fabry-Pérot mode-locked laser diode; PPG: pulse pattern generator; PD: photo-detector, BERT: Bit error rate tester (See appendix A for equipment specifications).
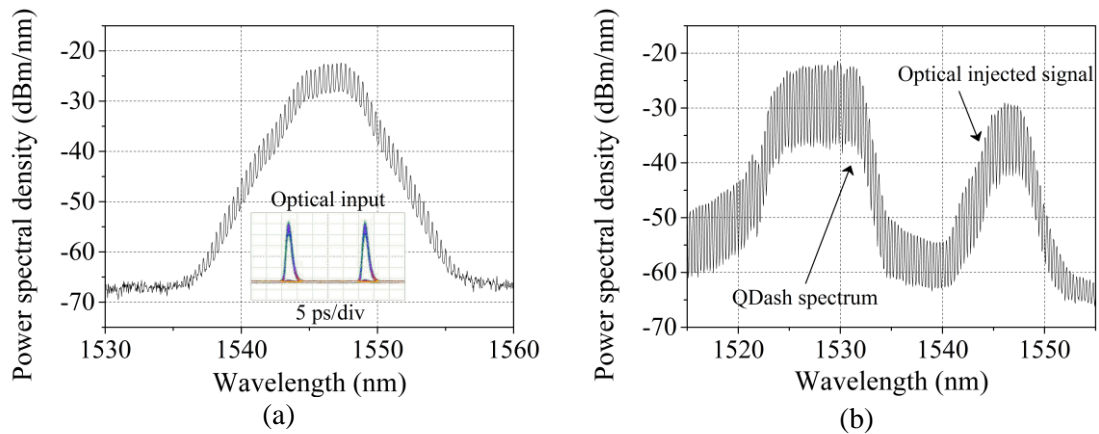
Figure 5.13: Optical spectra: (a) 40 Gb/s RZ-OOK optical input, Inset: eye diagram time trace, horizontal and vertical scales are 5 ps/div and 10 mV/div, respectively; (b) QDash-MLLD output before filtering.

The recovered optical clock is filtered out through OBPF-2 centered at 1530 nm and 5 nm bandwidth which is utilised to spectrally isolate the recovered clock at the QDash-MLLD output from the reflected injected data stream. Fig. 5.14 shows the optical spectrum of the recovered clock. Inset shows the time trace of the recovered clock retrieved by an electrical sampling oscilloscope. This signal looks like a sine wave due to the limitations in bandwidth of the electrical sampling oscilloscope utilised (LeCroy 100 H), being of 40 GHz.
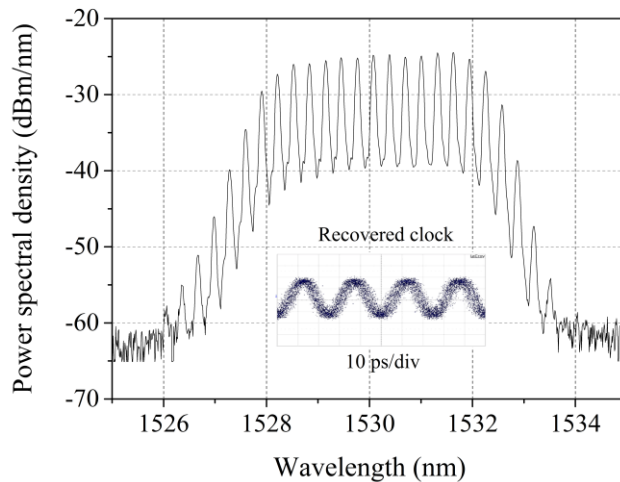
Figure 5.14: Recovered clock. Inset: time trace, horizontal and vertical scales are 10 ps/div and 100 mV/div, respectively.

77

5.4.2 Analysis and results

5.4.2.1 Phase noise and timing jitter

The optical clock is then converted to the electrical domain by using a 50 GHz PD (SHF 41210B) and a 40 GHz RF amplifier (RF-AMP) for triggering a bit error rate (BER) tester (SHF 11100B) or to assess the recovered clock in the RF domain with an ESA (ESA-3, Rohde & Schwarz FSU67). Fig. 5.15(a) shows the RF spectrum of the QDash-MLLD in free running (black) and the one synchronised to the 40 Gb/s RZ-OOK signal (red). The traces have been offset by 40 GHz. The reduction in the RF beat-tone linewidth in the locking state to <1 kHz is clearly visible, as compared to free running. The RF linewidth of the synchronised clock exhibits a value of ~10 Hz, when measured with a span of 600 Hz and resolution bandwidth of 10 Hz, as was demonstrated in the previous Section. In addition, this is in agreement with previous studies of mode-locking with these types of devices [26], [30]. For this experiment, we had access to an ESA Rohde & Schwarz FSU, 20 Hz to 67 GHz. This instrument combines the features of a spectrum analyser and a highly sophisticated phase noise tester. In addition, it allows calculations of the timing jitter from the phase noise measurement. Fig. 5.15(b) shows the single sideband phase noise spectral density (SSB-PSD) of the back-to-back (B2B) 40 GHz clock signal, i.e. the electrical clock signal provided by the transmitter, along with the corresponding traces of the recovered 40 GHz clock under injection of the 40 Gb/s (red trace), retrieved from the ESA. From this figure, it is possible to observe that the reference clock is slightly noisier than the recovered clock at low frequencies. From the trace corresponding to the recovered clock, it is possible to identify three regions [28]: in the first region from 100 Hz to 200 kHz, the phase noise from the injected input signal dominates, in between 200 kHz and ~ 2 MHz there is a transition region, in which the noise is dominated by the contribution of the free running QDash-MLLD. In this region, an increase in the timing jitter would be expected followed by its stabilisation. For frequencies higher than 4 MHz, the noise is determined by the QDash-MLLD and its filtering property, where a trending decrease in the phase noise level confirms it. In this region sudden increments in the timing jitter would not be expected.
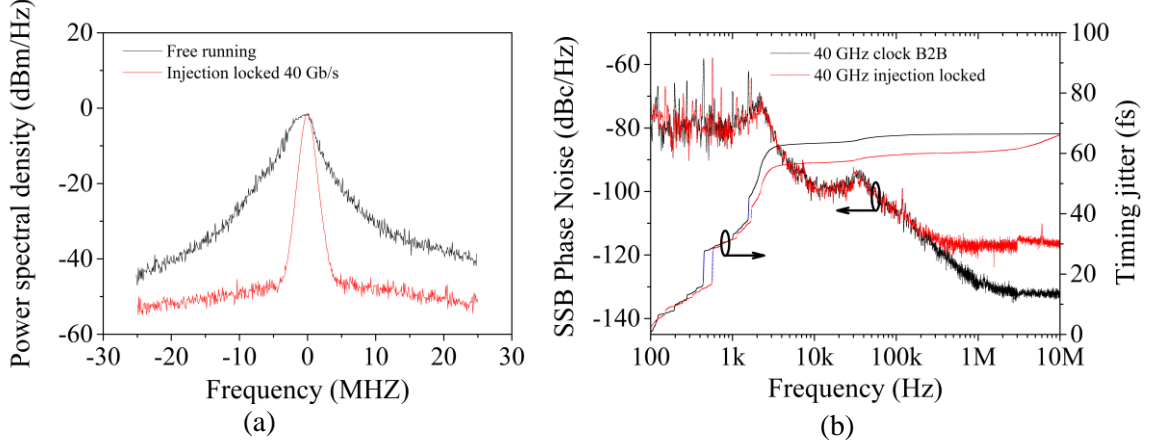
Figure 5.15: (a) Comparison of the RF spectra at the QDash-MLLD output, free running and injection locked. ESA set at a resolution of 1 MHz and span of 50 MHz; (b) Comparison of the single sideband phase noise of back-to-back and recovered clock.

In order to evaluate the timing jitter σ_J and to confirm the measurement retrieved from the ESA, equation (5.1) is used [31]:

$$\sigma_J = \frac{1}{2\pi f_R} \sqrt{\int_{f\,min}^{f\,max} L(f)df} \tag{5.1}$$

where, L(f) is the phase-noise spectral density, f_R is the repetition-rate, and $f$min and $f$max are boundaries of the frequency range. The timing jitter calculations, on the vertical right hand side axis, for the B2B and recovered clock are shown in Fig. 5.15(b). These traces represent the accumulated timing jitters which are calculated considering the $f$min as 100 Hz and the $f$max varied all along the frequencies retrieved from the phase noise trace. From the timing jitter traces, the regions where the phase noise from the recovered clock and B2B signal differ can be better monitored. The major difference between the phase noise trace corresponding to the recovered clock and the B2B is in the region from 2 to 3 kHz, which is possibly due to a random fluctuation of the clock from the transmitter. After that region of frequencies both signals show similar features and the timing jitter increases again for the recovered clock signal after 800 kHz. However, owing to the filtering properties of the QDash-MLLD the timing jitter from the recovered clock should not increase significantly. For the values of timing jitter reported in this Section, the integration boundary is from 100 Hz to 10 MHz. The recovered 40 GHz clock has a timing jitter of 66 fs.

5.4.2.2 Characterisation of the power locking range

Determination of the dynamic power locking range is achieved by varying the optical power injected into the QDash-MLLD whilst preserving the same driving bias current to the QDash-MLLD, and no optimization of the state of polarisation of the input signal is sought (after adjusting the polarisation from an initial state of polarisation resulting in the locking condition). The optical power is varied from -3 dBm to +4 dBm at the input of the QDash-MLLD-2. The initial state of the QDash-MLLD is in free running and then a given power is injected. The phase noise trace from the RF signal of the recovered clock is analysed for all the input optical powers and their accumulated timing jitter is calculated using equation (5.1). Fig. 5.16 shows the timing jitter dependence of the QDash-MLLD as a function of the injection optical power. The timing jitter of the synchronised QDash-MLLD presents almost a flat behaviour. This indicates no power dependence and a long range of utilisation of the clock recovery based on QDash-MLLD. Furthermore, it demonstrates that once the QDash-MLLD is locked, it is stable and the phase noise and the associated timing jitter are approximately constant with an average value of 65 fs. Note that for power levels outside the power range considered, the synchronisation is not stable. However, these optical power values might be adjusted depending on the operational conditions of the QDash-MLLD when synchronisation is sought.
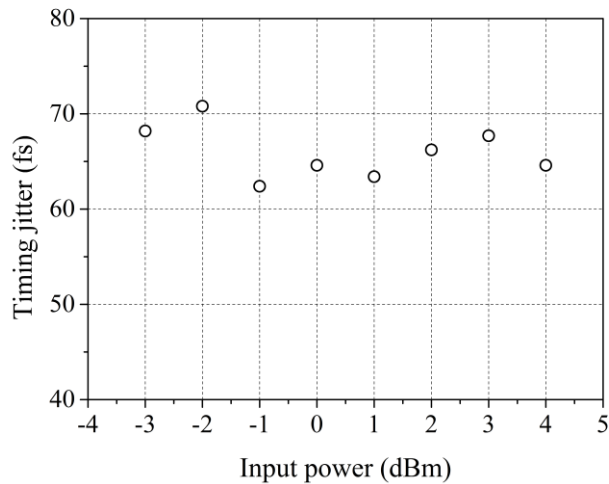
Figure 5.16: Timing jitter versus input power of the recovered clock from QDash-MLLD.

5.4.2.3 Clock recovery pattern length dependence

Additional investigation of the clock recovery is performed by analysing the BER measurements on the incoming data signal synchronised by the recovered clock for 2^7-1 and 2^{31} -1 long patterns. Fig. 5.17 shows the single sideband phase noise spectrum density (SSB-PSD) of the recovered 40 GHz for the two pattern lengths. From this figure, it is possible to observe the three regions mentioned previously for Fig. 5.15(b), where in the first region from 100 Hz to 200 kHz, the phase noise from the injected input signal dominates; in the transition region between 200 kHz and ~2 MHz, the noise is dominated by the contribution of the free running QDash-MLLD. In this region, an increase in the timing jitter would be expected followed by its stabilisation. For frequencies higher than 4 MHz, where the noise is determined by the QDash-MLLD and its filtering property, the decreasing trend in the phase noise level prevails. In general, the SSB-PSDs obtained from the RF spectra of the recovered clock after synchronisation by the input signal for both pattern lengths are similar. This indicates that the recovered clock system based on the QDash-MLLD is not dependent on the pattern length. Besides, after calculating the accumulated timing jitter is it found that for 2^7-1 and 2^{31}-1 long patterns the timing jitter is 66 fs and 69.1 fs, respectively [31]. This low timing jitter is a reference to verify the stability and high quality of the recovered clock pulses after synchronisation from 40 Gb/s RZ-OOK data signals.
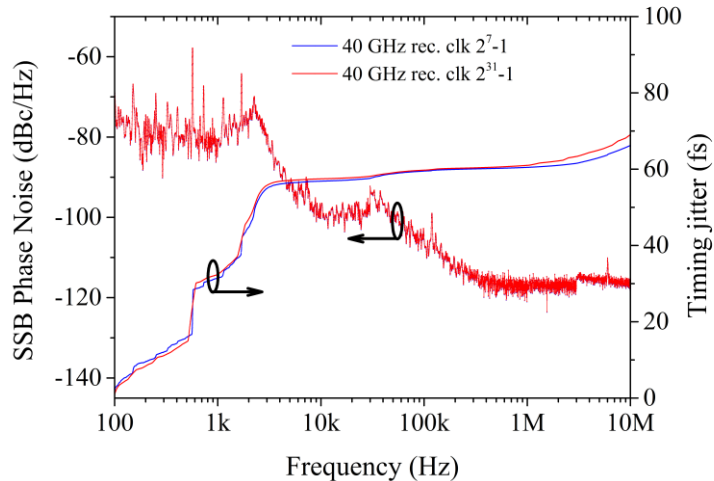
Figure 5.17: Comparison of single sideband phase noise of the recovered clock under injection of 40 Gb/s RZ-OOK signals at different pattern length.

Figs. 5.18(a) and 5.18(b), depict a comparison between the BER curves on the received 40 Gb/s incoming data signals (measured with the VOA-2 at the receiver of the BERT) when the BERT

is triggered by the original clock from the transmitter, referred as back-to-back (B2B) measurement, and with the recovered clock resulting from the synchronised QDash-MLLD by the 40 Gb/s (2^7-1) long data sequence Fig. 5.18(a) and to the (2^{31}-1) long data sequence Fig. 5.18(b). The operational conditions of the QDash-MLLD in terms of temperature are similar for both data pattern lengths, but not in terms of bias current and optical injected power, being 100 mA and -1 dBm for a 2^7-1 long pattern and 150 mA and 1 dBm for a 2^{31}-1 long pattern [30]. From these figures, it is possible to determine that there is no penalty for clock recovery for an input signal with a 2^7-1 long pattern, whilst a penalty of 0.5 dB exists for the recovered clock for an input signal with a 2^{31}-1 long pattern. Besides, in both cases is achieved error free ($10e^{-9}$) for received optical powers of at least -14.5 dBm and -14 dBm for data sequences of (2^7-1) and the (2^{31}-1) long pattern, respectively. These results validate the good performance and independence of the recovered clock to data pattern lengths.
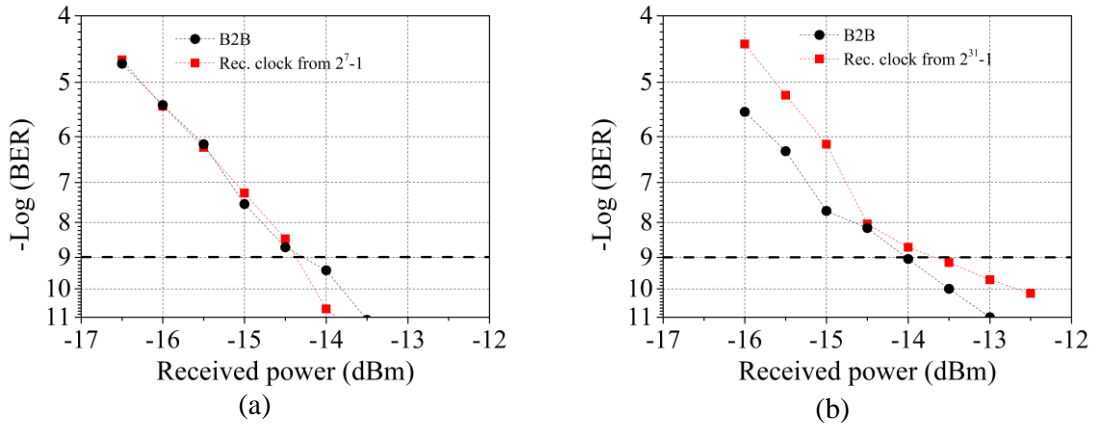
Figure 5.18: (a) BER results for an input with pattern length 2^7-1; black dots, B2B; red squares, recovered clock; (b) BER results for an input with pattern length 2^{31}-1; black dots B2B; red squares, recovered clock.

5.5 Summary

Two Dash-MLLDs were utilised to achieve synchronisation to incoming data signals at 40 Gb/s. The first QDash-MLLD-1, unpackaged laser, was synchronised to a NRZ data format signal and an optical clock signal was retrieved. The quality of the optical recovered clock signal was evaluated through the analysis of the RF beat-tone signal after its synchronisation to the incoming data. Good performance in terms of the RF peak power-to-noise-ratio, RF beating linewidth and timing jitter within a wavelength range of 23 nm. After achieving this reliable

optical clock signal, it was used to accomplish a 3R regeneration function (limited by the poor re-shaping function) with the bonus of an all-optical data format conversion from NRZ to RZ.

Furthermore, the QDash-MLLD-2 (packaged laser), was synchronised to incoming RZ data signal over 17 nm of separation between the recovered clock and data signal injected. In this case, the clock was further analysed with phase noise and timing jitter measurements from the RF beat-tone signal retrieved from an ESA. The clock signal exhibits a timing jitter value of ~ 65 fs. In addition, it displays a dynamic power locking range of 8 dB. Moreover, assessment on the dependence of the recovered clock to its synchronisation to injected data with pattern lengths of 2^7-1 and 2^{31}-1 was performed through BER measurements on the received data signals, demonstrating no penalty and 0.5 dB penalty, respectively.

The results presented in this Chapter validate the transparency of the QDash-MLLD to be synchronised to NRZ and RZ data formats, as well as to their pattern lengths. In addition, clock recovery based on the QDash-MLLD has the potential to give rise to the demonstration of more functions such as all-optical wavelength conversion and data format conversion.

References

[1]   C. Bornholt, J. Slovak, M. Mohrle, and B. Sartorius,"Jitter analysis of all-optical clock recovery at 40 GHz," *Optical Fiber Communications Conference* (OFC 2003), *Technical Digest.*, vol. 1, Paper 10.1109, pp. 120-121, Mar. 2003.

[2]   J. Lasri, P. Devgan, R. Tang, and P. Kumar, "Ultra-low timing jitter 40 Gb/s clock recovery using a novel electro-absorption modulator based self-starting optoelectronic oscillator," *Lasers and Electro-optics society. (LEOS 2003), 16 th IEEE Annual meeting*, Paper TuY6, pp. 390-391, vol. 1, Oct. 2003.

[3]   J. Parra-Cetina, S. Latkowski, R. Maldonado-Basilio and P. Landais, "Timing jitter and all-optical clock recovery based on a quantum-dash Fabry-Pérot semiconductor laser," *International conference on transparent optical Networks (ICTON 2010)*. We.D4.6. pp. 1-4, Munich, Germany, Jul. 2010.

[4]   J. Renaudier, B. Lavigne, F. Lelarge, M. Jourdran, B. Dagens, O. Legouezigou, P. Gallion, and G.-H. Duan, "Standard compliant jitter transfer function of all-optical clock recovery at 40 GHz based on a quantum dot self-pulsating semiconductor laser," *IEEE Photonics Technology Letters*, vol. 18, no. 11, pp. 1249-1251, Jun. 2006.

[5]   B.K. Mathason, P.J. Delfyett, G.A. Alphonse, and J.C. Connolly, "All-optical clock recovery and dynamics using mode-locked semiconductor lasers," *Optical Fiber Communications Conference (OFC 1998), Technical Digest*, Paper WM12, pp. 190-191, Feb. 1998.

[6]   X. Tang, J. C. Cartledge, A. Shen, F. V. Dijk, and G-H. Duan, "All-Optical Clock Recovery for 40-Gb/s MZM-Generated NRZ-DPSK Signals Using a Self-Pulsating DBR Laser," *IEEE Photonics Technology Letters*, vol. 20, no. 17, pp. 1443-1445, Sep. 2008.

[7]   Y. Yu, X. Zhang, E. Zhou, and D. Huang, "All-Optical Clock Recovery From NRZ Signals at Different Bit Rates via preprocessing by an Optical Filter," *IEEE Photonics Technology Letters*, vol. 19, no. 24, pp. 2039-2041, Dec. 2007.

[8]   G. Contestabile, N. Calabretta, E. Ciaramella, and M. Presi, "A novel 40 Gb/s NRZ all-optical clock recovery," *Laser & Electro-optics Conference (CLEO 2005)*, Paper CMZ2, vol. 1, pp. 452-454, May. 2005.

[9]   S. Arahira, H. Takahashi, K. Nakamura, H. Yaegashi, and Y. Ogawa, "Polarization-, wavelength-, and filter-free all-optical clock recovery in a passively mode-locked laser

diode with orthogonally pumped polarization-diversity configuration," *IEEE Journal of Quantum Electronics*, vol. 45, no. 5, pp. 476-487, May. 2009.

[10] J. Yu, Z. Jia, L. Yi, Y. Su, G.-K. Chang, and Ting Wang, "Optical Millimeter-Wave Generation or Up-Conversion Using External Modulators," *IEEE Photonics Technology Letters*, vol. 18, no. 1, pp. 265-267, Jan. 2006.

[11] J. C. Cartledge, X. Tang, M. Yañez, A. Shen, A. Akrout, and G.-H. Duan, "All-optical clock recovery using a quantum-dash Fabry-Perot laser," *in Proceedings IEEE Microwave Photonics Conference (MWP 2010) IEEE Topical Meeting on*, Paper TH3-1, pp. 201-204, Oct. 2010.

[12] H. J. Lee, H. G. Kim, J. Y. Choi and H. K. Lee, "All-optical clock recovery from NRZ data with simple NRZ-to-PRZ converter based on self-phase modulation of semiconductor optical amplifier," *Electronics letters*, vol. 35, no. 12, pp. 989-990, Jun. 1999.

[13] W. Mao, Y. Li, M. Al-Mumin, and G. Li, "All-optical clock recovery for both RZ and NRZ data," *IEEE Photonics Technology Letters*, vol. 14, no. 6, pp. 873-875, Jun. 2002.

[14] A. D. Ellis, K. Smith and D. M. Patrick, "All optical clock recovery at bit rates up to 40 Gb/s," *Electronics Letters*, vol. 29, no. 15, pp. 1323-1324, Jul. 1993.

[15] E. Tangdiongga, J. P. Turkiewicz, G. D. Khoe, and H. de Waardt, "Clock Recovery by a Fiber Ring Laser Employing a Linear Optical Amplifier," *IEEE Photonics Technology Letters*, vol. 16, no. 2, pp. 611-613, Feb. 2004.

[16] L. Wang, N. Zhu, W. Li, and J. Liu, "A frequency-doubling optoelectronic oscillator based on a dual parallel Mach–Zehnder modulator and a chirped fiber Bragg grating," *IEEE Photonics Technology Letters*, vol. 23, no. 22, pp. 1688–1690, Nov. 2011.

[17] H.C.H. Mulvad, E. Tangdiongga, H.de Waardt, and H. J. S. Dorren, "40 GHz clock recovery from 640 Gbit/s OTDM signal using SOA-based phase comparator," *Electronics Letters*, vol. 44, no. 2, pp. 146-148, Jan. 2008.

[18] T. Ono, T. Shimizu, Y. Yano, and H. Yokoyama, "Optical clock extraction from 10 Gbit/s data pulses by using monolithic mode-locked laser diodes," *in Proceedings Techical Digest Optics Fiber Communications Conference (OFC 1995)*, Feb. 1995, pp. 288–289, Paper ThL4.

[19] T. Ohno, K. Sato, T. Shimizu, T. Furuta, and H. Ito, "Recovery of 40 GHz optical clock from 160 Gbit/s data using regeneratively mode-locked semiconductor laser," *Electronics Letters*, vol. 39, no. 5, pp. 453–455, Mar. 2003

[20] X. Tang, J. C. Cartledge, A. Shen, F. van Dijk, A. Akrout, and G.-H. Duan,

"Characterization of all-optical clock recovery for 40 Gb/s RZ-OOK and RZ-DPSK data using mode-locked semiconductor lasers," *IEEE Journal of Lightwave Technology*, vol. 27, no. 20, pp. 4603–4609, Oct. 2009.

[21] F. Lelarge, B. Dagens, J. Renaudier, R. Brenot, A. Accard, F. van Dijk, D. Make, O. Le Gouezigou, J.-G. Provost, F. Poingt, J. Landreau, O. Drisse, E. Derouin, B. Rousseau, F. Pommereau, and G.-H. Duan, "Recent advances on InAs/InP quantum dash based semiconductor lasers and optical amplifiers operating at 1.55 µm," *IEEE Journal of Selected Topics in Quantum Electronics*, vol. 13, no. 1, pp. 111–124, Jan./Feb. 2007.

[22] F. Lelarge, F. Pommereau, F. Poingt, L. Le Gouezigou, and O. Le Gouezigou, "Active mode-locking of quantum dot Fabry-Pérot laser diode," *IEEE International Semiconductor Laser Conference*, 1708132, pp. 153-154, 2006.

[23] G.-H. Duan, A. Shen, A. Akrout, F. V. Dijk, F. Lelarge, F. Pommereau, O. LeGouezigou, J.-G. Provost, H. Gariah, F. Blache, F. Mallecot, K. Merghem, A. Martinez, and A. Ramdane, "High performance InP-based quantum dash semiconductor mode-locked lasers for optical communications," *Bell Labs Technical Journal*, vol. 14, pp. 63-84, Autumn 2009.

[24] X. Tang, S. H. Chung, J. C. Cartledge, A. Shen, F. V. Dijk, and G.-H. Duan, "Transmission performance of 40 Gb/s DPSK all-optical clock recovery based on a self-pulsating DBR laser," *in European conference and exhibition on optical communication (ECOC 2008)*, Paper Tu4D1, pp. 1-2, Brussels, Belgium, Sep. 2008.

[25] G.-H. Duan, B. Lavigne, J. Renaudier, F. Lelarge, O. Legouezigou, B. Dagens, and A. Accard, "Importance of the beating spectral linewidth on the performance of the recovered clock at 40 Gbit/s using self-pulsating lasers," *in Lasers and Electro-optics, (CLEO 2006)*, Long Beach, California, Paper CMN3, pp.1-2, May. 2006.

[26] J. Parra-Cetina, S. Latkowski, R. Maldonado-Basilio, P. Landais, "Wavelength tunability of all-optical clock recovery based on quantum dash mode-locked laser diode under injection of a 40 Gb/s NRZ data stream," *IEEE Photonics Technology Letters*, vol. 23, no. 9, pp. 531-533, May. 2011.

[27] R. Maldonado-Basilio, S. Latkowski, , J. Parra-Cetina and P. Landais, "All-optical 40 Gb/s 3R regeneration assisted by clock-extraction based on a passively mode-locked quantum-dash Fabry-Pérot laser," *European Conference and Exhibition on Optical Communication (ECOC) 2010*, 10.119. pp. 1-3, Torino, Italy, Sep. 2010.

[28] J. Renaudier, B. Lavigne, P. Gallion, and G-H. Duan, "Study of Phase-Noise Properties and Timing Jitter of 40-GHz All-Optical Clock Recovery Using Self-Pulsating Semiconductor Lasers," *IEEE Journal of Ligthwave Technology*, vol. 24, no. 10, pp.

3734-3742, Oct. 2006.

[29]   J. Parra-Cetina, S. Latkowski, R. Maldonado-Basilio and P. Landais, "All-optical clock recovery based on a quantum-dash Fabry-Pérot semiconductor laser in a 3R regenerator with modulation format conversion at 40 Gb/s," *China-Ireland International Conference on Information and Communications Technologies, CIICT*, Wuhan, China, Oct. 2010

[30]   R. Maldonado-Basilio, S. Latkowski, S. Philippe, and P. Landais, "40 GHz mode-beating with 8 Hz linewidth and 64 fs timing jitter from a synchronized mode-locked quantum-dash laser diode," *Optics Letters*, vol. 36, no. 16, pp. 3142-3144, Aug. 2011.

[31]   J. Lasri, P. Devgan, R. Tang, and P. Kumar, "Self-start optoelectronic oscillator for generating ultra-low-jitter high-rate (10 GHz or higher) optical pulses," *Optics Express*, vol. 11, no. 12, pp. 1430-1435, Jun. 2003.

Chapter 6

Sub-harmonic all-optical clock recovery and demultiplexing at 40 Gb/s

6.1 Introduction

The development of novel optical devices is of great importance to realising an optical time division multiplexing (OTDM) system that will enable ultrafast signal processing functions beyond the speed capabilities of conventional electronics [1-3]. Moreover, the possibility of processing signals in the all-optical domain, with these devices, will allow reducing the energy consumption in networks and systems. As mentioned in the previous Chapter, all-optical clock recovery (OCR) is one of the crucial technologies in the ultra-high speed OTDM front end, in particular where synchronous operations are required to be performed such as in demultiplexing and 3R regeneration (re-amplification, re-shaping and re-timing) [2], [4] and [5]. Clock recovery at the line rate is indispensable for 3R regeneration, while sub-harmonic clock recovery is required at the network nodes to allow both demultiplexing and 3R regeneration operations on individual channels [5]. An OCR system capable of retrieving a high quality clock signal synchronised to the original data signal is mandatory in order to achieve error free demultiplexing [6]. In addition to that, in order to make sub-harmonic clock recovery practical, it is crucial to ensure that the discrete phase jump caused by the random nature of an optical data pattern multiplexed at high bit rates is suppressed [7]. Sub-harmonic clock recovery has been investigated using different methods, such as optoelectronic oscillators (OEO) [8-10], optical phase-locked loops [4-5], [11-14], and mode-locked lasers [15-21]. Normally, the techniques based on OEO and PLLs are used in combination with nonlinear elements such as periodically poled lithium niobate (PPLN) [12], semiconductor optical amplifiers (SOAs) [13], [22], or electro-absorption modulators (EAMs) [4], [5], [11], and [14]. These schemes feature a complex and bulky structure, which increases the cost of the system, energy consumption and makes

them difficult to implement. In addition, not all of them systematically meet the requirement of timing-jitter for ultra-high baud-rate OTDM systems. Among these three methods, all-optical clock recovery using mode-locked semiconductor laser diodes (MLLD) has shown great performance because of its extremely simple configuration, stable operation, cost effectiveness, low energy consumption and ability to generate high quality optical pulses [5]. Recently, sub-harmonic clock recovery based on quantum dot/dash (QDot/QDash) lasers has been achieved with good performance in terms of frequency stability and low timing jitter [20], [23- 25] because of their narrow beat-tone linewidth (<50 kHz) and small associated phase noise [26-28]. Moreover, the fast locking time of the QDash-MLLD allows the possibility to exploit the OCR for burst mode operation [29], [30]. Although an OCR based on a QDash-MLLD followed by a high speed photo-detector and an electro-optical modulator as time demultiplexing has been demonstrated for optical signals up to 160 Gb/s [31]. Recently, one of the first demonstrations have been conducted on QDash-MLLD based OCR operation using high speed return-to-zero on-off keying (RZ-OOK) featuring no component at 40 GHz [32], [33], [34], which is a break-through, as any 40 GHz component strongly contributes to the synchronisation of 40 GHz free running frequency of the MLLD.

This Chapter details those results and some others in the following manner: firstly, two butterfly packaged QDash-MLLDs with the same features are studied. The first device, namely QDash-MLLD-2 (the laser is the one used in Chapter 5 to perform synchronisation under 40 Gb/s RZ-OOK). It will be subject to the injection of coherent 80 and 160 Gb/s RZ-OOK incoming data. The second packaged laser is referred to QDash-MLLD-3, and is subject to the injection of coherent 320 Gb/s RZ-OOK incoming data. The performance of the recovered clocks from both QDash-MLLDs are demonstrated over a large wavelength detuning between the data and recovered clock over the C-band, with phase noise and timing jitter measurements. Finally, an application of the recovered clocks to perform demultiplexing of these high speed data signals to 40 Gb/s tributaries is demonstrated and evaluated with bit error rate (BER) measurements.

6.2 Sub-harmonic all-optical clock recovery based on a mode-locked quantum dash laser diode

6.2.1 Experimental setup

The experimental setup to investigate the sub-harmonic all-optical clock recovery based on a QDash-MLLD under injection of RZ-OOK data signals at 80, 160 and 320 Gb/s is shown in Fig. 6.1. It consists of two major blocks: an OTDM RZ-OOK transmitter (in the red box) and the clock recovery system based on the QDash-MLLD (in the blue box). In the black dotted box, the transmission link block is shown, which will be described below. The transmission block only applies for signals at 80 and 160 Gb/s data speeds.
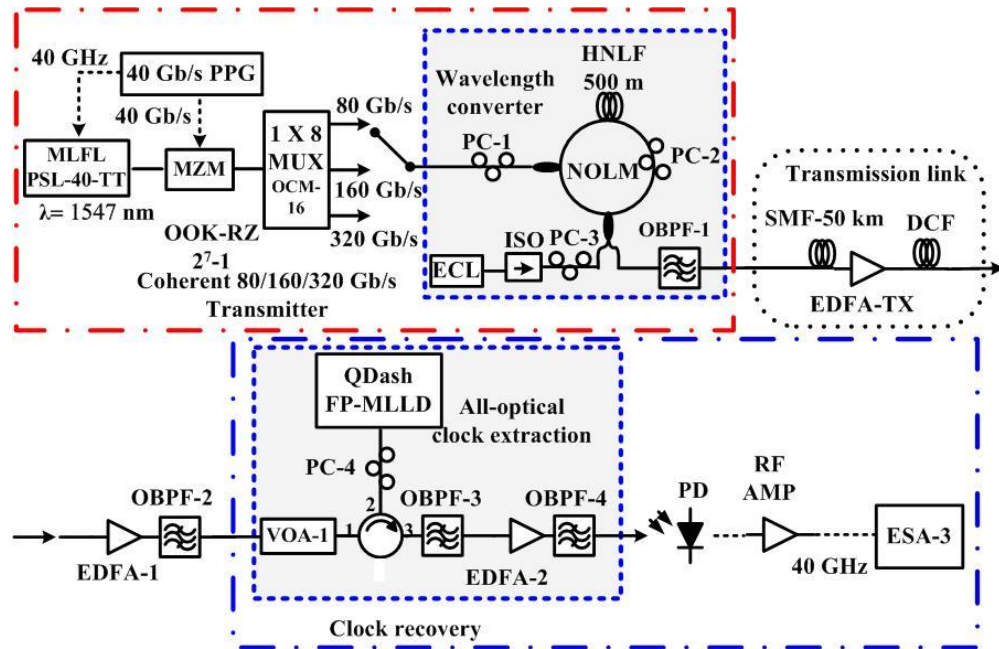
Figure 6.1: Sub-harmonic all-optical clock recovery experimental setup for high speed RZ-OOK: MZM: Mach-Zehnder modulator; ISO: optical isolator; MLFL: mode-locked fibre laser; PC: polarisation controller; ECL: external cavity laser; SMF: single-mode fibre; DCF: dispersion compensation fibre; EDFA: erbium-doped fibre amplifier; RF Amp: RF amplifier; OBPF: optical band pass filter; VOA: variable optical attenuator; QDash-FP-LD: quantum dash Fabry-Pérot laser diode; PPG: pulse pattern generator; MUX: multiplexer; HNLF: highly nonlinear fibre; PD: photo-detector, BERT: Bit error rate tester (See appendix A for equipment specifications).

In the OTDM RZ-OOK transmitter, a 40 Gb/s optical data stream is generated from a mode-locked fibre laser (MLFL, Calmar Laser PSL-40-TT) after being modulated by a 40 Gb/s 2^7-1

data signal. This 40 Gb/s data stream is optically time multiplexed via a fibre based interleaver (PriTel OCM-16) in order to produce the 80, 160 and 320 Gb/s OTDM RZ-OOK signals at a central wavelength of 1547 nm. Furthermore, the data pattern of the stream is limited to a length of 2^7-1 symbol, due to the time interleaver. This high data rate multiplexing method still introduces a 40 GHz spectral component originated by the MLFL. In order to obtain a stable and phase coherent RZ-OOK signal, the original OTDM signal at 80, 160 or 320 Gb/s is wavelength converted. The high speed OTDM signals are fed into a nonlinear optical loop mirror (NOLM) based wavelength converter (WC) as the control signal, while a coherent CW light from an external cavity laser (ECL, Agilent 81989A) centered at λs=1558 nm or 1559 nm, is used as the probe. The principle of operation of the NOLM based wavelength converter has been reported in [35], [36]. At the output of the NOLM, the data information of the 80, 160 or 320 Gb/s RZ-OOK sequence is replicated to the coherent CW probe light.

At the output of the NOLM configuration, a 6 nm optical band pass filter with the center wavelength located at the coherent CW light is used to select out the phase coherent 80, 160, or 320 Gb/s RZ-OOK signal. The coherent data signals at 80, 160 and 320 Gb/s are amplified by an Erbium-doped amplifier (EDFA-1) and filtered (OBPF-2) before being launched into the all-optical clock recovery setup based on the QDash-MLLD. In the case of 80 Gb/s and 160 Gb/s both signals can be also passed through a dispersion compensated 52 km transmission link. This transmission block is composed of 50 km of single mode fibre (SMF), 2 km of dispersion compensating fibre (DCF) with -220 ps/nm*km dispersion, and an EDFA-TX for amplification after the 50 km of SMF.

The generation of the 80, 160 and 320 Gb/s RZ-OOK signal is obtained after the multiplexing 1x2, 1x4, and 1x8 of the original 40 Gb/s signal from the MLFL, as explained above. Fig. 6.2 depicts the optical spectra of wavelength conversion, in red, and of the phase coherent RZ-OOK signals after filtering by OBPF-1 and 13 dB of amplification, in blue, for a bit-rate of 80 Gb/s (Fig. 6.2(a)), 160 Gb/s (Fig. 6.2(b)), and 320 Gb/s (Fig. 6.2(c)), respectively, taken with resolution bandwidth (RBW) of 0.06 nm (OSA-3, Agilent 86142B). Before the filtering stage (OBPF-1), the WC spectra are characterised by a main peak at 1547 nm (control signal) and a secondary peak at 1558 nm (in the case of 80 and 160 Gb/s) and at 1559 nm (for 320 Gb/s) due to the probe signal. The difference in wavelength between the optical spectra of the original high speed input signal and the wavelength converted signal (given by the ECL) is selected in order to avoid their overlapping during the wavelength conversion process inside the NOLM. From Fig. 6.2 it is possible to observe that for the three spectra at the output of the WC stage there is a spurious 40 GHz spectral component on the original OTDM signal. However, after filtering, it can be clearly verified that the WC and coherent signals produced at 80, 160 and 320 Gb/s are free of the 40 GHz spectral component. In addition, by this wavelength conversion method, the phase jump inherent to multiplexed signal is eliminated [7]. The separation between

optical modes is measured as 0.66, 1.32 and 2.64 nm, resulting from the bit rate of the transmitter, at 80, 160 and 320 Gb/s, respectively. The insets in Fig. 6.2, present the eye diagrams of the optical input data signals before WC and after WC. For the cases of 80 and 160 Gb/s, there are also provided the eye diagrams of the WC signals with and without transmission. The pulses are separated by 12.5 ps (a), 6.25 ps (b), and 3.125 ps (c) respectively. The extinction ratios for the eye diagrams are of 10 dB. These optical WC data signals can be injected directly into the QDash-MLLD or launched beforehand into a 52 km dispersion compensated transmission link with an injection power of 6 dBm. The signals going through the transmission stage (80 Gb/s or 160 Gb/s) are first amplified to 11 dBm, filtered and then fed into the clock recovery block based on QDash-MLLD.
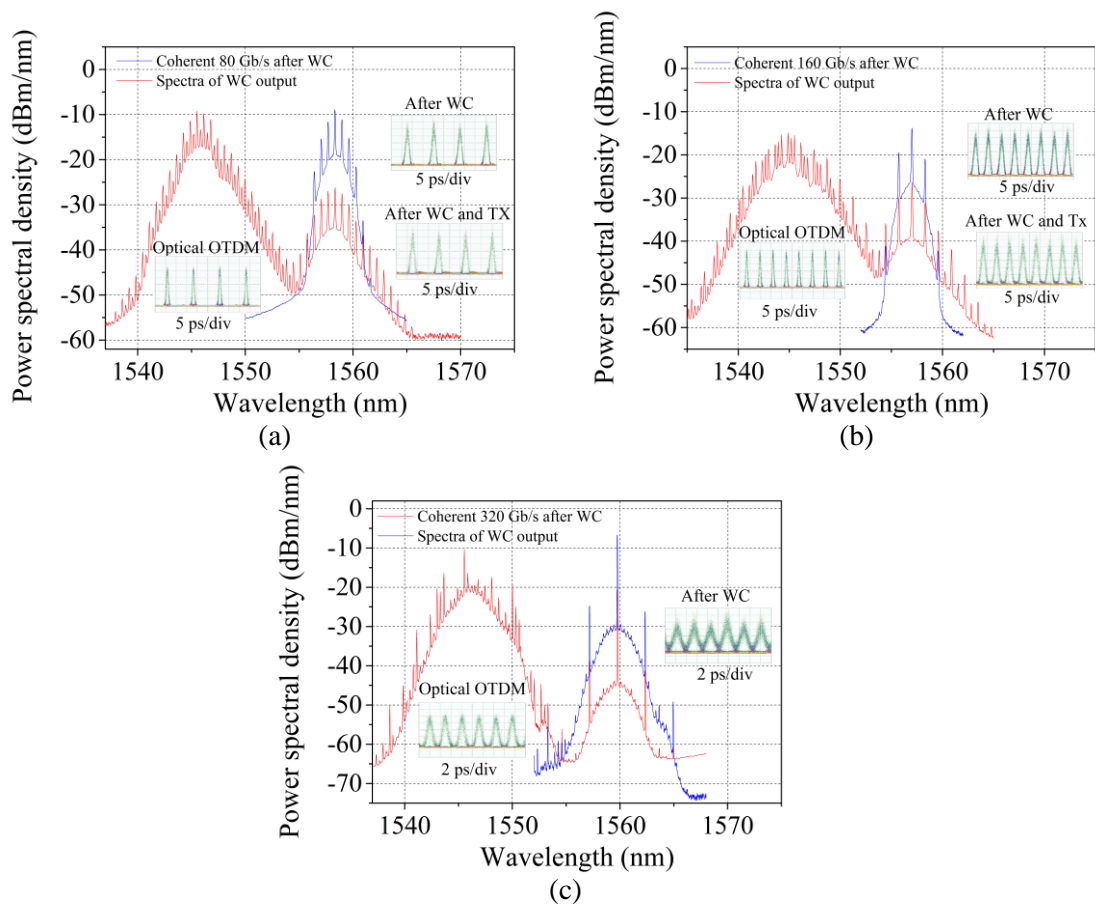
Figure 6.2: Optical spectra at the output of the WC stage: (a) for input at 80 Gb/s, with RBW: 0.06 nm. Inset: time traces of the corresponding signals, x-scale 5 ps/div.; (b) for input at 160 Gb/s, with RBW: 0.06 nm. Inset: time traces (taken with the electrical sampling oscilloscope Agilent 86100C) of the corresponding signals, x-scale 5 ps/div.; (c) for input at 320 Gb/s, with RBW: 0.06 nm. Inset: time traces of the corresponding signals, x-scale 2 ps/div.

The 40 GHz sub-harmonic optical clock recovery is achieved by injection locking the QDash-MLLD with the optical RZ-OOK signals at 80, 160 and 320 Gb/s. In this investigation, two packaged QDash-MLLDs with the same characteristics (except for the optical power emitted) are utilised, as mentioned in the introduction. These lasers will be referred throughout the Chapter as: QDash-MLLD-2 and QDash-MLLD-3. It is worth noting that the QDash-MLLD-2 is the same laser utilised in Chapter 5, when clock recovery under injection of RZ-OOK at 40 Gb/s was investigated. In this Chapter, the QDash-MLLD-2 will be used for synchronisation under injection of 80 and 160 Gb/s coherent data signal and QDash-MLLD-3 will be employed for synchronisation under injection coherent 320 Gb/s RZ-OOK data signal.

In the case of achieving synchronisation under 80 and 160 Gb/s coherent RZ-OOK signals, the QDash-MLLD-2 is operated with bias current of 86 mA and controlled at room temperature at 25 ℃. The coherent 80 and 160 Gb/s RZ-OOK data signals before being injected into the QDash-MLLD are optimised in polarisation by the (PC-4). The polarisation dependence can be solved by cascading a bulk and a quantum dash mode-locked laser [37] or by using a semiconductor optical amplifier in a dual pump configuration [38]. However, these elements were not available at the moment of doing these experiments. The injection power is within the range of 4 dBm and 5 dBm in the case of incoming signals at 80 Gb/s and 160 Gb/s, respectively. At room temperature and at the same optical power injected levels it was not possible to achieve synchronisation of the QDash-MLLD-3 under injection of coherent 320 Gb/s RZ-OOK. This can be explained better by reviewing the synchronisation mechanism of optical injection locking in Fabry-Pérot lasers along with some properties of the QDash material.

The quantum dash material possesses an ultra-wide broad bandwidth [26], [39]. This large bandwidth allows its interaction with a signal even outside the emitted gain spectrum visible by the longitudinal modes. The strong optical power with data impinged into it causes a modulation of the refractive index, which modifies the carrier density and the gain. These changes in the refractive index affect the frequency and the phase of the longitudinal modes and improve their phase correlation, giving rise to an effect similar to active mode-locking. In addition, by these modifications in the refractive index and gain there is a cavity resonance shift and bandwidth enhancement [26], [40], [41]. As a consequence of these last statements, it can be understood that when increasing the bit rate of the signal injected into the QDash-MLLD, the modulation of the refractive index caused by this data signal is not enough anymore to modify the cavity resonance frequency which results in the synchronisation of the QDash-MLLD and its subsequent stable pulse generation. In other words, the fundamental frequency of the input signal interacts with a smaller QDash-MLLD high-harmonic spectral component making it more difficult to lock in. With regard to synchronisation at 320 GHz, a modification in the refractive index has to take place, which can be done by a combination of changes involving the

temperature, optical power and/or the DC-bias applied to the QDash-MLLD. Consequently, in order to achieve the synchronisation of the QDash-MLLD and therefore the clock recovery from a 320 Gb/s data signal, the QDash-MLLD operational conditions such as the bias current and temperature are changed to 117 mA and 21.7 °C, respectively. Furthermore, the optical injection power is increased to 7 dBm.

Fig. 6.3 (a), Fig.6.3 (b) and Fig. 6.3 (c) represent the optical output of the QDash-MLLD under synchronisation before filtering from OBPF-3, in red, and of the recovered clock (after filtering) in blue, at bit rates of 80 Gb/s ,160 Gb/s and 320 Gb/s respectively. The optical spectrum of the synchronised signal centered at 1532 nm features a free-spectral range of 0.33 nm, corresponding to a frequency of 40 GHz. In the three figures, it can be noticed that even though the injected signals are at 80 Gb/s, 160 Gb/s, or 320 Gb/s the synchronised signal is invariably set at 40 GHz, which is also confirmed with the insets, showing the eye diagrams of the recovered clocks.

In summary, the QDash-MLLD is therefore able to synchronise to an incoming data signal at a multiple of its internal free running frequency and within a wavelength detuning of more than 23 nm between the injected signal and the recovered clock optical spectra [34]. It is worth noting that it is difficult to observe a clear sine wave for the recovered clock from the figures and the difference among them. This is due to the limited bandwidth of the photo-detector (~ 40 GHz) and of the internal detection system in the electrical sampling oscilloscope utilised to retrieve the traces (LeCroy 100 H). As a consequence, it is required to do further analysis of the extracted clock. In this regard, the optical clock is photo-detected (PD, SHF 41210B) and amplified by an RF amplifier. The retrieved electrical clock is analysed through an electrical spectrum analyser (ESA-3, Rohde&Schwarz FSU67) as will be described in the following Section.
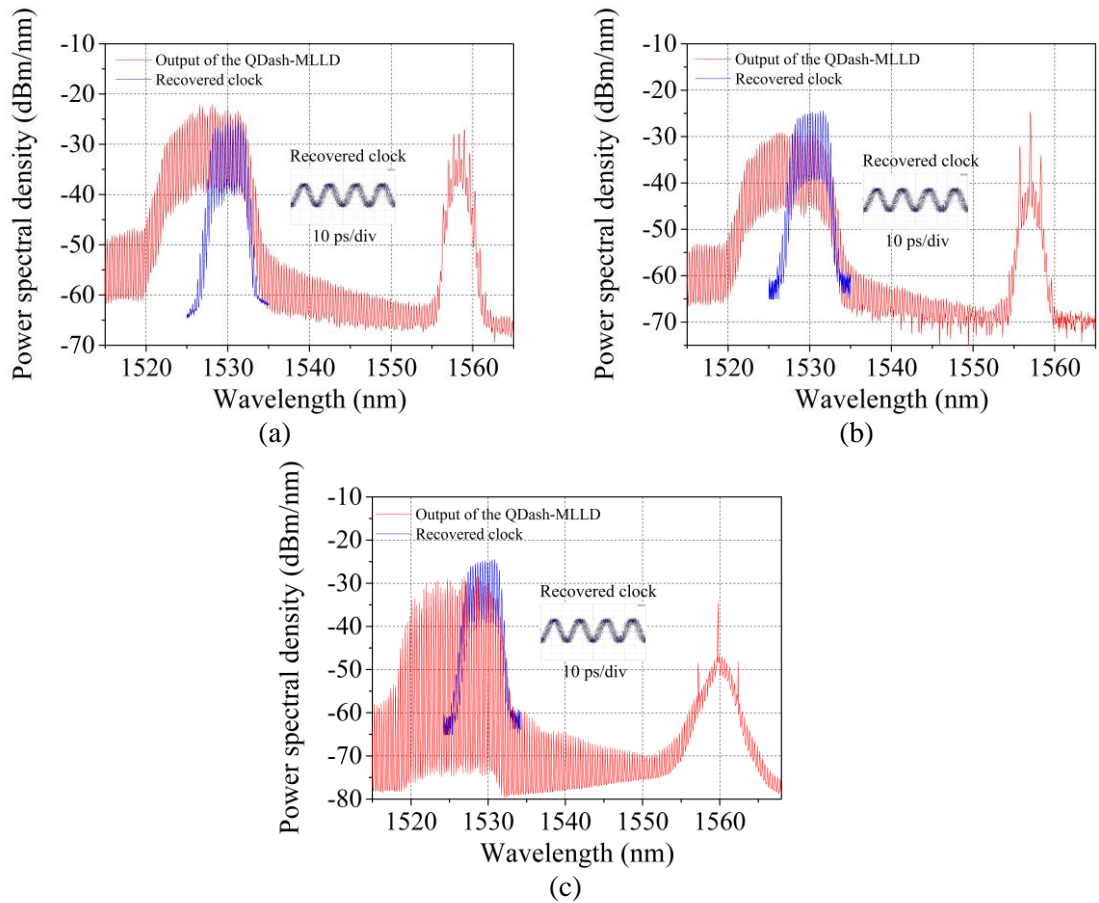
Figure 6.3: Optical spectra at the output of the QDash-MLLD: (a) for input at 80 Gb/s, with RBW: 0.06 nm; (b) for input at 160 Gb/s, with RBW: 0.06 nm; (c) for input at 320 Gb/s, with RBW: 0.06 nm. Insets: recovered clock eye diagrams, x-scale 10 ps/div.

6.2.2 Analysis of the all-optical clock recovery from coherent 80 Gb/s and 160 Gb/s RZ-OOK with and without transmission over 52 km of optical fibre

6.2.2.1 Phase noise and timing jitter analysis of the recovered clock under synchronisation of coherent 80 Gb/s RZ-OOK data signal

Fig. 6.4 is dedicated to the analysis of the response of the QDash-MLLD-2 under optical injection of a 80 Gb/s data sequence detuned by 23 nm. Fig. 6.4(a) shows the RF spectra of the photocurrent from the beating of the QDash-MLLD lasing modes. The figure has been offset by 40 GHz. In the black colour line, the RF beating signal of the QDash-MLLD in free running operation is shown. As demonstrated in Chapter 3, it features a Lorentzian distribution with a

linewidth of 25 kHz, which is largely narrower than that of any of the optical longitudinal modes of its optical spectrum. The synchronised RF beating after WC spectra with and without transmission (TX) (red and blue traces, respectively) are shown in Fig. 6.4(a), retrieved with span of 50 MHz and resolution bandwidth of 1 MHz. For the two traces, when measured with a span of 1 kHz and resolution bandwidth of 20 Hz, they exhibit a RF linewidth of <1 kHz, as was also demonstrated in Chapter 5. This compression of the RF linewidth and change in distribution confirm the synchronisation of the QDash-MLLD to the optical injected signals. Since the laser beating linewidth results from the phase noise of the optical modes, the phase noise of each mode must be highly correlated.

Fig. 6.4(b) exhibits the single side band power spectral density (SSB-PSD) of the back-to-back (B2B) 40 GHz clock signal, i.e. the electrical clock signal provided by the transmitter along with the corresponding traces of the recovered clock under injection of the 80 Gb/s with and without transmission over fibre (TX) (red and blue traces, respectively). The SSB-PSD traces are retrieved directly from the ESA which enables that analysis. Note that the SSB traces in this figure for both synchronised signals are similar in the region below 1 kHz, but a few spikes make them higher than the reference clock phase noise trace. The spikes are due to the absence of 40 GHz components on the coherent signals injected into the QDash-MLLD. In between 60 kHz and ~ 2 MHz a transition region is clearly visible, in which the noise is dominated by the contribution of the free running QDash-MLLD. In this region, an increase in the timing jitter of the recovered clock signals would be expected. For frequencies higher than 4 MHz, the noise is then dominated by the QDash-MLLD and its filtering property. This is confirmed by a decrease in the phase noise which is in agreement with previous observations [42], [43]. The timing jitter is calculated from the SSB-PSD, using equation (5.1), introduced in Chapter 5 and shown again below:

$$\sigma_J = \frac{1}{2\pi f_R} \sqrt{\int_{f\min}^{f\max} L(f)df}$$

(6.1)

where, L(f) is the phase-noise spectral density, f_R is the repetition-rate, and $f$min and $f$max are the boundaries of the frequency range. For the values of timing jitter reported in this Chapter, the integration boundary is from 100 Hz to 10 MHz.

The timing jitter accumulated from 100 Hz to 10 MHz is of 50 fs for the reference B2B signal. The 40 GHz recovered clock signal under injection of the 80 Gb/s coherent wavelength converted signal has a timing jitter of 62 fs. In the same condition, but after 52 km of data transmission in SMF and DCF, the timing jitter is 83 fs. The penalty is mostly due to the chromatic dispersion of the fibre as would be expected.

Figure 6.4: (a) Comparison of the RF spectra at the QDash output, in free running and under locking conditions with a frequency span of 50 MHz and resolution bandwidth of 1 MHz; (b) Comparison of single sideband phase noise of back-to-back with recovered clock under injection of coherent 80 Gb/s RZ-OOK with and without transmission.

6.2.2.2 Phase noise and timing jitter analysis of the recovered clock under synchronisation of coherent 160 Gb/s RZ-OOK data signal

Similar experiments have been carried out to analyse the recovered clock under injection of coherent 160 Gb/s RZ-OOK signal. Fig. 6.5(a) depicts the comparison of the RF spectra of the QDash-MLLD in free running (black line), and as a result of the synchronisation from the injected signal at 160 Gb/s with and without transmission (TX)) (red and blue traces, respectively), retrieved with a span of 50 MHz and resolution bandwidth of 1 MHz. In the same way as previously shown for the signals at 80 Gb/s, they reveal a distribution different from that of the laser in free running, exhibiting a RF linewidth of <1 kHz. The compression in their linewidths demonstrates again that the 40 GHz QDash-MLLD is synchronised, but in this case by a 160 Gb/s data stream. In Fig 6.5(b), the SSB-PSD of the B2B from the electrical 40 GHz clock signal (black trace) is compared with the synchronised signals from the injection of the 160 Gb/s coherent signal with and without transmission over 52 km of dispersion compensated fibre link (red and blue traces, respectively). These two SSB-PSD traces present an initial major amount of phase noise than the B2B trace in the region of 1 kHz and between them there is a slight difference, which can be attributed to the changes in amplitude and chromatic dispersion as a consequence of the transmission over the fibre link. In this case, it is expected to find more timing jitter than the shown by the reference clock, which is confirmed through their corresponding timing jitter traces shown in Fig. 6.5(b). Then, there is the transition region between 60 kHz and approximately 2 MHz, in which the noise is dominated by the contribution of the free running QDash-MLLD. In this region, an increase in the timing jitter of the

97

recovered clock signals would be expected. For frequencies higher than ~ 2 MHz, the expected reduction in phase noise of the synchronised signals is confirmed as a consequence of the direct influence of the QDash-MLLD filtering attribute [21]. Consequently, the timing jitter would not be expected to increase drastically. The timing jitter accumulated from 100 Hz to 10 MHz is 50 fs for the reference B2B signal. The added timing jitters resulting from the synchronisation of the QDash-MLLD from the injected signal at 160 Gb/s with or without transmission within a frequency span of 100 Hz and 10 MHz are 84 fs and 92 fs, respectively. The difference is only 8 fs at 10 MHz. These results make the recovered clock of the same quality regardless of the transmission of the 160 Gb/s coherent data signal.

According to these results in terms of timing jitter on the recovered clock signals from data streams at 80 and 160 Gb/s, this study has been pushed at higher bit rate to find out the eventual limitation of the optical recovered clock system, as will be shown in the next Subsection.
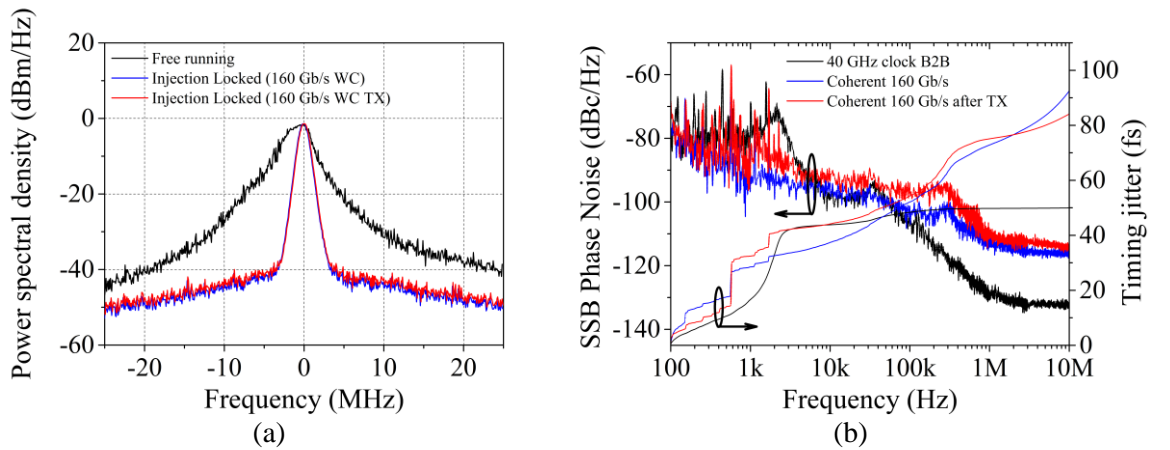
Figure 6.5: (a) Comparison of the RF spectra at the QDash-MLLD output, in free running and under locking conditions with a frequency span of 50 MHz and resolution bandwidth of 1 MHz; (b) Comparison of single sideband phase noise of back-to-back with recovered clock under injection of coherent 160 Gb/s RZ-OOK with and without transmission.

6.2.2.3 Phase noise and timing jitter analysis of the recovered clock under synchronisation of coherent 320 Gb/s RZ-OOK data signal

In this Section, the analysis of the response of the QDash-MLLD-3 under injection of a 320 Gb/s data sequence is analysed. Fig. 6.6(a) depicts, in the black colour line, the RF spectrum of the QDash-MLLD output in free running along with the corresponding RF spectrum of the QDash-MLLD under synchronisation from the 320 Gb/s injected optical data, in the blue colour line. In the same manner as in the two previous studies, the RF beating

linewidth features a value of <1 kHz when synchronised to an optical data signal. This compression of the RF linewidth and change in distribution when compared to free running conditions is a signature of synchronisation and enhancement of phase correlation of the optical modes. As a consequence, a low level of timing jitter for the optical signal generated from the QDash-MLLD output is expected. This can be confirmed through phase noise and timing jitter measurements. Fig. 6.6(b) exhibits the comparison of SSB-PSD of the back-to-back 40 GHz clock signal and the corresponding SSB-PSD trace of the recovered clock under injection of 320 Gb/s. In the region below 60 kHz, it is possible to see spikes attributed to the coherent injected signal. From 60 kHz is the transition region [21], it contains the noise contributions from both the incoming signal and the laser itself. At frequencies higher than 4 MHz, there is a decrease in the phase noise and as a consequence the timing jitter would be reduced, as it is confirmed in its analogous timing jitter trace in Fig. 6.6(b). Finally, the synchronised and recovered clock signal features an accumulated low timing jitter of 94 fs when integrated from 100 Hz to 10 MHz.

It is important to mention that in spite of only showing the phase noise traces up to 10 MHz, it is expected that for frequencies above 10 MHz the phase noise gets reduced due to the filtering effect imposed by the QDash-MLLD which derives in a settling down of the timing jitter value which would be represented by a no more rapid increase in the accumulated timing jitter trace at a value around 100 fs.
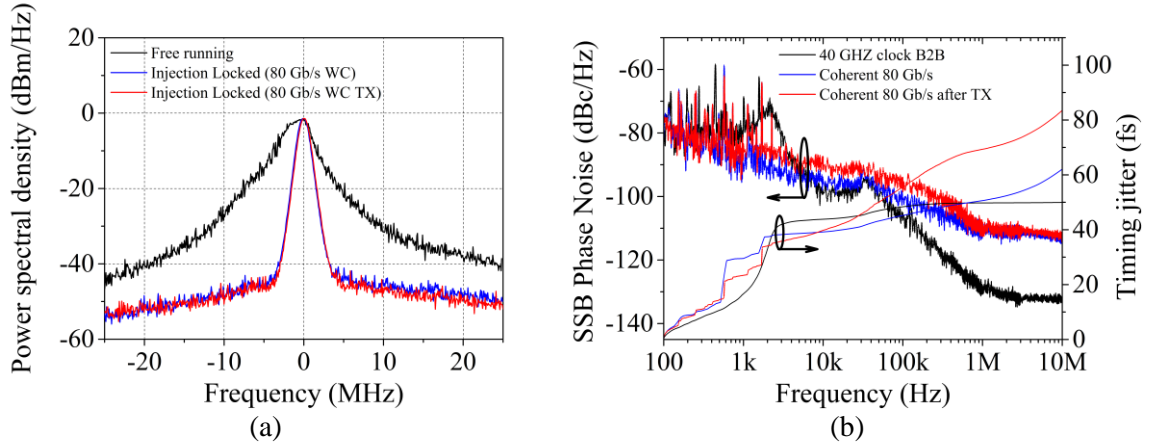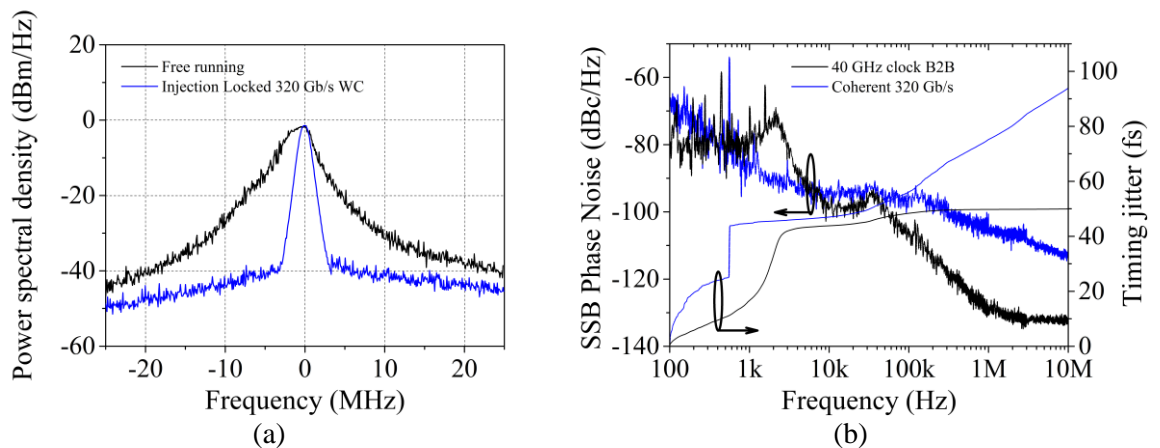

Figure 6.6: (a) Comparison of the RF spectra at QDash output, in free running and under locking conditions with a frequency span of 50 MHz and resolution bandwidth of 1 MHz; (b) Comparison of single side band phase noise of back-to-back with recovered clock under injection of coherent 320 Gb/s RZ-OOK.

6.2.2.4   Characterisation of the dynamic power locking range

With the intention to verify the clock recovery performance for implementation in a real network it is worth assessing the dynamic power locking range for optical injection of 80 Gb/s, 160 Gb/s and 320 Gb/s data sequences. This analysis is achieved by varying the optical power injected into the QDash-MLLD whilst preserving the same driving bias current and temperature of the QDash-MLLD in which synchronisation was achieved and analysed in previous Subsections for each of the three data rates injected into it; and no optimisation of the state of polarisation of the input signal is sought. The optical input power is controlled to vary from 3.5 dBm to 4.5 dBm for an optical input data rate at 80 Gb/s, from 4.5 to 5.5 dBm at 160 Gb/s and from 6 dBm to 8 dBm at 320 Gb/s. The RF signal of the recovered clock is analysed by retrieving the phase noise trace from the ESA and calculating the accumulated timing jitter. Fig. 6.7 shows the timing jitter dependence of the recovered clock from the QDash-MLLD as a function of the optical input power at data rates of 80 Gb/s, 160 Gbs and 320 Gb/s. From Fig. 6.7, two important results are found. Firstly, the dynamic range at 80 Gb/s and 160 Gb/s is 1 dB and both present an increment in the timing jitter as the optical input power increases. These traces are labeled with black squares for 80 Gb/s and black circles for 160 Gb/s, averaging timing jitter values of 75 fs and 100 fs, respectively. This increase in the timing jitter with the increase in optical power injected is due to the added noise from the EDFA-1 and the induced wavelength shift between the QDash-MLLD and the input signals at such data rates. The shift of the QDash-MLLD longitudinal spectrum is a consequence of variations in the gain and refractive index of the cavity under high power injection. The timing jitter of the synchronised QDash-MLLD at 320 Gb/s data sequence presents a decreasing trend with the increase of input power, represented in black triangles. This indicates that the interaction among the modes in the QDash-MLLD with the wavelength of the input signal at this data rate is better detuned with the increment in power, giving rise to an enhancement of the phase correlation of the QDash-MLLD, averaging 110 fs. The second result derived from Fig. 6.7, is that in order to achieve the synchronisation of the QDash-MLLD at higher bit rates it is necessary to increase the power injected into the QDash-MLLD, leading to an increase in the phase noise and associated timing jitter but decreasing the dynamic power locking range when compared to the results derived from a base-line synchronisation, as analysed in Chapter 5.

It is worth mentioning that outside the limits of the dynamic range values shown in Fig. 6.7, for lower power input unstable synchronisation is achieved. At higher values of optical power injected in the case of incoming data signals at 80 and 160 Gb/s the synchronisation is lost, but for 320 Gb/s it would be improved. Due to limitations in the equipment available, however, it was not possible to inject more optical power.
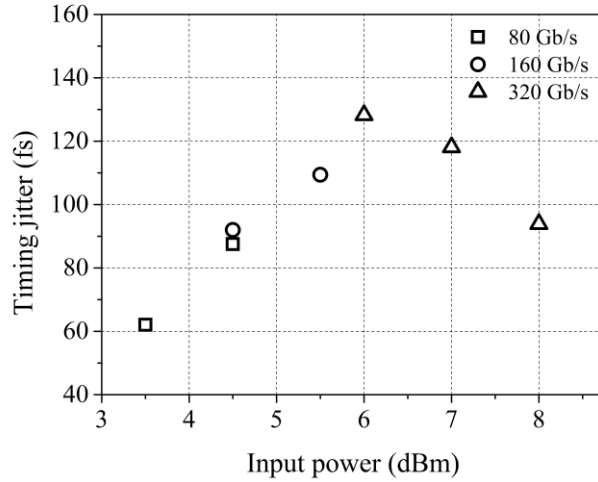
Figure 6.7: Timing jitter vs. input power of recovered clock from QDash-MLLD under injection of coherent 80, 160 and 320 Gb/s RZ-OOK.

6.2.2.5 Summary and comparison of clock recovery results

Having characterised the recovered optical clock signals for different incoming data rates, it is worth comparing the results obtained. Table 6.1 summarises the main attributes of the recovered clock for each of the data rates considered without transmission. First of all, two QDash-MLLDs were utilised, QDash-MLLD-2 and QDash-MLLD-3. The former laser was used to achieve synchronisation to incoming coherent 80 and 160 Gb/s RZ-OOK signals, and the latter one to accomplish synchronisation to coherent 320 Gb/s RZ-OOK. On one hand, the QDash-MLLD-2 was operated at room temperature and only 1 dB of optical power penalty to achieve synchronisation at a higher bit rate. On the other hand, operation of the QDash-MLLD- 3 at room temperature was not possible and it had to be controlled at a lower temperature to accomplish synchronisation at 320 Gb/s. As the bit rate increases more injected optical power is required. The main reasons for these differences have been given in Subsection 6.2.1; it is also expected that synchronisation of a QDash-MLLD at high speed relies on fewer modes due to the increase in the mode spacing at higher multiples of the original mode spacing of the QDash-MLLD spectrum. To compensate for the reduction in the number of modes, the contributing modes must be more powerful. This can explain a deterioration in the RF peak to noise ratio of the RF spectra (as analysed in Chapter 5) resulting in more phase noise as well as timing jitter (see table 6.1). Nevertheless, based on the experimental works carried out in this Section, some good ways to overcome the increment of phase noise associated to the increase in the bit rate of the injected data signal can be identified. This can be done by injecting more optical power into the QDash-MLLD (as mentioned above for the dynamic range analysis) as

101

well as an adjustment to lower temperatures of the laser from the room temperature (25 °C), (see table 6.1). The changes in temperature help to reduce the amount of spontaneous emission and as a consequence the longitudinal phase correlation of the modes is stable enough to achieve the synchronisation.

The results presented in table 6.1 are consistent with our expectations as it was shown previously in Chapters 3 and 5. It can be concluded in this regard, that once the synchronisation of the QDash-MLLD to incoming optical data signals is achieved, the RF spectral linewidth is reduced (when compared to its free running condition) and a linewidth of less than 1 kHz is resolved. Moreover, an increment in the timing jitter of the recovered clock signal is obtained with the increase in the data speed of the incoming optical data signals but still providing less than 300 fs. In terms of temperature control, they indicate that it is still possible to reach lower timing jitter for 80 Gb/s and 160 Gb/s than the ones listed in table 6.1 if a reduction in the operating temperature is implemented. Furthermore, these results allow speculating that it would be possible to achieve synchronisation to a 640 Gb/s data signal. Even more important are the outcomes shown in this Chapter, as the synchronisation is demonstrated with injected signals lacking in the 40 GHz component [34]. Otherwise, the synchronisation would be easier for an incoming signal with such a spectral component. This reinforces the explanation on the dependence of the power injection with the bit rate.

Finally, the low values of timing jitter displayed in table 6.1 are also suitable for demultiplexing of data signals, as will be shown in the next Section of this Chapter.

Bit rate	80 Gb/s	160 Gb/s	320 Gb/s
QDash-MLLD:	2	2	3
Temperature (QDash-MLLD):	25 °C	25 °C	21.7 °C
Bias current (QDash-MLLD):	86 mA	86 mA	117 mA
Power injected:	4 dBm	5 dBm	7 dBm
RF linewidth:	< 1 kHz	< 1 kHz	< 1 kHz
Timing jitter (100 Hz to 10 MHz):	62 fs	92 fs	94 fs

Table 6.1: Comparison of the QDash-MLLD operational conditions and main attributes of the recovered clock signal for the three data rates analysed for the sub-harmonic synchronisation without transmission over fibre.

6.3   Demultiplexing of high bit rate signals

As demonstrated in the previous Section, the recovered clock from the high speed data rates used in this work presents an exceptionally low timing jitter. This feature allows using the

recovered clock to demultiplex the incoming signals into tributaries at 40 Gb/s providing a direct evaluation of the clock recovery based QDash-MLLD as well as enabling more functions for the OTDM high speed networks. Demultiplexing is an important element as it allows the establishment of a direct connection between the ultrafast optical signals on OTDM systems and the lower speed electronic systems at the receiver end [31]. In this Section, demultiplexing of the incoming data signals to tributaries at 40 Gb/s is performed and analysed with BER measurements by using two techniques available in the laboratory. These techniques involve the use of an EAM for demultiplexing of incoming signals at 80 and 160 Gb/s and a fibre based NOLM configuration to all-optical demultiplexing of incoming signals at 320 Gb/s.

The optical demultiplexing of the signals based on an EAM is performed by electrically driving the EAM with the recovered base-line clock signal. The optical demultiplexing of signals employing a single EAM has been used for demultiplexing of signals up to 160 Gb/s with good performance [44-46]. EAMs are suitable for demultiplexing owing to their advantages in terms of stability, easy controlling, and high integrability [11], [47]. However, it presents some drawbacks due to its relatively high insertion loss and relatively wide time switching window. This may cause adjacent-channel crosstalk limiting its performance when demultiplexing signals beyond 160 Gb/s. In order to go beyond 160 Gb/s, it would be required to increase the complexity of the system by using some other components, such as another EAM, RF amplifiers, etc., which would increase its cost [48]. In this regard, a fibre based method such as the use of a NOLM is a good solution. The NOLM has been demonstrated for all-optical demultiplexing of signals beyond 160 Gb/s [49-52]. It is based on the Sagnac interferometric configuration, where two interfering light beams follow the same path in opposite directions [35], [36], [53-54]. Basically, it consists of two couplers, one of which is a bidirectional coupler, whose two outputs are connected to a fibre loop as depicted in Fig. 6.8. The other coupler, which is a WDM coupler, is used to introduce the control pulses into the loop. The input OTDM data field (signal) is divided by the directional coupler into two counter propagating pulse streams. The control pulse (clock pulse) propagating on the clockwise direction is synchronised to the OTDM target channel (in red) in the fibre loop with nonlinear coefficient. In the absence of the control signal, the device acts as a mirror and the signal is returned to the input. Inside the fibre, the two counter propagating signals interact through cross phase modulation (XPM) and are phase shifted creating constructive interference switching the pulse from one output arm to the other of the coupler [49-52], [54]. As it is shown in Fig. 6.8, the target channel is transmitted by the NOLM as the demultiplexed field, while the remaining OTDM channels are reflected. Normally, an optical bandpass filter is used at the output of the NOLM to block the control pulses.
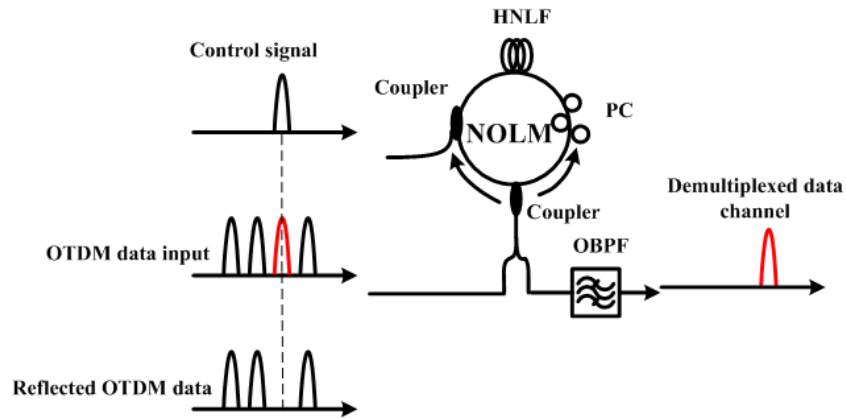
Figure 6.8: Representation of the NOLM based demultiplexer.

6.3.1 Demultiplexing of 80 Gb/s and 160 Gb/s RZ-OOK data signals to 40 Gb/s tributaries

6.3.1.1 Experimental setup

The experimental setup to investigate the synchronisation and demultiplexing of the 80 and 160 Gb/s data rate signals is depicted in Fig. 6.9. The synchronised 40 GHz optical pulses, after being photo-detected and amplified, are fed into an electro-absorption modulator (EAM, OKI OM5642W-30B) optical demultiplexer to select each of the two 40 Gb/s tributaries of the 80 Gb/s or four tributaries of the 160 Gb/s signals, respectively. This selection of channels is performed through the optical delay line (ODL). The obtained 40 Gb/s channels are then detected and tested by a bit error rate tester (BERT, SHF 11100B), which is also triggered by the recovered 40 GHz clock. It is worth mentioning that it is not possible to demultiplex the OTDM 320 Gb/s signal with this scheme, since beyond 160 Gb/s the switching window of OTDM based on fast electro-optical-modulators (EOM) is too large to resolve the high speed modulated pulses. This leads to a larger crosstalk as the data rate increases and thus to a larger power penalty, as previously mentioned at the beginning of this Section.
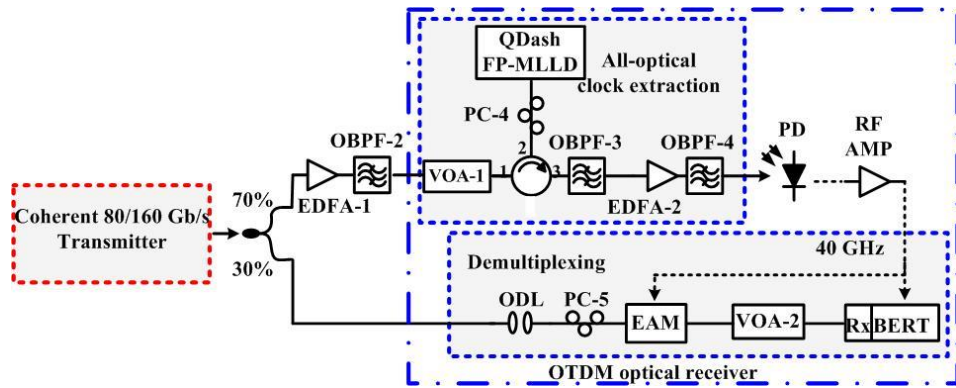
Figure 6.9: Experimental setup for the demultiplexing of 80 and 160 Gb/s RZ-OOK data signals.

6.3.1.2 Analysis of results

The BER results are given in Fig 6.10. They provide a direct evaluation of the quality of the clock and the performance of the 80-to-40 Gb/s demultiplexer. The 80 Gb/s back-to-back (B2B) BER curves labelled by a black dot are achieved by varying the optical power of the original OTDM signal received into the demultiplexer and using the electrical clock signal provided by the transmitter. They are used as the reference for the measurement of the power penalty. The BER curves are similar since they represent the two tributary contributions to the 80 Gb/s channel. The 80 Gb/s B2B after WC curves have been achieved by varying the optical power of the wavelength converted signal going into EAM based optical demultiplexer while triggering the EAM with 40 GHz clock from the transmitter. They are labelled with red squares. The 80 Gb/s BER curves after wavelength conversion and demultiplexing by the optical recovered clock signal are labelled with a blue star. With the same scheme but after 52 km of SMF, the curves are labelled with a reverse green triangle. It can be seen from these two curves that the optical synchronised signal can be used as a 40 GHz optical clock for the demultiplexing of optical signals achieving error free ($10e^{-9}$) for an optical injection power of at least -12 dBm. A power penalty of 1.5 dB is measured when compared with the B2B [34]. The primary source of this penalty is the pulse broadening of the input signals (caused by the chromatic dispersion of the HNLF) and the extra amplitude noise introduced during the wavelength conversion scheme at this bit rate.
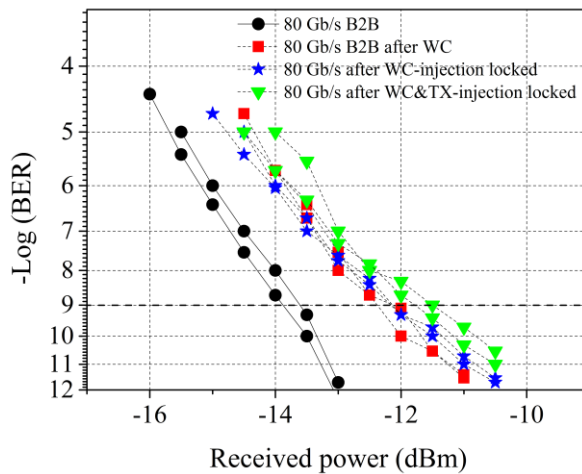
Figure 6.10: BER results for an input at 80 Gb/s; black dots, B2B; red squares, B2B after WC; blue stars, after WC and using the recovered clock; green inverted triangles, after WC and transmission using the recovered clock.

Similar experiments have been carried out at 160 Gb/s (see Fig. 6.11). In the case of 160 Gb/s, four tributaries at 40 Gb/s are demultiplexed. It can be observed that when the power dependence of the BER of the original B2B 160 Gb/s OTDM signal is compared with that of the phase coherent 160 Gb/s RZ-OOK a 1.5 dB penalty is present. It can be concluded that the WC is the main source of power penalty. This is due to the data pulse broadening and extra amplitude noise introduced during the wavelength conversion. In addition, there is an interesting result when comparing between the BER traces of the phase coherent WC 160 Gb/s RZ-OOK without transmission, while using the original clock and the recovered clock, respectively. It is found that there is a negligible penalty between the two cases, which indicates that the recovered clock, in spite of having 34 fs more timing jitter than the original clock (see Fig. 6.5), is still very good quality (sufficiently low timing jitter) and capable of efficiently demultiplexing a 160 Gb/s data signal. The transmission over 52 km introduces a further power penalty of 1.5 dB. The overall penalty of the tributaries after transmission is 3 dB with respect to the B2B electrical scheme. However, the BER is still error free ($10e^{-9}$) for a reasonable received optical power of -8 dBm.

An important fact from these results when comparing BER traces at 80 Gb/s and at 160 Gb/s with the transmission scheme and reaching error free ($10e^{-9}$) is that by doubling the data rate, it was necessary to increase power by 4 dB, as can be seen by comparing Figs. 6.10 and 6.11.
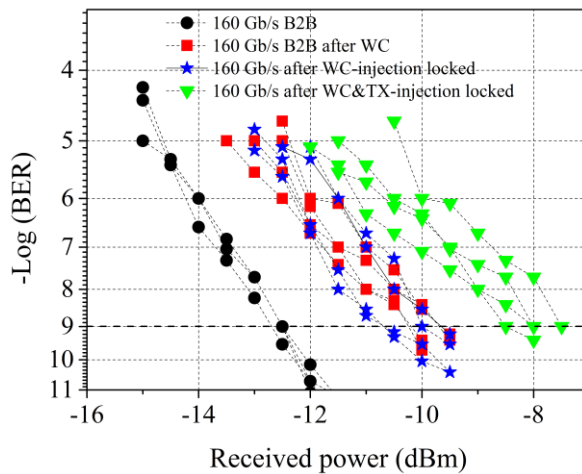
Figure 6.11: BER results for an input at 160 Gb/s; black dots, B2B; red squares, B2B after WC; blue stars, after WC and using the recovered clock; green inverted triangles, after WC and transmission using the recovered clock.

6.3.2 All-optical demultiplexing of coherent 320 Gb/s RZ-OOK data signal to 40 Gb/s tributaries

6.3.2.1 Experimental setup

Fig. 6.12 shows the experimental setup corresponding to the receiver for demultiplexing of the coherent 320 Gb/s RZ-OOK. As it is not possible to demultiplex the 320 Gb/s signal with the previous scheme, for the reasons already given in the introduction to this Section, an all-optical scheme based on a nonlinear optical loop mirror (NOLM) is used. At the output of the injection locked QDash-MLLD, the recovered optical 40 GHz clock is selected out through a 5 nm optical band-pass filter (OBPF-3). Owing to the positive chirp of the optical pulses, 125 m SMF (piece of fibre available) are deployed to compress the pulses to a 1.9 ps width. The 40 GHz optical clock pulse is then amplified (EDFA-2) and filtered (OBPF-4) before being fed into the NOLM to all-optically time demultiplex the 320 Gb/s into 8x40 Gb/s tributaries. The selection of tributaries is performed with the ODL. After the all-optical time demultiplexing, the 40 Gb/s signals are detected and analysed by a BERT (SHF 11100B), which is clocked by the recovered 40 GHz clock.
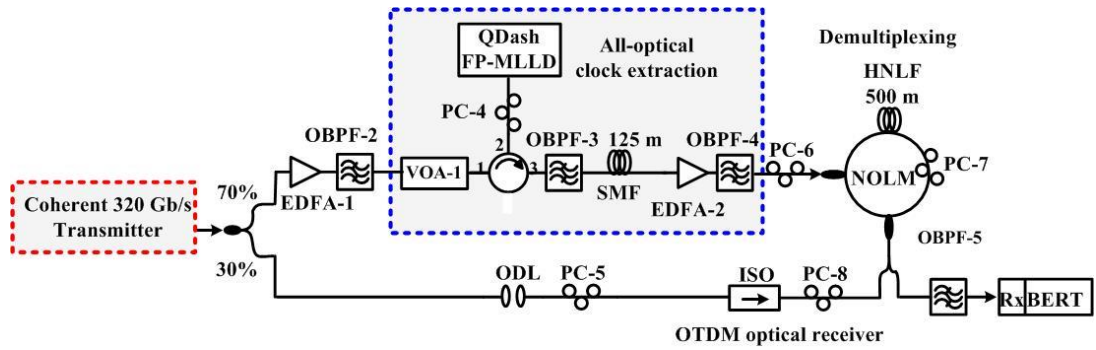
Figure 6.12: Experimental setup for all-optical demultiplexing of coherent 320 Gb/s RZ-OOK.

6.3.2.2   Analysis of results

The BER results are given in Fig 6.13. They provide a direct evaluation of the quality of the clock and the performance of the 320-to-40 Gb/s all-optical demultiplexer. In this figure, the 40 Gb/s back-to-back (B2B) BER curve labelled by a black dot is achieved by using the 40 GHz optical clock from the transmitter. This curve is used to benchmark the performance of the QDash-MLLD. The B2B BER curves of the coherent 320 Gb/s OTDM signal demultiplexed by the 40 GHz optical clock pulses directly provided by the transmitter are labelled with red squares. In addition, the BER curves of the 320 Gb/s signal demultiplexed by using the 40 GHz optical clock pulse recovered from the QDash-MLLD are shown in blue stars. They provide similar performance to the 320 Gb/s B2B BER curves, and have only a 1 dB penalty when compared to the 40 Gb/s B2B BER curve. These results indicate that in spite of 44 fs more timing jitter in the recovered clock signal, when compared to the original clock from the transmitter (see Fig. 6.6), the timing jitter of the recovered clock is low and sufficiently enough to achieve high quality pulses to efficiently demultiplex data signals at 320 Gb/s. Moreover, it can be seen from these two curves that the optical synchronised signal can be used as a 40 GHz optical clock for the demultiplexing of optical signals achieving error free performance for an optical injection power at the receiver of at least -10 dBm, reaching the same performance as for 160 Gb/s, as can be seen in Fig. 6.11.
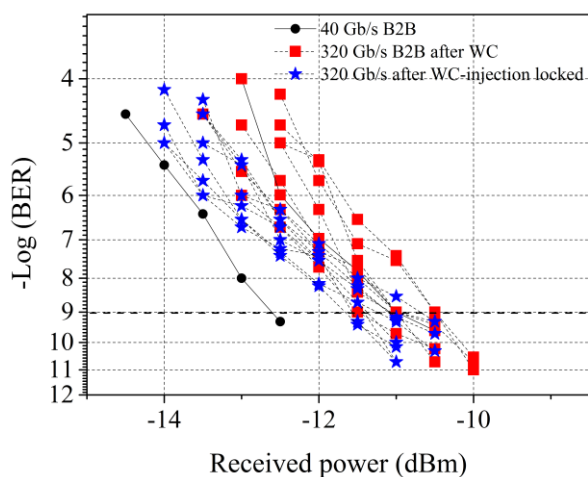
Figure 6.13: BER results for an input at 320 Gb/s; black dots, B2B; red squares, B2B after WC and using clock from the transmitter; blue stars, after WC and using recovered clock.

6.4 Summary

In this Chapter, sub-harmonic all-optical clock recovery for data rates up to 320 Gb/s was demonstrated. Two packaged Dash-MLLDs were utilised. The first QDash-MLLD-2 was synchronised to incoming coherent RZ-OOK data signals at 80 and 160 Gb/s and an optical clock signal was recovered. In addition, this investigation was expanded by propagating such signals over 52 km of optical fibre. The quality of the optical clock signals were evaluated through the analysis of the RF beat-tone signal with phase noise and timing jitter measurements. The recovered clocks have timing jitter values of less than 100 fs. Furthermore, the second QDash-MLLD-3 was subjected to synchronisation of coherent RZ-OOK data signal at 320 Gb/s. The assessment of the recovered clock was performed in the same way as that for the synchronisation to 80 and 160 Gb/s. The recovered clock features a timing jitter of 94 fs. For the three different data speeds, the clock recovery systems based on the QDash-MLLDs demonstrated good results within no less than 20 nm of detuning between the recovered clock and input data optical spectra.

Owing to the good performance of the recovered clock signals obtained from the synchronisation to the incoming data signals at 80, 160 and 320 Gb/s, the next step was to enable them to demonstrate more functions for the high speed OTDM system. In this regard, the optical clock pulses were used to demultiplex the incoming signals to tributaries of 40 Gb/s. Firstly, the demultiplexing of the signals at 80 and 160 Gb/s with and without transmission to 40 Gb/s tributaries were performed using an EAM, clocked by the recovered pulses from QDash-MLLD, and assessed through BER measurements and retrieving error free performance.

Finally, a 320 Gb/s to 40 Gb/s all-optical demultiplexing system was demonstrated by using a NOLM, also achieving error free performance.

The results presented in this Chapter confirm that the QDash-MLLD is a reliable and cost-effective solution to all-optical signal processing at high bit rates. In the next Chapter, a further analysis of the QDash-MLLD dynamic is carried out in order to investigate the capability of the device to achieve clock recovery for burst/packet switched networks.

References

[1] H. Yokoyaina, Y. Hashimolo, H. Kmila, and I. Ogura, "Two-stage all-optical subharmonic clock recovery using modelocked semiconductor lasers," *Electronics Letters*, vol. 36, no. 18, pp. 1577-1578, Aug. 2000.

[2] R. Salem, A. A. Ahmadi, G. E. Tudury, G. M. Carter, and T. E. Murphy, "Two-photon absorption for optical clock recovery in OTDM networks," *IEEE Journal of Lightwave Technology*, vol. 24, no. 9, pp. 3353-3362, Sep. 2006.

[3] H. Murai, M. Kagawa, H. Tsuji, and K. Fujii, "EA-modulator-based optical time division multiplexing/demultiplexing techniques for 160-Gb/s optical signal transmission," *Journal of Selected Topics in Quantum Electronics*, vol. 13, no. 1, pp. 70-78, Jan/Feb. 2007.

[4] E. S. Awad, P. S. Cho, and J. Goldhar, "Simultaneous four-wave mixing and cross-absorption modulation inside a single EAM for high-speed optical demultiplexing and clock recovery," *IEEE Photonics, Technology Letters*, vol. 17, no. 7, pp. 1534-1536, Jul. 2005.

[5] E. S. Awad, P. S. Cho, N. Moulton, and J. Goldhar, "Subharmonic optical clock recovery from 160 Gb/s using time-dependent loss saturation inside a single electroabsorption modulator," *IEEE Photonics Technology Letters,* vol. 15, no. 12, pp. 1764-1766, Dec. 2003.

[6] R. Ludwig, U. Feiste, C. Schmidt, J. Berger, E. Hilliger, M. Kroh, T. Yamamoto, C. M. Weinert, and H. G. Weber, "Enabling transmission at 160 Gbit/s," *in Proceedings of Optical Fiber Communications Conference, OFC 2002*, paper TuA1, pp. 1-2, Anaheim, CA, Mar. 2002.

[7] L. Moller, Y. Su, C. Xie, R. Ryf, X. Liu, X. Wei, and C.R. Doerr, "Enabling 160 Gbit/s transmitter and receiver designs," *in Optical Fiber Communications Conference,2005, OFC 2005,* vol. 4, paper OThR3, Mar. 2005.

[8] H. Tsuchida, "Subharmonic optoelectronic oscillator," *IEEE Photonics Technology Letters,* vol. 20, no. 17, pp. 1509-1511, Sep. 2008.

[9] J. Lasri, P. Devgan, R. Tang, and P. Kumar, "Ultra-low timing jitter 40Gb/s clock recovery using a novel electroabsorption-modulator-based self-starting optoelectronic oscillator," *in the 2003 Annual Meeting of the IEEE Lasers and Electro-Optics Society*

(LEOS'03) , 2003, paper TuY6.

[10] H. Tsuchida and M. Suzuki, "40-Gb/s clock recovery using an injection-locked optoelectronic oscillator," *IEEE Photonics Technology Letters,* vol. 17, no. 1, pp. 2611–213, Jan. 2005.

[11] C. Boemer, C. Schubert, C. Schmidt, E. Hilliger, V. Marembert, J. Berger, S. Ferber, E. Dietrich, R. Ludwig, and H.G Weber, "160 Gbitk clock recovery with electro-optical PLL using bidirectionally operated eleetroabsorption modulator as phase comparator," *in Optical Fiber Communications Conference,2003, OFC 2003*, vol. 2, pp. 670-671, paper FF3.

[12] L.K. Oxenlowe, F. Gomez-Agis, C. Ware, S. Kurimura, H. C. H. Mulvad, M. Galili, H. Nakajima, J. Ichikawa, D. Erasme, A. T. Clausen, and P. Jeppesen, "640-Gbit/s data transmission and clock recovery using an ultrafast periodically poled lithium niobate device," *IEEE Journal of Lightwave Technology*, vol. 27, no. 3, pp. 205-213, Feb. 2009.

[13] H. C. H. Mulvad, E. Tangdiongga, H.de Waardt, and H. J. S. Dorren, "40 GHz clock recovery from 640 Gbit/s OTDM signal using SOA-based phase comparator," *Electronics Letters*, vol. 44 , no. 2, pp. 146-147, Jan. 2008.

[14] N. Jia, T. Li, K. Zhong, J. Sun, M. Wang, and J. Li, "Simultaneous clock enhancing and demultiplexing for 160-Gb/s OTDM signal using two bidirectionally operated electroabsorption modulators," *IEEE Photonics Technology Letters*, vol. 23, no. 21, pp. 1615–1617, Nov. 2011.

[15] M. Jinno and Matsumoto, "All-optical timing extraction using 1.5 mm self pulsating multielectrode DFB LD," *Electronics Letters*, vol. 24, no. 23, pp. 1426–1427, 1988.

[16] H. Yokoyama, Y. Hashimoto, H. Kurita, and I. Ogura, "All-optical subharmonic clock recovery and demultiplexing," *in Proceedings of Optical Fiber Communications Conference, 2000, OFC, 2000*, vol. 3, pp. 232–234, Mar. 2000.

[17] T. Ohno, K. Sato, T. Shimizu, T. Furuta, and H. Ito, "Recovery of 40 GHz optical clock from 160 Gbit/s data using regeneratively modeloked semiconductor laser," *Electronics Letters*, vol. 39, no. 5, pp. 453–455, Mar. 2003.

[18] S. Arahira, S. Sasaki, K. Tachibana, and Y. Ogawa, "All-optical 160-Gb/s clock extraction with a mode-locked laser diode module," *IEEE Photonics Technology Letters*, vol. 16, no. 6, pp. 1558–1560, Jun. 2004.

[19] S. Arahira and Y. Ogawa, "Retiming and reshaping function of alloptical clock extraction at 160 Gb/s in monolithic mode-locked laser diode," *IEEE Journal of Quantum Electronics*, vol. 41, no. 7, pp. 937–944, Jul. 2005.

[20] J. C. Cartledge, X. Tang, M. Yañez, M. Shen, A. Akrout, and G. H. Duan, "All-optical clock recovery using a quantum-dash Fabry-Pérot laser," *in Proceedings of IEEE Microwave. Photonics Conference, 2010*, paper TH3-1. pp. 201-204, Oct. 2010.

[21] J. Renaudier, B. Lavigne, P. Gallion, and G.-H. Duan, "Study of Phase-Noise Properties and Timing jitter of 40-GHz all-optical clock recovery using self-pulsating semiconductor lasers," *IEEE Journal of Ligthwave Technology*, vol. 24, no. 10, pp. 3734-3742, Oct. 2006.

[22] L. K. Oxenlowe, D. Zibar, M. Galili, A. T. Clausen, L. J. Christiansen and P. Jeppesen, "Clock recovery for 320 Gb/s OTDM data using filtering-assisted XPM in an SOA," *in Lasers and Electro-optics Europe, 2005, CLEO/Europe,* Conference on. C13-4-MON, Munich, Germany, Jun. 2005.

[23] V. Roncin, A. O'Hare, S. Lobo, E. Jacquette, L. Bramerie, P. Rochard, Q.-T. Le, M. Gay, J.-C. Simon, A. Shen, J. Renaudier, F. Lelarge, and G.-H. Duan, "Multi-data-rate system performance of a 40-GHz all-optical clock recovery based on a quantum-dot Fabry-Pérot laser," *IEEE Photonics Technology Letters*, vol. 19, no. 19, pp. 1409-1411, Oct. 2007.

[24] M. Costa e Silva, A. Lagrost, L. Bramerie, M. Gay, P. Besnard, M. Joindot, J. C. Simon, A. Shen, and G.H. Duan, "Up to 425 GHz all-optical frequency down-conversion clock recovery based on quantum dash Fabry-Pérot mode-locked laser," *IEEE Journal of Ligthwave Technology*, vol. 29, no. 4, pp.609-615, Feb. 2011.

[25] R. Maldonado-Basilio, S. Latkowski, S. Philippe, and P. Landais, "Experimental investigation of harmonic and subharmonic synchronization of 40 GHz mode-locked quantum dash laser diodes," *Optics letters,* vol. 36, no. 9, pp. 1569-1571, May 2011.

[26] F. Lelarge, B. Dagens, J. Renaudier, R. Brenot, A. Accard, F. van Dijk, D. Make, O. Le Gouezigou, J.-G. Provost, F. Poingt, J. Landreau, O. Drisse, E. Derouin, B. Rousseau, F. Pommereau, and G.-H. Duan, "Recent advances on InAs/InP quantum dash based semiconductor lasers and optical amplifiers operating at 1.55 μm," *IEEE Journal of Selected Topics in Quantum Electronics,* vol. 13, no. 1, pp. 111-124, Jan./Feb. 2007.

[27] F. Lelarge, F. Pommereau, F. Poingt, L. Le Gouezigou, and O. Le Gouezigou, "Active mode-locking of quantum dot Fabry-Pérot laser diode," *in IEEE 20th International Semiconductor Laser Conference, 2006. Conference Digest. 2006*, 1708132, pp. 153-154, 2006.

[28] G.-H. Duan, A. Shen, A. Akrout, F. V. Dijk, F. Lelarge, F. Pommereau, O. LeGouezigou, J.-G. Provost, H. Gariah, F. Blache, F. Mallecot, K. Merghem, A. Martinez, and A. Ramdane, "High performance InP-based quantum dash semiconductor mode-locked lasers for optical communications," *Bell Labs Technical Journal*, vol. 14,

no. 3, pp. 63-84, Nov. 2009.

[29] R. Maldonado-Basilio, J. Parra-Cetina, S. Latkowski, Nicola Calabretta, and P.Landais, "Experimental investigation of the optical injection locking dynamics in single section quantum-dash Fabry-Perot laser diode for packet-based clock recovery applications," *IEEE Journal of Lightwave Technology*, vol. 31, no.6, pp. 860-865, Mar. 2013.

[30] J. Luo, J. Parra-Cetina, and P. Landais, H. J. Dorren, and N. Calabretta, "40G burst mode optical clock recovery after 52 km transmission enabled by a dynamically switched quantum dash mode-locked laser," *presented in the 39th European Conference and Exhibition on Optical Communication, ECOC 2013*, London, UK, paper Th.2.A.2. Sep. 2013.

[31] M. Yañez, and J. Cartledge, "Single harmonically driven electroabsorption modulator for OTDM demultiplexing," *IEEE Journal of Lightwave Technology*, vol. 29, no. 10, pp. 1437-1444, May. 2011.

[32] J. Luo, J. Parra-Cetina, and S. Latkowski, R. Maldonado-Basilio, P.Landais, H. Dorren, and N. Calabretta, "Quantum dash mode-locked laser based open-loop optical clock recovery for 160 Gb/s transmission system," *Optical Fiber Communications Conference 2013,OFC 2013*, Anaheim, California, USA, paper OTh4D.6, Mar. 2013.

[33] N. Calabretta, J. Luo, and J. Parra-Cetina, S. Latkowski, R. Maldonado-Basilio, P.Landais, and H. Dorren, "320 Gb/s all-optical clock recovery and time demultiplexing enabled by a single quantum dash mode-locked laser Fabry-Perot optical clock pulse generator," *Optical Fiber Communications Conference, OFC 2013*, Anaheim, USA, paper OTh4D.5, Mar. 2013.

[34] J. Parra-Cetina, J. Luo, N. Calabretta, S. Latkowski H. J. S. Dorren, and P. Landais, "Sub-harmonic all-optical clock recovery of up to 320 Gb/s signals using a quantum dash Fabry-Pérot mode-locked laser," *IEEE Journal of Lightwave Technology*, vol. 31, no. 19, pp. 3127-3134, Oct. 2013

[35] K. A. Rauschenbach, K. L. Hall, J. C. Livas and G. Raybon, "All-optical pulse width and wavelength conversion at 10 Gb/s using a nonlinear optical loop mirror," *IEEE Photonics Technology Letters*, vol. 6, no. 9, pp. 1130-1132, Sep. 1994.

[36] S. J. B. Yoo, "Wavelength conversion technologies for WDM network applications," *IEEE Journal of Lightwave Technology*, vol. 14, no. 6, pp. 955-966, Jun. 1996.

[37] B. Lavigne, J. Renaudier, F. Lelarge, O. Legouezigou, H. Gariah, and G.-H. Duan, "Polarisation-insensitive low timing jitter and highly optical noise tolerant all-optical 40-GHz clock recovery using a bulk and a quantum-dots-based self-pulsating laser cascade," *IEEE Journal of Lightwave Technology*, vol. 25, no. 1, pp.170-176, Jan. 2007.

[38] H. Soto, D. Erasme, and J. Zitlalpopoca, "Polarization-insensitive wavelength conversion with a constant output linear polarization allowing the realization of an active polarization controller," *Microwave and Optical Technology Letters*, vol. 29, no. 5 pp. 344-348, Jun. 2001.

[39] A. Somers, W. Kaiser, J. P. Reithmaier, A. Forchel, M. Gioaninni, and I. Montrosset, "Optical gain properties of InAs/InAlGaAs/InP quantum dash structures with a spectral gain bandwidth of more than 300 nm," *Applied Physics Letters*, vol. 89, no. 6, pp. 061107-3, Aug. 2006.

[40] Y. J. Wen, D. Novak and H. F. Liu, "Mode-locking of long cavity Fabry-Perot semiconductor laser at millimetre wave frequencies by subharmonic optical injection," *Electronics Letters*, vol. 36, no. 10, pp. 879-881, May. 2000.

[41] A. Murakami, K. Kawashima, and K. Atsuki, "Cavity resonance shift and bandwidth enhancement in semiconductor lasers with strong light injection," *IEEE Journal of Quantum Electronics*, vol. 39, no. 10, pp. 1196-1204, Oct. 2003.

[42] R. Maldonado-Basilio, S. Latkowski, S. Philippe, and P. Landais, "40 GHz mode-beating with 8 Hz linewidth and 64 fs timing jitter from a synchronised mode-locked quantum-dash laser diode," *Optics Letters*, vol. 36, no. 16, pp. 3142-3144, Aug. 2011.

[43] J. Parra-Cetina, S. Latkowski, R. Maldonado-Basilio, and P. Landais, "Wavelength tunability of all-optical clock-recovery based on quantum-dash mode-locked laser diode under injection of a 40-Gb/s NRZ data stream," *IEEE Photonics Technology Letters,* vol. 23, no. 9, pp. 531-533, May. 2011.

[44 H. Murai, M. Kagawa, H. Tsuji, and K. Fuji, "EA-modulator-based optical time division multiplexing/demultiplexing techniques for 160-Gb/s optical signal transmission," *IEEE Journal Selected Topics in Quantum Electronics,* vol. 13, no. 1, pp. 70–78, Jan. 2007.

[45] F. Futami, S. Ono, and S. Watanabe, "160-Gb/s optical demultiplexing with enhanced timing tolerance by unequally aligning pulse position," *in European Conference and Exhibition on Optical Communication,2005. ECOC 2005*, Glasgow, U.K., vol. 3, pp. 387-388, paper We2.2.6, Sep. 2005.

[46] H. F. Chou, J. E. Bowers, D. J. Blumenthal, "Compact 160Gb/s add-drop multiplexer with a 40 Gb/s base rate using electroabsorption modulators," *IEEE Photonics Technology Letters*, vol. 16, no. 6, pp. 1564- 1566, Jun. 2004.

[47] M. Chen, G. Tao-rong, D. Lu, B. Lv, L. Tang-jun, S-S. Jian, "Clock recovery and demultiplexing for 80Git/s OTDM system," *Photonics and Optoelectronics, 2009. SOPO 2009. Symposium on*, Digital Object Identifier: 10.1109/SOPO.2009.5230248, pp. 1-3, Aug. 2009.

[48] N. Deng, C.-K. Chan, and L.-K. Chen, "A hybrid OTDM scheme with enhanced demultiplexing performance," *IEEE Photonics Technology Letters*, vol. 19, no. 19, pp. 1454-1456, Oct. 2007.

[49] M. Galili, H.C.H. Mulvad, L.K. Oxenlowe, H. Hu, E. Palushani, A.T. Clausen, and P. Jeppesen, "Generation and detection of 2.56 Tbit/s OTDM data using DPSK and polarization multiplexing," *Optical Fiber Communication (OFC), Collocated National Fiber Optic Engineers Conference, 2010 Conference on.* pp. 1-3, paper OThV2, Mar. 2010.

[50] A. T. Clausen, A. I. Siahlo, J. Seoane, L. K. Oxenlowe, and P. Jeppesen, "320 to 10 Gbit/s demultiplexing using NOLM based on commerically available components," *Electronics Letters*, vol. 41, no. 5, pp. 265–266, Mar. 2005.

[51] T. Yamamoto, E. Yoshida, and M. Nakazawa, "Ultrafast nonlineal optical loop mirror for demultiplexing 640 Gb/s TDM signals," *Electronics Letters*, vol. 34, no. 10, pp. 1013-1014, May. 1998.

[52] E. Palushani, H. Hu, M. Galili, H. C. H. Mulvad, R. Slavik, L.K Oxenlowe, A. T Clausen, and P. Jeppesen, "640 Gbit/s polarisation-independent demultiplexing in a standard nonlineal optical loop mirror using cascaded long-period grating pulse shaper," *annual meeting IEEE Photonics society, 2010*, pp. 203-204, paper. 10.1109, Nov. 2010.

[53] N. J. Doran, and D. Wood, "Nonlinear-optical loop mirror," *Optics Letters*, vol. 13, no. 1, pp. 56-58, Jan. 1988.

[54] D. Wang, A. Golovchenko, A. N. Pilipetskii, C. R. Menyuk, and M. F. Arend, "Nonlinear-optical loop mirror," *IEEE Journal of Lightwave Technology,* vol. 15, no. 4, pp. 642-646, Apr. 1997.

Chapter 7

Experimental investigation on the dynamics of a quantum dash mode-locked laser towards the synchronisation and clock recovery of data packets

7.1 Introduction

We have seen in Chapter 4 that the QDash-MLLD is capable of generating optical pulses as well as of being synchronised to series of pulses. The recovered synchronised signal comprises stable 40 GHz clock pulses featuring a pulse-width of 1.8 ps and sub-picosecond timing jitter [1]. That was the first step towards the investigation of the capability of the device to synchronise its frequency to OTDM data or in other words, to achieve clock recovery.

In Chapters 5 and 6 all-optical clock recoveries at line bit rate of 40 Gb/s and sub-harmonic from up to 320 Gb/s data rate were demonstrated, respectively. As has been already mentioned in Chapter 1, clock recovery is a key function for all-optical signal processing at high bit rate, not only for OTDM systems but also for packet switching data in current and future optical networks. In this sense, the next step is to demonstrate that the QDash-MLLD can be used for clock recovery of data packets.

Current optical networks are not fully deployed with packet switching technology due to technological constraints directly associated with the switching operation at the receivers of the nodes of the network [2-5]. However, in the metro access networks (MAN) optical burst switching (OBS) is used as an alternative technology [3], [4]. In OBS, a burst data consists of multiple packets which are grouped and switched through the network all-optically [2], [5]. As

mentioned above, one of the main issues in present burst networks, is regarding the receiver. Burst-mode receivers have to be dynamic to the arrival of the data packets [2], [6].

An important function to study in the receivers is its synchronisation to incoming data. Indeed, a system where an asynchronous packet based clock extraction circuitry at the receiver end operates at very fast locking and unlocking times (few tens of ns) is necessary. For instance, assuming packets typically comprised of 1500 bytes and transmitted at 100 Gb/s data rate, it results in time slots of 120 ns per packet. To optimise the load at which such a system can operate, the guard times between the packets have to be small, in the order of a few tens of nanoseconds. In current MANs, clock recovery is achieved by using optoelectronic means such as global clocks or phase-locked loop (PLL) oscillators. However, they are limited to the speed of their electronic components [3], [6], [7]. Consequently, more work still has to be done in regard to faster data rates (>40 Gb/s). There have been a variety of approaches for clock recovery; in some of these techniques, CR circuits still based on electronic phase-locked loops and mode-locked ring-lasers exhibit a relatively long time for synchronisation and are not suitable for asynchronous short optical packets. On the other hand, a synchronisation time of 1 ns has been reported after extracting an inline bit rate clock signal from 10 Gb/s data packets using a SPL based on a distributed Bragg reflector with detuned gratings [8]. Packet based clock recovery approaches featuring a faster response have also been investigated utilising low finesse Fabry-Pérot filters (FPF). An instantaneous synchronisation and a 400 ps persistence time (or de-synchronisation) from short and closely spaced optical packets at 40 Gb/s has been obtained using a FPF followed by an ultrafast nonlinear interferometer based on a semiconductor optical amplifier (SOA) [9]. A photonic integrated version of this concept but utilising a Mach-Zehnder interferometer was reported in [10]. Unlike the aforementioned experiments with on-off keying (OOK) return-to-zero (RZ) pulsed data streams, inline bit rate optical clock has also been extracted from 10 Gb/s non-return-to-zero (NRZ) differential phase shift keying data utilising a FPF followed by an SOA gate [11]. Instantaneous synchronisation and de-synchronisation was obtained. Despite the remarkable achievements in terms of ultrafast synchronisation and de-synchronisation times, the complexity, bulkiness, and limited operation speed of some experimental demonstrations, in addition to a reduction of the components (which eventually translates into less energy consumption for operation) seem to be motivating aspects for further improvement. In this sense clock recovery based on quantum dash mode-locked lasers are potentially a good option owing to their small size, low energy consumption, and low cost as well as some of the other features previously mentioned in Chapters 1 and 3.

This Chapter presents experimental investigations of the fast dynamic characteristics of the QDash Fabry-Pérot (FP) passively mode-locked laser diode (PML-LD) for all-optical packed based clock recovery applications. Firstly, in Section 7.2, the switching on and characteristic times of the passive mode-locking mechanism with pulsed biasing current are assessed.

Secondly, in Section 7.3, the locking and unlocking characteristic times of the QDash-MLLD subject to external optical injection are estimated by using two methods. The first method, is based on the concept presented in [12] and focuses on an analysis of the instantaneous frequency of the 40 GHz beat-tone signal measured at the output of the laser under investigation, which after a frequency down-conversion (FDC) stage, is recorded by a real-time oscilloscope (RTO). The second method is based on a direct measurement with an electrical sampling oscilloscope synchronised to the incoming burst data signal [13].

7.2 Switch-on and passive mode-locking times of a quantum dash mode-locked laser diode

In this Section, investigation of the switch-on and passive mode-locking times of the QDash-MLLD is carried out. This study is important as a first step prior to determining the suitability of the device to be employed as an active element for packet/burst switching clock recovery applications.

7.2.1 Experimental setup

The experimental setup to investigate the switching on and passive locking/unlocking times when the bias current of the QDash-PML-LD is turned on and off is depicted in Fig. 7.1. The pulsed bias current is provided by a synthesized clock generator (Stanford research system CG635) set at 40 kHz and 50 % duty cycle, with low and high current levels set at 0 and 100 mA, respectively. The temperature of the QDash-MLLD is set to 25°C (room temperature). The selected frequency of the clock generator allows an efficient use of the real-time scope (Agilent DSO-81004B) in terms of its internal buffer size and sampling rate, whereas it is sufficient to observe the dynamic behavior of the tested device. Moreover, the selection of the high level of the bias current relies on the operating conditions at which the QDash-PML-LD synchronises to an externally injected signal, as seen in Chapters 4, 5 and 6 [1], [14-18]. In this experiment the QDash-MLLD in its unpackaged presentation is utilised. The optical power emitted from the laser is collected through a lensed fibre and passed through an optical isolator (ISO) to avoid back reflections and the ~ 40 GHz beat-tone signal is detected on a fast (50 GHz) photo-detector (PD, u^{2}t XPDV2020R) followed by an RF amplifier. Taking into account the features of the real-time oscilloscope used in this experiment (10 GHz frequency bandwidth and 40 GSa/s sampling rate), the beat-tone signal of interest is frequency down-converted (FDC) to ~ 1 GHz by using an RF-mixer and a local oscillator (LO, Rohde & Schwarz SMR 40) set at

~ 39 GHz. It is worth mentioning two aspects merit consideration in this study. Firstly, the signal from the LO features a linewidth of a few hertz, affecting to a minimal extent the characteristics of the ~ 40 GHz beat-tone signal measured at the mixer output. Secondly, in order to obtain the passive mode-locking characteristic times with the supplied pulsed current reported in this Section, the time delay experienced by the electric signals biasing the QDash-MLLD (i.e, from the clock synthesizer to the laser p-n junction) and the synchronised beat-tone (i.e, from the QDash-MLLD output to the real-time oscilloscope) have been taken into account.
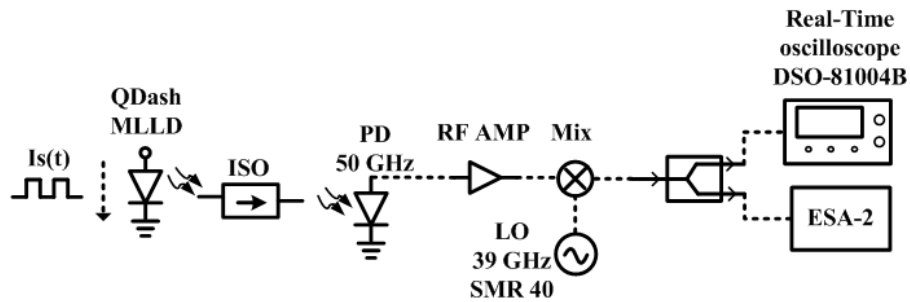
Figure 7.1: Experimental setup. Continuous (—) and dashed (---) lines denote optical and electrical links, respectively. QDash-MLLD: quantum dash mode-locked laser diode; ISO: optical isolator; PD: photo-detector; RF Amp: RF amplifier; Mix: electrical mixer; LO: local oscillator; ESA: electrical spectrum analyser (see Appendix A for equipment specifications).

7.2.2 Analysis and results

Firstly, the study of the free-running (neither external optical injection nor electrical modulation is applied to the laser) operation of the QDash-MLLD biased at 100 mA is performed. Fig. 7.2(a) shows the FDC beat-tone measured with the real-time oscilloscope within a span of 20 µs. A stable frequency component of ~ 1 GHz is observed in this signal, as depicted in the zoom-in trace of Fig. 7.2(b) within a span of 22 ns and with the help of an electrical spectrum analyser (ESA-2, Anritsu MS2668C), set at a resolution of 30 kHz and a span of 5 MHz, in Fig. 7.2(c). Moreover, the full width at half maximum (FWHM) linewidth of the down-converted signal is less than 25 kHz.
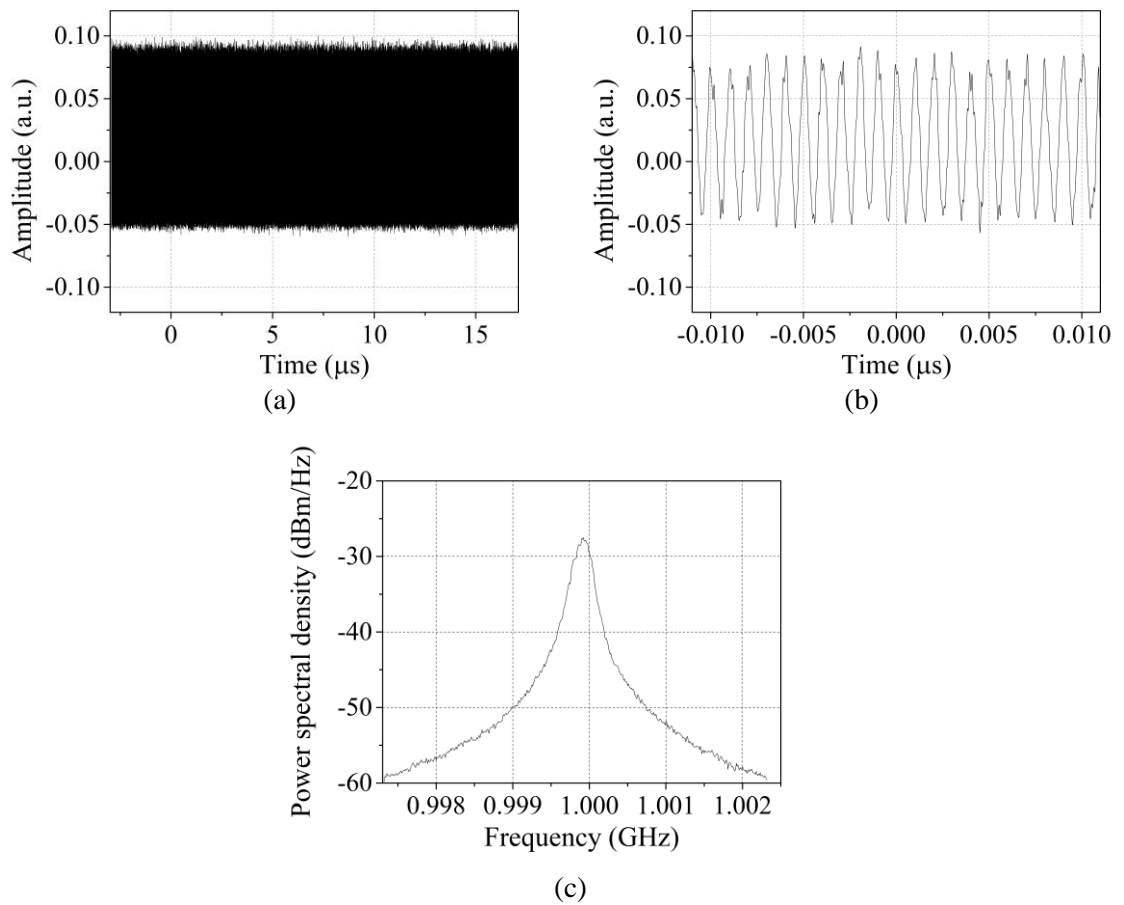
Figure 7.2: Frequency down-converted beat-tone in constant current conditions. (a)-(b) Measured with real-time oscilloscope. (c) Measured with electrical spectrum analyser set at a resolution of 30 kHz and a span of 5 MHz.

As a second part of the experiment, the current applied to the QDash-PML-LD is modulated by a clock signal at 40 kHz as shown in Fig. 7.3(a). Analysing this signal more in detail, it is measured a rising time of 41 ns (from 10% to 90% of the pulsed biasing current level) and a falling time of 39 ns (from 90% to 10 % of the pulsed biasing current level), as depicted in Figs. 7.3(b) and 7.3(c), respectively [19].
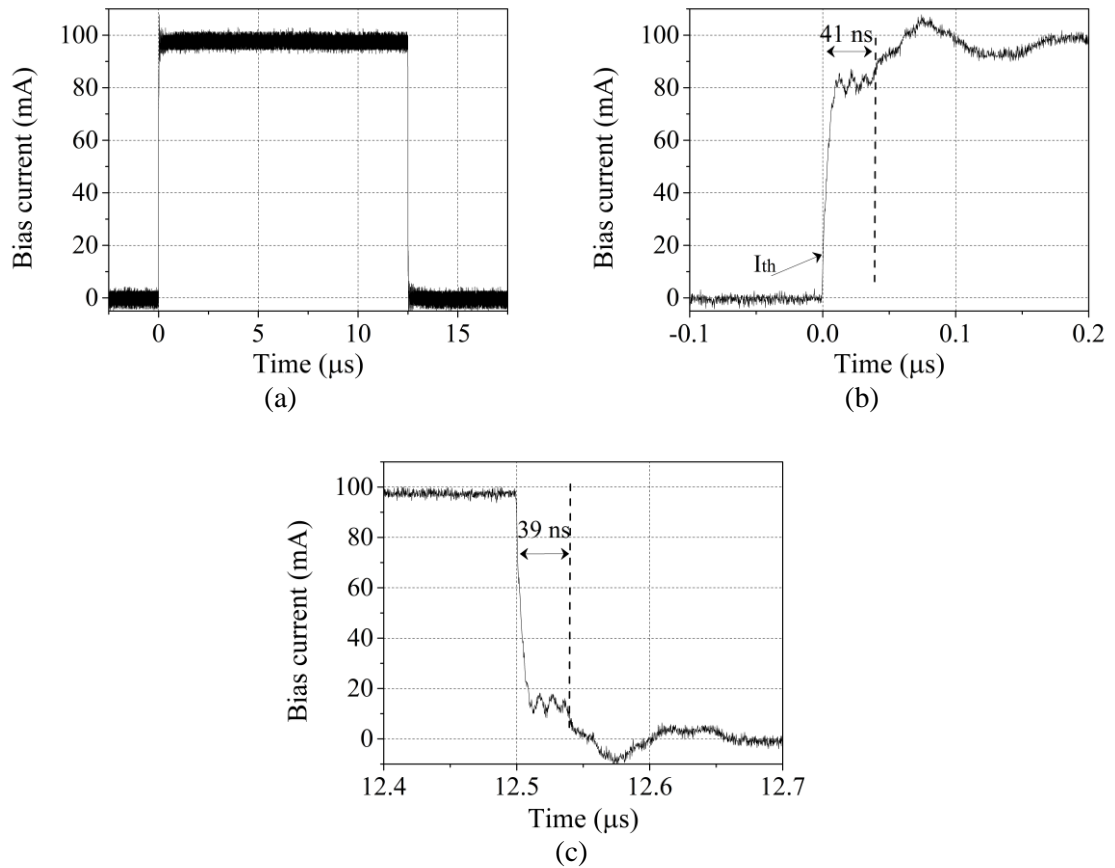
Figure 7.3: Time traces of the modulating bias current source: (a) full span, (b)-(c) zoom-in, of rising and falling times, respectively.

The time domain trace of the FDC beat-tone taken with the real-time scope is shown in Fig. 7.4(a). The starting point (time=0) of the FDC beat-tone signal is obtained after triggering the real-time oscilloscope with the electric signal biasing the QDash-MLLD visualised in another channel and adjusting the delay to a time equal to zero on both signals. Analysing the emitted power of the QDash-PML-LD (visualised in these plots as the envelope of the beat-tone), it does not exhibit an instantaneous response with the current supplied, particularly after the threshold current (I_{th}) has been reached. By zooming in the trace within 300 ns span in its leading edge, a switch-on time τ_0 of around 30 ns is observed, as showed in Fig. 7.4(b). In the same manner, Fig. 7.4 (c) illustrates the zoom in trace within a span of 300 ns for the falling edge. A mark at the time 12.539 μs indicates the point corresponding to the modulating current square shape falling time at 10% [19], [20].
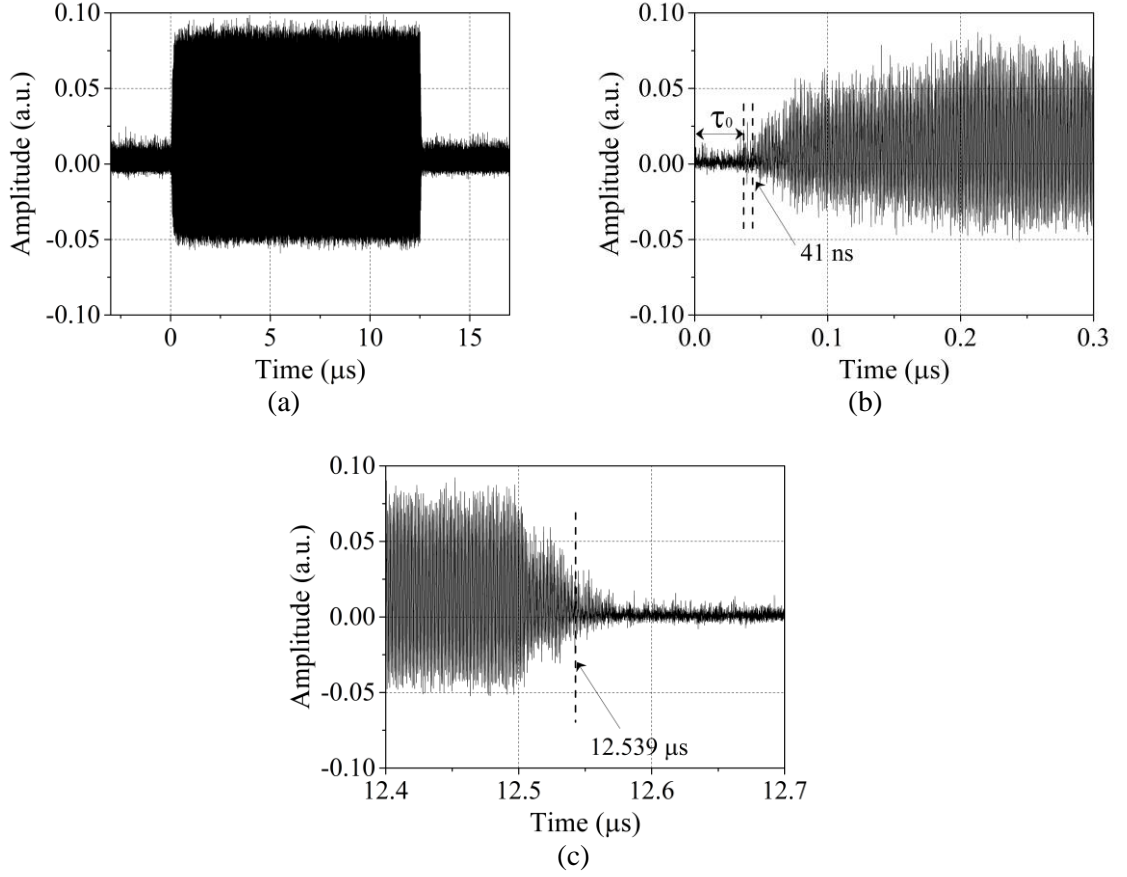
Figure 7.4: Time traces of the FDC beat-tone taken with the real-time scope: (a) full span, (b)-(c) leading and falling edges, respectively.

Furthermore, in order to determine the passive mode-locking characteristic time, relative to the point where the 90% of the supplied bias current is reached (which occurs at 41 ns), the instantaneous frequency exhibited by the recorded FDC beat-tone over 20 µs is analysed. The analysis is performed by implementing a fast-Fourier-transform (FFT) calculation in time-windows or frames of 10 ns size. The selected window sets a resolution of ~ 100 MHz for the calculation of the instantaneous frequency of the down-converted beat-tone signal. The instantaneous frequency exhibited by the recorded FDC beat-tones is shown in Fig. 7.5(a). The red and black traces represent the frequency of the beat-tone when the passively QDash-MLLD is constantly DC-biased at 100 mA and with the 40 kHz modulated current, respectively. In the case of constantly DC-biasing the laser, a stable frequency of 1 GHz is observed in the entire time 20 µs span, whereas for a modulated DC-bias two regions are identified. One of the regions depicts a random frequency magnitude and another one with a stable frequency value corresponding to 1 GHz. This stabilisation in the frequency allows determining the time in which the passive mode-locking condition is reached. A trace of the frequency power spectrum of one of the frames analysed at a time corresponding to the range from 5.0035 µs to 5.0135 µs

in the total 20 μs of the recorded data is displayed in Fig. 7.5(b). This figure shows the frequency of the FDC beat-tone signal at a stable frequency of approximately 1 GHz.

In order to analyse in detail the time in which the passive mode-locking occurs, the analysis of the FDC signal is extended. By maintaining the same frame size and as a consequence the same resolution, the FFT analysis is performed five times within a time span of 60 ns around both end regions where the stabilisation is not maintained and which correspond to the leading (0 to 60 ns) and trailing edges (12.5 μs to 12.56 μs) of the FDC signal. This approach would allow only 6 frames in that span, but additionally, each frame is time shifted by 2 ns. The first analysis is carried out for the time frame [0 ns, 10 ns], the second analysis for [2 ns, 12 ns], the third one for [4 ns, 14 ns] and so on and so forth, for the analysis of the leading edge for instance, 30 records for the establishment of the mode-locking are achieved between 0 ns and 60 ns [20]. The results of this analysis are presented in Fig. 7.5(c). They show that the frequency of the down converted beat-tones stabilises to a constant value of ~ 1 GHz after a response time τ_1, of approximately 42 ns. This means that the passive mode-locking process taking place in the QDash-MLLD occurs approximately 12 ns after the switch on time and only 1 ns after the 90% of the pulsed biasing current is reached. These results obtained with this method of analysis complement those obtained in [12], [19], [20], where a single analysis along the recorded data was performed and the information in each frame allowed an uncertainty of at least 10 ns from frame to frame, as demonstrated when the results are compared. Following the same approach, but for the expected falling edge region of the recorded FDC, unstable frequency beat-tones are retrieved and shown in Fig. 7.5(d). The passive mode-locking process exhibits a deterioration time τ_2 of 33 ns after the 90% of the pulsed biasing current falling time is achieved, which is less than the 39 ns that it takes to reach the 10%. This means that the passive mode-locking condition is still present meanwhile the threshold current is not reached.
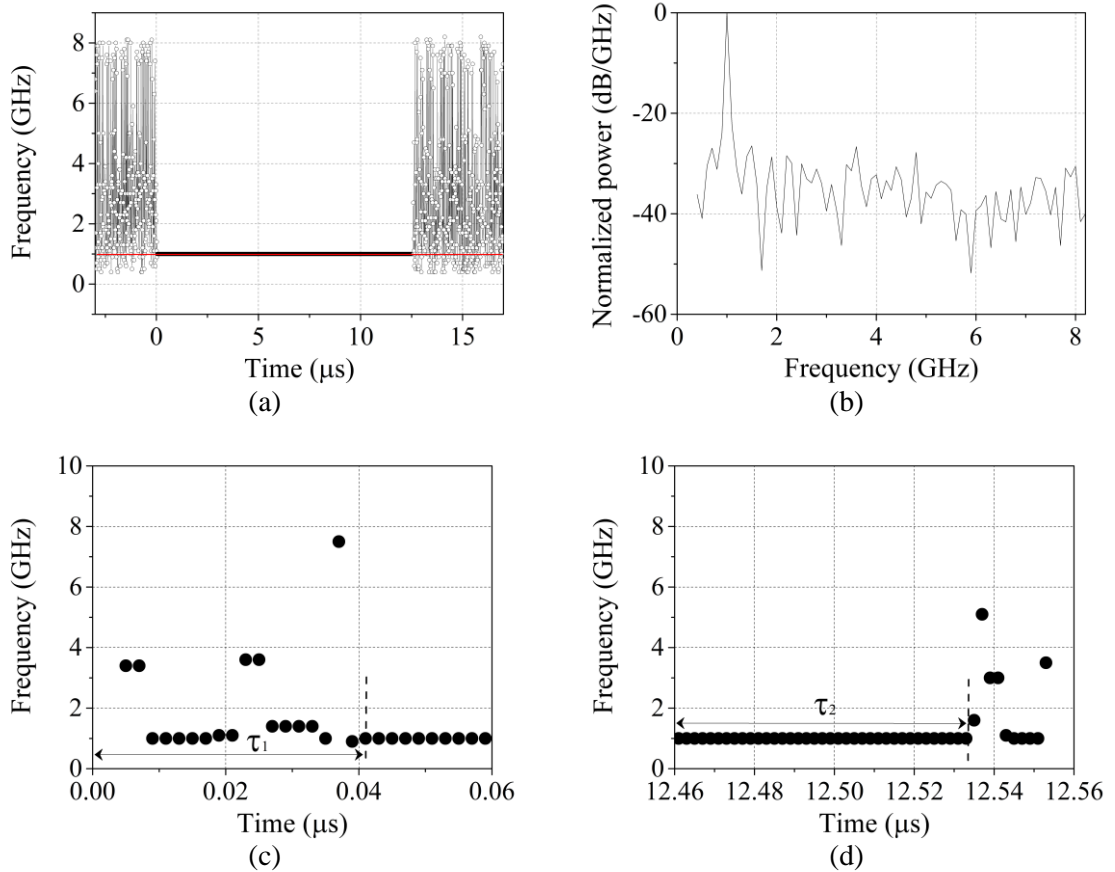
Figure 7.5: Instantaneous frequency of the recorded beat-tone: (a) full span, for both in constant current (red) and after current modulation (black); (b) for a frame of 10 ns span; (c)-(d) zoom in within a 60 ns span to measure the passive locking and unlocking times, respectively.

The results obtained in this Section suggest the suitability of the QDash-MLLD for clock recovery of burst data under transmission. It is even possible to imagine a solution where some energy can be saved up by keeping the device switched-off and switching it on only when needed. In the next Section, more investigations on the time dynamics of the laser are carried out in order to determine the time that takes the laser to synchronise to data packets.

7.3 Locking dynamics of the quantum dash under injection of data sequences

In this Section, investigation of the locking times of the QDash-MLLD under injection of data signals is performed. Two different methods are shown and analysed providing locking times in the order of nanoseconds, which support the possibility to use this device as an element for all-

signal processing in the optical networks. It is worth to mention that these two techniques were performed at different laboratories and times.

7.3.1   Method 1

7.3.1.1   Experimental setup

In this Section, the locking dynamics of the QDash-MLLD, under the injection of packets formed with 10 Gb/s non-return-to-zero (NRZ) pseudo-random binary sequences (PRBS) whilst it is DC-biased at 110 mA, are investigated [19]. The data rate of 10 Gb/s for this investigation was used due to the availability of equipment at the time of the experiment. The experimental setup is depicted in Fig. 7.6. A tunable external cavity laser (ECL, HP 8168F) set at a wavelength of 1540 nm is intensity modulated by 10 Gb/s PRBS NRZ data signals (Yokogawa AP9945). The generation of the 25 µs long packets is implemented by a built-in feature of the ECL, applying an internal direct modulation at 20 kHz through an embedded electrical square pulse signal. The optical 10 Gb/s NRZ signal is amplified by EDFA-1 and filtered out, to supress its spontaneous emission, through 2 nm optical bandpass filter (OBPF-1) centred at the input signal wavelength from ECL. This signal is injected into the QDash-MLLD, where at the upper level of the modulating signal, an average power of +6.5 dBm at the variable optical attenuator display (VOA-1) is measured, which is high enough to allow an external synchronisation to the PRBS NRZ data signal. Special care has been taken for optimizing the signal injected into the QDash-MLLD. To achieve synchronisation, the centre wavelength of the injected signal must match at a large extent one of the Fabry-Pérot weak resonances far away from the QDash-MLLD emission. When external synchronisation is accomplished, modulation sidebands in coincidence with adjacent Fabry-Pérot resonances (~40 GHz apart) appear in the optical spectrum (not shown here) created by four wave mixing [19]. This synchronisation is justified by the mechanism behind the passive mode-locking in the Fabry-Pérot semiconductor laser as explained in Chapter 2.

At the lower level of the modulating signal, an optical power of only around -12 dBm (measured at VOA-1 and supplied from the amplified spontaneous emission of the EDFA) is injected to the QDash-MLLD. In this case, synchronisation of the mode-locked laser diode to the injected signal is not achieved, and hence it operates in free-running conditions. Fig. 7.7 depicts the optical spectrum at the output of the QDash-MLLD before the band-pass filter (OBPF-2) after injection of the data signal within a span of 30 nm and RBW of 0.02 nm (OSA-1, Yokogawa AQ6370). The figure shows the optical spectra of both the QDash-MLLD (black trace) and the data signal (red trace). After injection to the QDash-MLLD, the recovered

clock signal is amplified (EDFA-2) and filtered by OBPF-2, which features a band-pass of 5 nm and central wavelength of 1530 nm. Synchronised (or de-synchronised) clock pulses are detected on a fast (50 GHz) photo-detector (PD, u^{2}t XPDV2020R) followed by an RF-amplifier. In a similar manner to the experiment shown in Section 7.2 of this Chapter, taking into account the features of the real-time oscilloscope used in this experiment (10 GHz frequency bandwidth and 40 GSa/s sampling rate, DSO-81004B), the beat-tone signal of interest is frequency down-converted to approximately 1 GHz by using an RF-mixer and a local oscillator (LO, Rohde & Schwarz SMR 40) set at around 39 GHz. The FDC signal is analysed via an electrical spectrum analyser (ESA-2, Anritsu MS2668C), a real-time oscilloscope, and an electrical sampling oscilloscope (SCOPE, Agilent 86100C). The injected PRBS NRZ data and recovered clock pulses at the input and output of the QDash-MLLD are also recorded by an electrical sampling oscilloscope, respectively. In this case, the output clock from the PRBS generator is connected to the trigger port of the sampling oscilloscope.
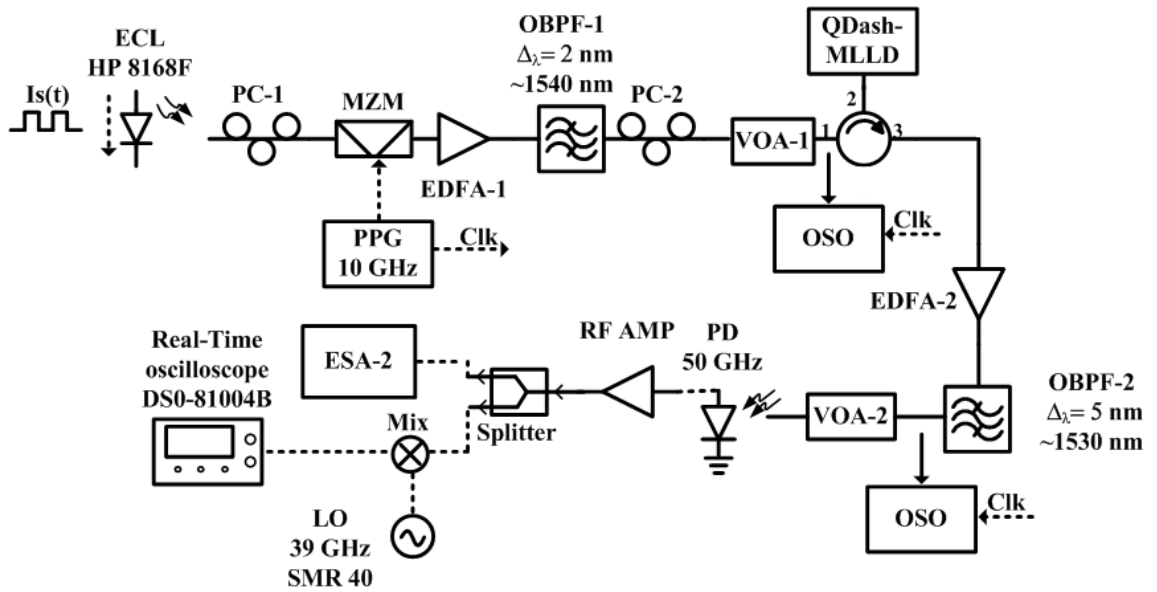
Figure 7.6: Experimental setup. Continuous (—) and dashed (- - -) lines denote optical and electrical links, respectively. ECL: external cavity laser; PC: polarisation controller; MZM: Mach-Zehnder modulator; QDash-MLLD: quantum dash mode-locked laser diode; PPG: pulse pattern generator; EDFA: Erbium-doped fibre amplifier; OBPF: optical band pass filter; VOA: variable optical attenuator; SCOPE: electrical sampling oscilloscope; PD: photo-detector; RF Amp: RF amplifier; Mix: electrical mixer; LO: local oscillator; ESA: electrical spectrum analyser (see Appendix A for equipment specifications).
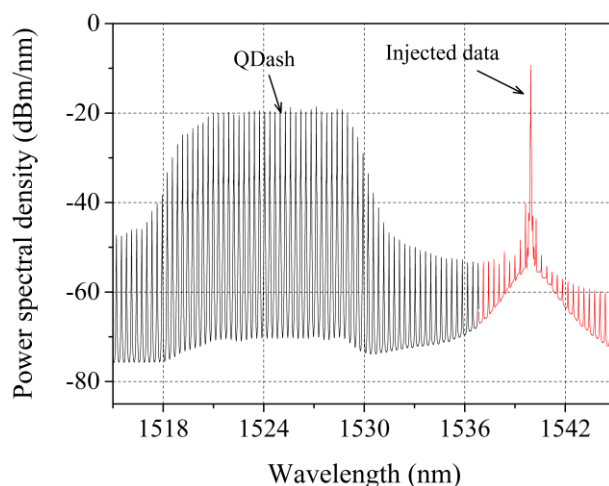
Figure 7.7: Optical spectrum at the output of the QDash-MLLD when synchronised to the input data signal.

7.3.1.2 Analysis of results

The dynamics of the QDash-MLLD are experimentally analysed by switching on and off the injected data stream at a frequency of 20 kHz. The bit rate of the injected NRZ data stream is set at 10 Gb/s, whilst the free-running frequency of the beat-tone occurs at 40 GHz. This implies that the QDash-MLLD is synchronised to the third harmonic of the incoming signal spectrum, which is not as efficient as a 40 Gb/s data stream. A period of the ECL's modulating signal is illustrated in Fig. 7.8(a) after being recorded by the real-time oscilloscope. A zoom-in of this trace is depicted in Fig. 7.8(b) and (c), where a rising (from 10% to 90% of the ECL's modulating signal amplitude) and falling time (from 90% to 10% of the ECL's modulating signal amplitude) of 100 and 27 ns are estimated, respectively [19].
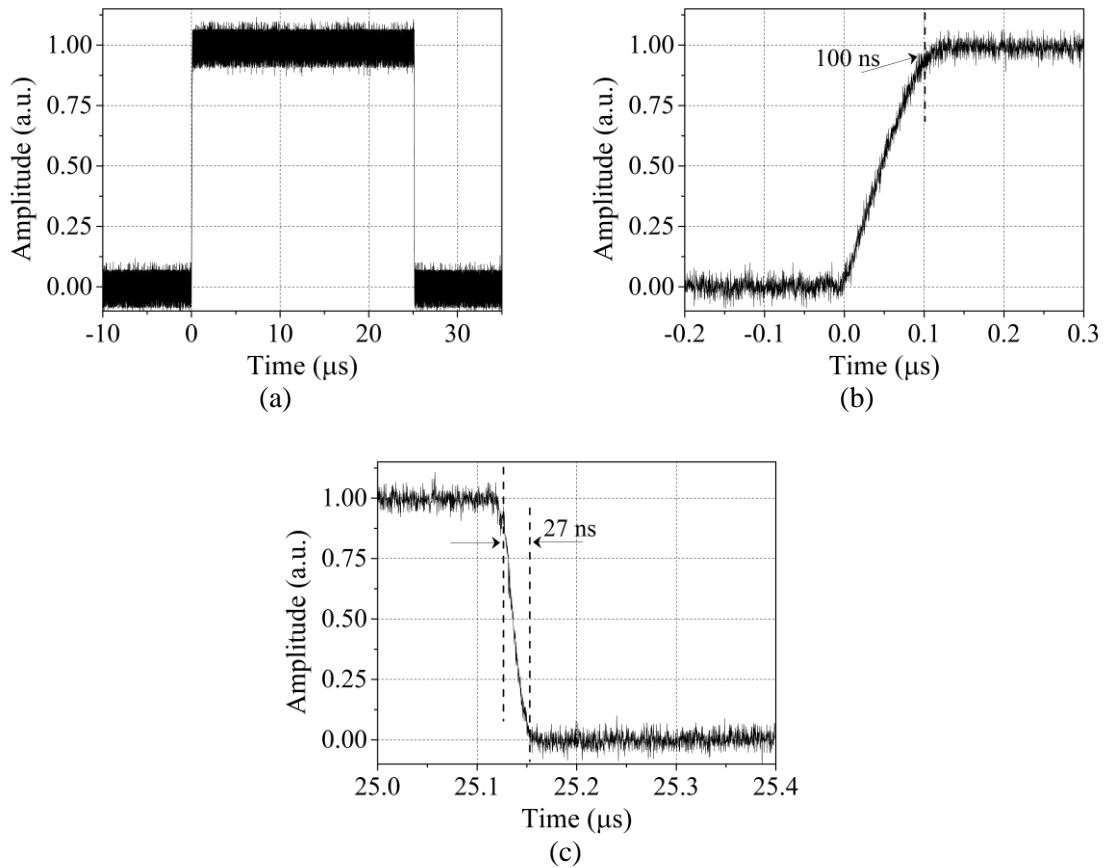
Figure 7.8: (a) Normalised electrical square pulse signal utilised for modulating the intensity of the ECL. (b)-(c) zoom-in illustrating the rising and falling times of the modulating signal, respectively.

The analysis of the FDC synchronised signal is performed by direct measurements from the real-time oscilloscope. As shown in Fig. 7.9(a), a change in the amplitude of the recorded FDC beat tones is observed whilst switching from free-running to external synchronisation and vice-versa. Unlike the free-running operation, the FDC beat tones exhibit an amplitude reduction while the QDash-MLLD is externally synchronised. The reduction in the amplitude of the FDC can be attributed to the decrease of the QDash-MLLD emitted power as a consequence of the decrement of the laser gain by depletion of the carrier density caused by the external optical signal applied into the QDash-MLLD. In addition, relative to the 100 ns mark imposed by the rising time of the electrical modulating signal applied to the ECL (red dashed-line), synchronisation of the QDash-MLLD to the injected data signal is achieved in 25 ns after the emission of the ECL is switched on, as depicted in Fig. 7.9(b). Once the synchronising signal is switched off, the mode-locked laser diode switches to the free-running condition in 20 ns after a holding time of around 128 ns (Fig. 7.9(c)). Note that the 100 ns turn on time of the directly modulated external cavity laser obeys to the response of its embedded modulation function

which is represented by the square modulating signal illustrated in Fig. 7.8(b). The ECL emission turns on only after the 90% of the relative amplitude of the internal control signal is reached. Before the 100 ns mark, the input optical power at the QDash-PMLL diode is very small (and is contributed only by the filtered amplified spontaneous emission of the EDFA). For this reason, in Fig. 7.9(b) is observed no transition from free-running to synchronisation of the QDash-MLLD until after the 100 ns mark is reached. This also indicates that there is no holding time for this transition. As illustrated in Fig. 7.9(b), a clear transition from free-running to external synchronisation is exhibited by the beat-tone signal relative to this reference mark, making possible the assessment of the synchronisation time.
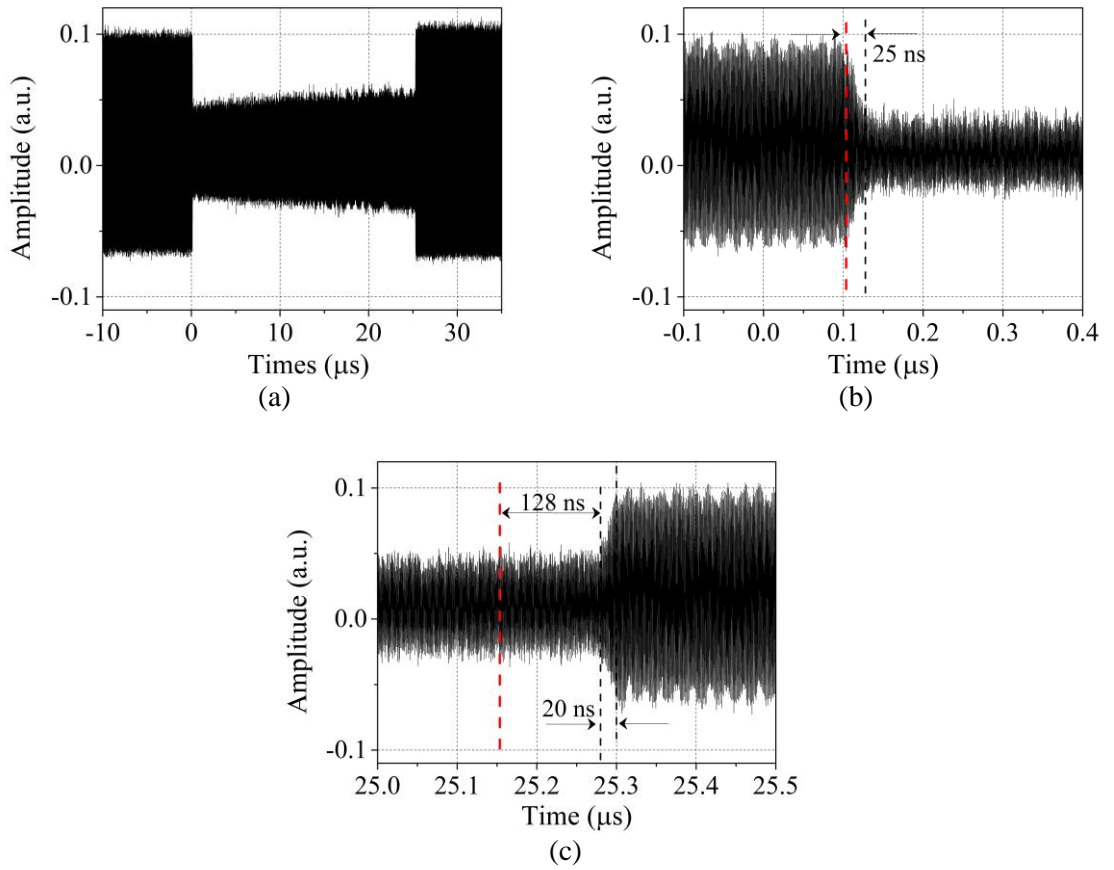
Figure 7.9: (a) Normalized frequency down-converted beat-tones measured at the output of the RF-mixer. (b)-(c) zoom-in of the beat-tones illustrating the synchronisation and de-synchronisation characteristic times, respectively.

The reported dynamics in the QDash-MLLD for packet based all-optical clock recovery are hence conclusive. At 10 Gb/s, the injection locking characteristic times indicate that the QDash-MLLD synchronises after 250 bits of the incoming data signals. Furthermore, a holding

time of 128 ns implies that the device under investigation can remain in a synchronised condition after a train of 1280 consecutive zero-data bits.

The reported synchronisation and de-synchronisation times are obtained after taking into account the delays from the electric modulating signal to the real-time oscilloscope, from optical components to the QDash-MLLD input as well as from the laser output to the input of the photodiode plus the delay from this point to the real-time oscilloscope.

Illustrated in Fig. 7.10 are the two frequency components obtained after computing the FFT from the 50 μs long recorded signal of the FDC beat-tones: a spectral component is retrieved while the QDash-MLLD is synchronised (0 to 25 μs) and another one while it is de-synchronised (25 to 50 μs).

The spectral analysis reveals a reduction of the amplitude under synchronisation (component around 1 GHz) relative to the free-running condition (component around 1.01 GHz), which is consistent with the normalized frequency down converted beat-tones depicted in Fig. 7.9. In addition, the beat-tone retrieved for the synchronisation condition features a larger linewidth, which in this case is a result of a frequency drift (in the order of a few megahertz) of the external cavity laser utilised in this experiment whilst operating in direct modulation mode [19]. It is worth mentioning that in this experiment, it was not possible to analyse the FDC in frames of time and to calculate the FFT on them, as there were not enough points in the recorded data to provide reliable results.
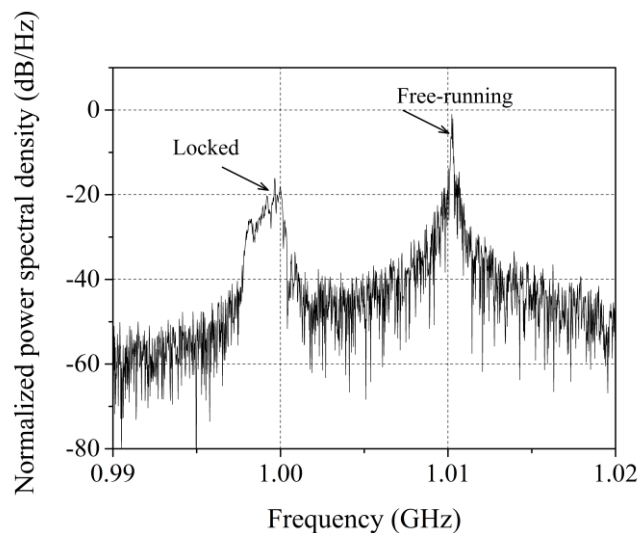
Figure 7.10: FFT computed from the recorded FDC beat-tones for the entire time span of 50 μs.

7.3.2 Method 2

7.3.2.1 Experimental setup

The experimental setup to evaluate the QDash-MLLD based on burst mode optical clock recovery (BMOCR) of 40 Gb/s return-to-zero on-off-keying (RZ-OOK) is depicted in Fig. 7.11 [13]. 40 Gb/s RZ-OOK packets are generated via a SHF RZ-OOK optical transmitter module (SHF 46210C) centered at 1550 nm. The data packet has a payload duration length of 286 ns (for the sake of simplicity, it consists of multiples of 2^7-1 PRBS patterns) and a guard time of 45 ns. The PRBS pattern length is limited by the payload duration. OCR based on QDash-MLLD with higher order PRBS pattern (2^{31}-1 PRBS) is also feasible [21]. The 40 Gb/s optical packets are first amplified to 10 dB and split with 99:1 power splitting ratio. 99% of the power signal is injected into the QDash-MLLD via an optical circulator; a polarisation controller is used before the QDash-MLLD to optimise the polarisation state of the external injected signal. 1% of the optical power is detected by a low speed optical receiver (622 Mb/s receiver) as the envelop detector to extract the packet envelope. The detected envelope signal is used as the control signal to switch on/off a current driver that powers up the QDash-MLLD. Hence the QDash-MLLD is activated only when a data packet arrives. Due to the lack of the proper current driver, a 400 MSa/s arbitrary waveform generator (AWG, LeCroy LW420) is used in this experiment. The AWG is externally triggered by the packet envelope signal. It produces a square gating current varying from 0 mA to 82 mA, with the same duration length as the data packets. The key device of the BMOCR is the QDash-MLLD. For this experiment, the QDash-MLLD referred to in Chapter 6 as QDash-MLLD-3 (butterfly packaged device) is used. The QDash-MLLD-3 is placed on a mounting board with an external RF current drive port, and is temperature stabilised at 20.5 °C. When the data packet is present, the packet envelope triggers the AWG output to activate the QDash-MLLD. Meanwhile, with the data packet injection, the QDash-MLLD is locked. When a data packet is absent, the QDash-MLLD is switched off without optical power output. Therefore, the QDash-MLLD is able to recover a packetized clock that is synchronised to the data packets. At the output of the BMOCR, the recovered clock is selected out by a 5 nm optical filter (OBPF-2) and detected by a 40 GHz photo-detector (SHF 41210B). The clock quality is analysed in an electrical spectrum analyser (ESA-3, Rohde & Schwarz FSU67) and electrical sampling oscilloscope (SCOPE, LeCroy 100 H). Further evaluation is implemented by mixing the recovered clock with the reference 40 GHz clock from the source. Time trace is acquired afterwards by using a real-time oscilloscope (Tektronix DPO-71254C) with a sampling rate of 1.25 GSa/s.
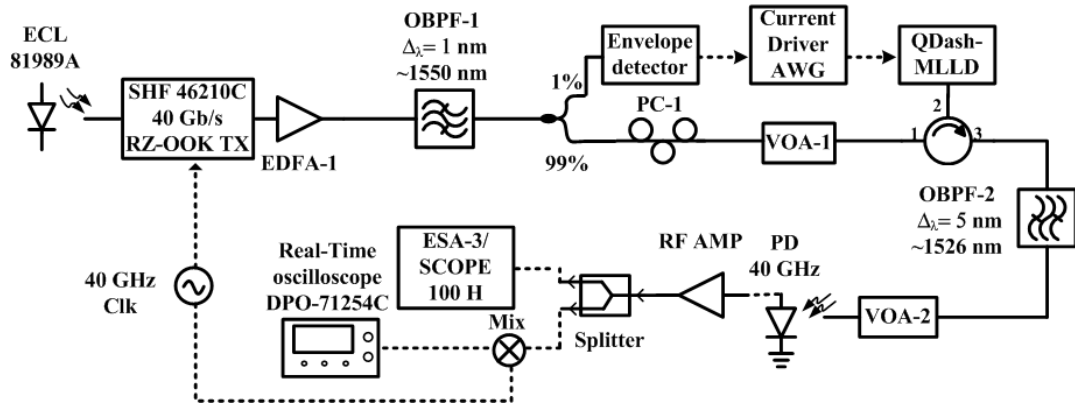
Figure 7.11: Experimental setup of burst mode optical clock recovery based on QDash-MLLD. ECL: external cavity laser; PC: polarisation controller; QDash-MLLD: quantum dash mode-locked laser diode; EDFA: Erbium-doped fibre amplifier; OBPF: optical band pass filter; VOA: variable optical attenuator; SCOPE: electrical sampling oscilloscope; PD: photo-detector; RF Amp: RF amplifier; AWG: arbitrary waveform generator; Mix: electrical mixer; ESA: electrical spectrum analyser (see Appendix A for equipment specifications).

7.3.2.2 Analysis of results

Fig. 7.12 shows the electrical spectrum of the recovered clock from data packets in a 1 kHz span. This demonstrates successful synchronisation of the QDash-MLLD to the incoming packets; the clock tone has a peak power signal-to-noise floor suppression ratio of 46 dB.
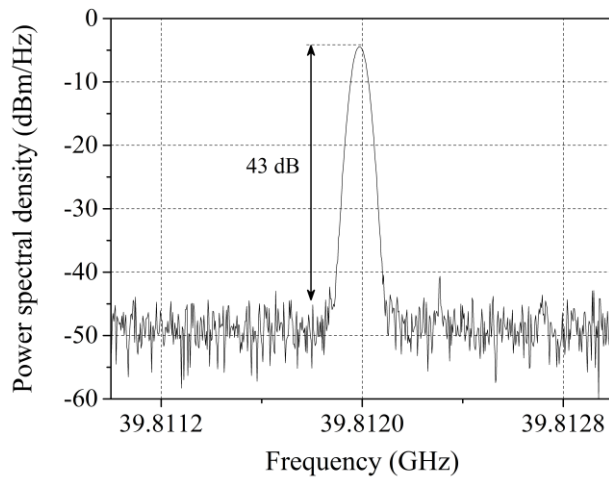
Figure 7.12: RF spectra of the QDash-MLLD when synchronised to the data packets.

The locking and unlocking times of the BMOCR are characterised with the injection of the 40 Gb/s RZ-OOK packets. The injected optical power is 4 dBm measured at the VOA-1 display.

Fig. 7.13 presents the time domain response of the QDash-MLLD under BMOCR operation. The traces are retrieved with the electrical sampling oscilloscope. Fig. 7.13(a) shows the time trace of the packets to be injected into the laser. Fig. 7.13(b) depicts the response of the QDash-MLLD (recovered clock) to the injected packets with the corresponding effect on its operation, determined by the envelope detector and the current driver. Insets of Fig. 7.13(b) show the magnification of the recovered clock at three different time positions. Fig. 7.13(b) shows that it takes approximately 25 ns to lock the QDash-MLLD to the incoming packets and to produce a synchronised clock. Moreover, it can be seen from the falling edge of the recovered signal that the QDash-MLLD unlocks instantly once the data burst is off, since the QDash-MLLD is not powered anymore [13]. The timing jitter of the recovered clock when synchronised to the data packets is approximately 82 fs.
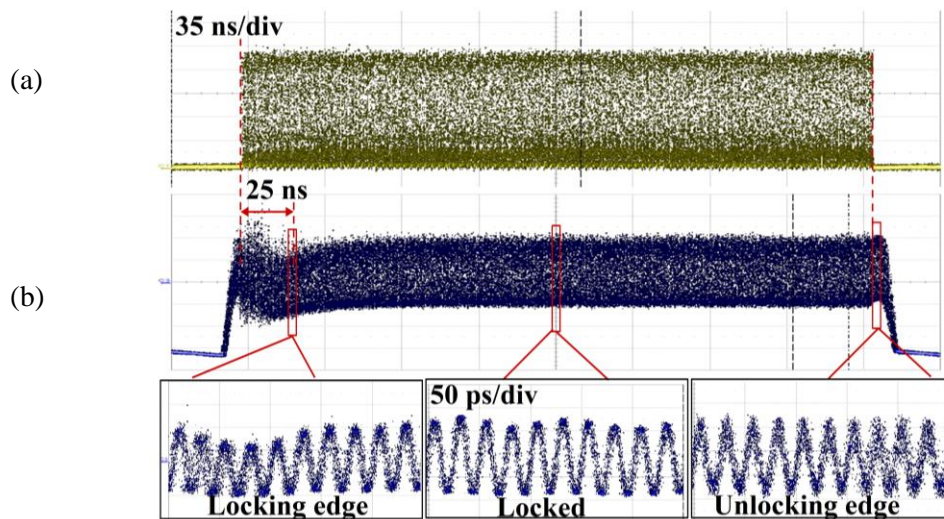
Figure 7.13: (a) time trace of the 40 Gb/s RZ-OOK packets that are injected into the QDash-MLLD; (b) time trace of the recovered 40 GHz packetized clock, insets are the clock time traces at locking edge, locked region, and the unlocking edge respectively.

Fig. 7.14 shows the time traces acquired by the real-time oscilloscope when mixing the recovered clock (~ 39. 81 GHz) with the original 40 GHz clock resulting in a down conversion of the recovered clock which is used to evaluate its quality. Each of the three traces corresponds to the signal mix-up taken at three different frames of data packets and the resulting signals are overlapped in one packet period. This is done in order to provide an average value in which the QDash-MLLD retrieves a stable optical clock signal from the data packets that are injected into the QDash-MLLD and that at the same time through their envelope turn the laser on and off. The results verify that circa 25 ns are needed to building up the frequency locking of the

QDash-MLLD, the phase difference at the leading edge of the traces indicate when the QDash-MLLD is not properly synchronised while the flat part of the trace indicates that the recovered clock holds the locked frequency.
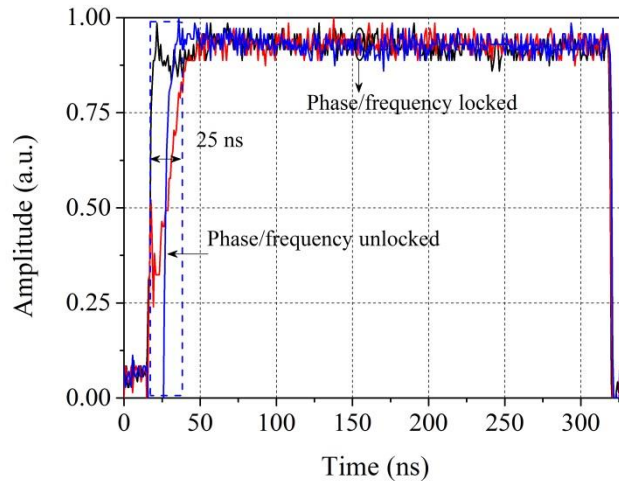
Figure 7.14: Time traces after mixing the recovered clock with the original 40 GHz clock from the transmitter side.

The two methods presented in this Section to estimate the time taken by a QDash-MLLD to synchronise its free-running frequency to the data signal and to retrieve a clock pulse differ in terms of the speed of the data injected (10 Gb/s and 40 Gb/s), the equipment and the complexity of the schemes and the analysis of the results. However, both methods have achieved very similar results in terms of the time the QDash-MLLD synchronises to the incoming data, being of approximately 25 ns.

In the case of the determination of the unlocking time, the results obtained with both methods were different but revealed two important phenomena. On one hand, using method 1, it is noted that the QDash-MLLD presents a memory-like behavior; in other words, the QDash-MLLD is not de-synchronised immediately after a long sequence of zeros. On the other hand, if method 2 is applied, an instantaneous switch off is reached. For clock recovery on packet or burst switching applications, method 2 would be the best option, with the advantage of energy saving for this clock recovery system.

7.4   Summary

In this Chapter a study of the dynamics of the QDash-MLLD was shown. In Section 7.2, the analysis of the switching on/off and passive mode-locking time allowed to determine that the QDash-MLLD switches on in a time of 30 ns. In addition, the passive mode-locking mechanism takes place 12 ns after the QDash-MLLD starts to lase. The deterioration of the passive mode-locking condition occurs 6 ns before the modulating bias current reaches its 10% of value, indicating that the passive mode-locking is still ongoing.

Furthermore, Section 7.3 introduced two different methods to estimate the locking and unlocking times of the QDash-MLLD under injection of data packets. Method 1 featured a technique where the QDash-MLLD was always DC-biased, but it used an optical modulated signal forming data packets to inject into the laser at 10 Gb/s. The second method dynamically switched the QDash-MLLD on and off depending on the presence or absence of the data packets to be injected into the laser, at a bit rate of 40 Gb/s. In both methods, locking times of 25 ns were achieved. However, the second method produced better results, not only in terms of obtaining an immediate device's unlocking or de-synchronisation, as the laser was switched-off, but also by providing another way to implement an all-optical burst-mode receiver with fast response. In conclusion, method 2 provides evidence that the QDash-MLLD is suitable for implementing a fast all-optical clock recovery system from packet or burst data. This fact, in combination with some other properties of the QDash-MLLD such as low power consumption, simplicity of operation and small footprint, suggest that the device is a good option to consider in current and future all-optical networks.

References

[1] R. Maldonado-Basilio, J. Parra-Cetina, S. Latkowski, and P. Landais, "Timing jitter, optical, and mode-beating linewidths analysis on subpicosecond optical pulses generated by a quantum-dash passively mode-locked semiconductor laser," *Optics Letters*, vol. 35, no.8, pp. 1184-1186, Apr. 2010.

[2] J. P. Jue, and V. M. Vokkarane, *Optical burst switched networks*, p. 145, USA: Springer, 2005

[3] *Optical packet switch and transport. A technical introduction*, pp. 1-10, Intune networks [online] *in* can be found at www.intunenetworks.com.

[4] A. I. A. El-Rahman, S. I. Rabia, and H. M. H. Shalaby, "MAC-layer performance enhancement using control packet buffering in optical burst-swicthed networks," *IEEE Journal of Lightwave Technology*, vol. 30, no. 11, pp. 1578-1586, Jun. 2012.

[5] S. J. B. Yoo, "Optical packet and burst switching technologies for the future photonic internet," *IEEE Journal of Ligthwave Technology*, vol. 24, no. 12, pp. 4468-4492, Dec. 2006

[6] C. Su, L.-K. Chen, and K.-W. Cheung, "Theory of burst-mode receiver and its applications in optical multi-access networks," *IEEE Journal of Lightwave Technology*, vol. 15, no. 4, pp. 590-606, Apr. 1997.

[7] N. Suzuki, K. Nakura, S. Kozaki, H. Tagami, M. Nogami, and J. Nakagawa, "Single Platform 10G-EPON 10.3-Gbps/1.25-Gbps dual rate CDR with fast burst-mode lock time employing 82.5 GS/s sampling IC and bit-rate adaptive decision logic circuit," *European Conference and Exhibition on Optical Communications, ECOC 2010*. Paper Mo.2.B.3, pp. 1-3, Sep. 2010.

[8] S. Bauer, C. Bornholdt, O. Brox, D. Hoffmann, M. Mohrle, G. Sahin, B. Sartorious, S. Schelhase, B. Lavigne, and D. Chiaroni, "Ultrafast locking optical clock for IP packet switching applications," *in Proceedings of Optical Fiber Communications Conference 2000*, *OFC 2000*, paper TuF5-1.

[9] E. Kehayas, L. Stampoulidis, H. Avramopoulos, Y. Liu, E. Tangdiongga, and H. J. S. Dorren, "40 Gb/s all-optical packed clock recovery with ultrafast lock-in time and low inter-packet guardbands," *Optics Express*, vol. 13, no. 2, pp. 475–480, 2005.

[10] E. Kehayas, D. Tsiokos, P. Bakopoulos, D. apostolopoulos, D. Pentrantonakis, L. Stampoulidis, A. Poustie, R. McDougall, G. Maxwell, Y. Liu, S. Zhang, H. J. S. Dorren, J. Seoane, P. Van Holm-Nielsen, P. Jeppesen, and H. Avramopoulos, "40-Gb/s all-optical processing systems using hybrid photonic integration technologies," *IEEE Journal of Lightwave Technology*, vol. 24, no. 12, pp. 4903–4911, Dec. 2006.

[11] M. Presi, N. Calabretta,G. Contestabile, and E. Ciaramella, "Wide dynamic range all-optical clock and data recovery from preamble-free NRZ-DPSK packets," *IEEE Photonics Technology Letters*, vol. 19, no. 6, pp. 372–374, Mar. 2007.

[12] R. Maldonado-Basilio, J. Parra-Cetina, S. Latkowski, N. Calabretta and P. Landais, "Mode-locking dynamics in a quantum dash Fabry-Pérot laser diode for packet based clock recovery," *in Optical Fiber Communications Conference, Technical Digest, OFC 2012*, paper JTh2A.14. Mar. 2012.

[13] J. Luo, J. Parra-Cetina, and P. Landais, H. J. S. Dorren, and N. Calabretta, "40G burst mode optical clock recovery after 52 km transmission enabled by a dynamically switched quantum dash mode-locked laser," *presented in the 39th European Conference and Exhibition on Optical Communication, ECOC 2013*, London, UK, paper Th.2.A.2.

[14] R. Maldonado-Basilio, S. Latkowski, S. Philippe, and P. Landais, "Experimental investigation of harmonic and subharmonic synchronisation of 40 GHz mode-locked quantum-dash laser diodes," *Optics Letters*, vol. 36, no. 9, pp. 1569–1571, May. 2011.

[15] R. Maldonado-Basilio, S. Latkowski, and P. Landais, "320 GHz time-domain multiplexed pulses from quantum-dash mode-locked semiconductor laser diodes," *Lasers and Electro-Optics Europe (CLEO EUROPE/EQEC 2011), Conference on, and12th European Quantum Electronics Conference*, p.1, May. 2011

[16] R. Maldonado-Basilio, S. Latkowski, S. Philippe, and P. Landais, "40 GHz mode-beating with 8 Hz linewidth and 64 fs timing jitter from a synchronised mode-locked quantum-dash laser diode," *Optics Letters*, vol. 36. no. 16, pp. 3142-3144, Aug. 2011.

[17] R. Maldonado-Basilio, S. Latkowski, J. Parra-Cetina, and P. Landais, "All-optical 40 Gb/s 3R regeneration assisted by clock-extraction based on a passively mode-locked quantum-dash Fabry-Pérot laser," *European Conference and Exhibition on Optical Communication (ECOC) 2010*, 10.119. pp. 1-3, Torino, Italy.

[18] J. Parra-Cetina, S. Latkowski, R. Maldonado-Basilio, and P. Landais, "Wavelength tunability of all-optical clock recovery based on quantum dash mode-locked laser diode under injection of a 40 Gb/s NRZ data stream," *IEEE Photonics Technology Letters*, vol. 23, no. 9, pp. 531-533. May. 2011.

[19] R. Maldonado-Basilio, J. Parra-Cetina, S. Latkowski, N. Calabretta, and P. Landais, "Experimental investigation of the optical injection locking dynamics in single section quantum-dash Fabry-Perot laser diode for packet-based clock recovery applications," *IEEE Journal of Lightwave Technology*, vol. 31, no. 6, JTL-2012-2235820, pp. 860-865, Mar. 2013.

[20] R. Maldonado-Basilio, J. Parra-Cetina, S. Latkowski, N. Calabretta, and P. Landais, "Characteristic switching-on and passive node-locking times in a quantum dash Fabry-Pérot laser diode," *in The International conference on transparent optical Networks (ICTON 2012),* Paper Mo.C4.4, pp.1-4, Coventry, United Kingdom.

[21] G. H. Duan, A. Shen, A. Akrout, F. van Dijk, F. Lelarge and F. Pommereau, O. LeGouezigou, J.-G. Provost, H. Gariah, F. Blache, F. Mallecot, K. Merghem, A. Martinez, and A. Ramdane, "High performance InP-based quantum dash semiconductor mode-locked lasers for optical communications, " *Bell Labs Technical Journal*, vol.14, no. 3, pp. 63-84, Nov. 2009.

Chapter 8

Conclusions and future work

8.1   Conclusions

The focus of this thesis has been the study of quantum dash passively mode-locked laser diodes for all-optical applications, mainly clock recovery. In Chapter 3, this type of laser was presented and characterised. From the series of basic experiments it was demonstrated that the quantum dash Fabry-Pérot laser exhibits a narrow RF beating linewidth of 25 kHz and that on average the optical linewidths of the 40 lasing modes (within the 3 dB bandwidth) are approximately 20 MHz. The difference of about three orders of magnitude between the RF beating linewidth and the optical mode linewidth helped to demonstrate the passive mode-locking mechanism in the QDash Fabry-Pérot semiconductor laser which was confirmed with the study of the pulse generation presented in Chapter 4. The laser is capable of producing ~ 40 GHz pulses as narrow as 720 ps and featuring a low timing jitter of less than 200 fs. In addition, in Chapter 4 the QDash-MLLD was validated as a pulse generator at frequencies of up to 160 GHz based on a time multiplexing system. The obtained pulses feature a full width at half maximum (FWHM) of 1.8 ps. Moreover, the demonstration of the synchronisation of the QDash-MLLD to pulses at 10, 20, 40, 80 and 160 GHz was carried out. The recovered 40 GHz optical pulses from these synchronisations exhibit a FWHM of around 1.8 ps regardless of the repetition rate of the injected pulses with low values of timing jitter (0.4 ps). The aforementioned results on pulse generation with short duration and low timing jitter as a result of the synchronisation, along with the position of the optical spectrum (~1530 nm) allowed for the use of the device for all-optical clock recovery. The synchronisation of the QDash-MLLD and demonstration of all-optical clock recovery to incoming data signals with a large tunability (over 23 nm within the C-band) for data at the base rate of 40 Gb/s with return-to-zero (RZ) and non-return-to-zero (NRZ) formats for all tested pattern lengths was successfully demonstrated. Moreover, it was verified that the QDash-MLLD provides a high quality ~ 40 GHz clock signal when synchronised with up to 320 Gb/s data rate signals even if they lack the 40 GHz fundamental component. This is an important outcome and contribution, as data signals with the fundamental component

facilitate the synchronisation of the device. The resulting clock pulses feature less than 100 fs of timing jitter and a RF linewidth below the ESA resolution, i.e. less than 8 Hz, confirming the high quality and stability of the recovered clock. These outstanding results on the recovered clock pulses from the QDash-MLLD allowed its use for implementation of another function, in this case to achieve demultiplexing of signals at 160 and 320 Gb/s to tributaries of 40 Gb/s with error free performance. Finally, the very fast switching-on and locking time of a QDash-MLLD when synchronised to optical data, achieving 8 ns and 25 ns, respectively, was measured. This fast synchronisation makes the device a promising and reliable option for developing all-optical clock recovery for packetised data.

It has been mentioned and demonstrated in this dissertation that the QDash-MLLD presents many benefits such as cost effectiveness, small size (which has possibilities for large scale integration), low energy consumption and stable operation. All these features and the results obtained and shown in this dissertation provide evidence of the great potential of this device to develop applications and solutions for all-optical signal processing in the future optical transparent networks, more specifically for all-optical clock recovery, demultiplexing, sampling and 3R regeneration.

8.2   Future work

A short list of future directions, related to the work presented in this thesis, that could be explored in the future include: an experimental verification of the clock recovery and demultiplexing of OTDM signals at 320 Gb/s after transmission over some kilometers of fiber. Furthermore, an experimental investigation of clock recovery for packet switching at bit rates beyond 80 Gb/s using the experimental setup provided in Chapter 7 and presented as method 2, where the QDash-MLLD is synchronised to burst data would be interesting to investigate.

Another series of experiments to demonstrate more applications of the QDash-MLLD for telecommunications would be in regard to employing the laser as a comb source for multi-channel transmission for metropolitan area networks (MAN) and access networks transporting advanced modulation formats. The main advantages of using a QDash-MLLD compared to single mode lasers are: only a single device is required to generate multiple modes or channels (~ 40 modes in the 3 dB bandwidth), the channel spacing is fixed band set by the FSR of the laser, the modes are coherent which allows achieving high spectral efficiency, in addition to making the channels more resistant to crosstalk [1-4], as well as no requirement of control on the individual channels. Some approaches have been demonstrated using passive mode-locked lasers for transmission of differential quadrature phase shift keying (DPSK) [3], conventional non-return-to-zero (NRZ) [4] and orthogonal frequency division multiplexing (OFDM) [5]. In

these experiments, two important parameters to consider are the phase noise and the relative intensity noise (RIN) of the longitudinal modes, as they have to be low. Only in [5] was injection locking of a Fabry-Pérot laser employed; in the other studies the lasers utilised were in their passive mode-locking condition.

Firstly, I propose to carry out a study on different methods to reduce the optical linewidths of the longitudinal modes such as optical feedback and external injection locking. The motivation for this study is to reduce the RIN of each longitudinal mode, since the RIN is a critical parameter to achieve low bit error rate at high speed modulation of each channel [1-4]. Some previous studies have demonstrated that external injection locking reduces the phase noise and the RIN in Fabry-Pérot based structures [6], [7].

Secondly, for the study of the QDash laser as a multi-carrier source, the laser would be subject to optical injection locking with a NRZ data signal at 40 Gb/s whose central wavelength would be outside the QDash-MLLD gain bandwidth. This injection locking will reduce the amount of phase noise and RIN associated to each of longitudinal modes of the QDash-MLLD. This would facilitate the transportation of data signals.

Thirdly, exploration of the optimum modulation format used on the transmitter and also verification of the ideal detection technique to be used would be carried out. The modulation formats to impose on the multicarrier signal emitted by the MLLD would include: quadrature amplitude modulation, standard on-off keying, differential quadrature phase shift keying, orthogonal frequency division multiplexing and quadrature phase shift keying. On the receiver side, examination by both direct and coherent detection depending on whether the system will be optically or electrically coherent would be carried out.

Fourthly, performance benchmarking of the QDash-MLLD in systems employing the various modulation formats will be carried out by using a Pilot Photonics comb source [8] available in the Radio and Optical Communications Laboratory research group at Dublin City University. The benefit reaped in terms of energy efficiency from the use of a multi-carrier transmitter (as opposed to multiple lasers) and direct detection schemes (vs coherent detection schemes) would be experimentally verified.

References

[1] D. Yin, A. Gubenko, I. Krestnikov, D. Livshits, S. Mikhrin, A. Kovsh, and G. Wojcik, "Laser diode comb spectrum amplification preserving low RIN for WDM applications," *Communications and Photonics Conference and Exhibition (ACP), 2009 Asia*, vol. 7631, pp. 1-7, Nov. 2009.

[2] G.-H. Duan, "InAs/InP based quantum dash mode-lcoked lasers for WDM transmission and millimetre wave generation," *Communications and Photonics Conference and Exhibition (ACP), 2009 Asia*, Paper FB1, pp. 1-2, Nov. 2009.

[3] Y. B. M'Sallem, Q. T. Le, L. Bramerie, Q-T. Nguyen, E. Borgne, P. Besnard, A. Shen, F. Lelarge, S. LaRochelle, L.A. Rusch and J. C. Simon, "Quantum-Dash mode locked laser as a source for 56 Gb/s DQPSK modulation in WDM multicast," *IEEE Photonics Technology Letters*, vol. 23, no. 7, pp. 453-455, Apr. 2011.

[4] A. Akrout, A. Shen, R. Brenot, F. V. Dijk, O. Legouezigou, F. Pommereau, F. Lelarge, A. Ramdane, and G.H. Duan, "Separate error-free transmission of eight channels at 10 Gb/s using comb generation in a quantum-dash based mode locked laser," *IEEE Photonics Technology Letters*, vol. 21, no. 23, pp. 1746-1748, Dec. 2009.

[5] H.-Y. Chen, C.-H. Yeh, C.-W. Chow, J.-Y. Sung, Y.-L. Liu, and J. Chen, "Investigation of using injection-locked Fabry-Perot laser diode with 10% front-facet reflectivity for short-reach to long-reach upstream PON access," *IEEE Photonics Journal*, vol. 5, no. 3, Jun. 2013

[6] X. Jin, and S. L. Chuang, "Relative intensity noise characteristics of injection-locked semiconductor lasers," *Applied Physics Letters*, vol. 77, no. 9, pp. 1250-1252, Aug. 2000.

[7] F. Xiong, W.-D. Zhong, and H. Kim, "Multimode-injection-locked Fabry-Perot laser diode as remote sensing," *Photonics Global Conference (PGC), 2010*, pp. 1-3, Dec. 2010.

[8] *Pilot Photonics optical wavelength comb source*, pp. 1-2, [online] Data sheet can be found at: www. pilotphotonics.com.

Appendix A

Main equipment used in this work

Device	Main specifications
Anritsu MS2661C- Electrical Spectrum Analyser (ESA-1)	- Frequency range: 9 kHz to 3 GHz. - Frequency span: 0 Hz, 1 kHz to 3.1 GHz. - Resolution bandwidth (RBW)(3 dB bandwidth)-Setting range: 1 kHz, 3 kHz, 10 kHz, 30 kHz, 100 kHz, 300 kHz, 1 MHz, 3 MHz (manually settable, or automatically settable according to frequency span). - Bandwidth accuracy: ± 20% (1 kHz to 1 MHz), ± 30% (3 MHz). - Selectivity (60 dB: 3 dB): < 15:1. - Video bandwidth: 1 Hz to 3 MHz (1-3 sequence), OFF Manually settable, or automatically settable according to RBW. - Frequency of reference oscillator: 10 MHz.
Anritsu MS2668C- Electrical Spectrum Analyser (ESA-2)	- Frequency range: 9 kHz to 40 GHz. - Frequency span: 0 Hz to 40 GHz. - Resolution bandwidth (RBW)(3 dB bandwidth)-Setting range: 1 kHz, 3 kHz, 10 kHz, 30 kHz, 100 kHz, 300 kHz, 1 MHz, 3 MHz (manually settable, or automatically settable according to frequency span). - Bandwidth accuracy: ± 20% (1 kHz to 1 MHz), ± 30% (3 MHz). - Selectivity (60 dB: 3 dB): 15:1. - Video bandwidth: 1 Hz to 3 MHz (1-3 sequence), OFF Manually settable, or automatically settable according to RBW. - Frequency of reference oscillator: 10 MHz.
Rohde&Schwarz FSU67- Spectrum Analyser (ESA-3) and Phase Noise Tester	- Frequency range: 20 Hz to 67 GHz. - Phase noise: (typ.) -133 dBc (1 Hz) at 640 MHz in 10 kHz from carrier. - Resolution bandwidth: 10 Hz to 50 MHz. - Video bandwidth: 1 Hz to 10 MHz. - Maximum span: full span sweep of 67 GHz. - Noise floor: -142 dBm (1 Hz RBW) at 40 GHz.

Yokogawa AQ6370- Optical Spectrum Analyser (OSA-1)	- Wavelength range: 600 to 1700 nm. - Wavelength span range: from 0.5 to full range (nm). - Maximum resolution: 0.02 nm. - Absolute level accuracy: +/- 0.4 dB. - Measurement level range: -90 dBm to +20 dBm. - Maximum input optical power: 20 dBm.
Apex AP2443B- Optical Complex Spectrum Analyser (OSA-2)	- Measurement wavelength range: 1520 to 1630 nm. - Wavelength span range: 80 pm to 110 nm. - Absolute level accuracy: +/- 0.3 dB. - Wavelength resolution: 20 MHz (0.16 pm) and 100 MHz (0.8 pm). - Measurement level range: -70 dBm to +10 dBm. - Maximum input optical power: 10 dBm.
Agilent 86142B- Optical Spectrum Analyser (OSA-3)	- Measurement wavelength range: 600 to1700 nm. - Wavelength span range: 0.2 nm to full range and zero span. - Absolute level accuracy: +/- 0.5 dB. - Maximum resolution: 0.06 nm. - Measurement level range: -60 dBm to +30 dBm. - Maximum input optical power: 30 dBm.
LeCroy Wave Expert 100 H- Equivalent Time Electrical Sampling Oscilloscope System (SCOPE)	**Electrical module:** - Sample rate: 1 MS/s. - Frequency range: DC- 40 GHz. - Time resolution: 100 fs rms. - Timebase range: 1 ps/div- 1 ms/div. - Maximum record length: 100 k samples. - Jitter: 1 ps. - Input voltage: 2 V_{pp}. *Trigger* - Input Amplitude: $\pm$ 1 V. - Max. input voltage: $\pm$ 2.5 V. **Optical module:** - Bit rate: 40 Gb/s.
Agilent 86100C- Equivalent Time Electrical Sampling Oscilloscope (SCOPE)	**Mainframe(86100C)** - Trigger modes: Free run, Internal and External. - Horizontal full scale: Min. 2ps/div, max 1 s/div. - Jitter: < 10 ps. - Vertical system (resolution): 14 bit A/D converter. **Optical interface (86106b)** 28 GHz optical/ 40 GHz electrical module. - Wavelength range: 1000 to1600 nm. - Maximum average input power: 2 mW. - Maximum electrical input power: $\pm$ 2 V_{pp}. **Clock module-Precision time base(86107A)** - Maximum input: $\pm$ 2V_{pp}. - Clock input frequencies: 10, 20 & 40 GHz. - Time base jitter: < 200 fs.

	86119A(optical sampler) • Optical frequency bandwidth: 700 GHz.
Picosolve PSO-101 Optical Sampling Oscilloscope (OSO)	• Wavelength range: C-1525 to 1563 nm, L-1575 to 1608 nm. • Optical bandwidth: > 500 GHz. • Timing jitter: < 100 fs. • Signal sensitivity: 2 mW. • Maximum input peak power: 200 mW. • Maximum input average power: 100 mW. • External clock frequency range: 0.001 to 12.5 GHz. • Time resolution: 0.83 ps.
Agilent Infiniium DSO 81004B- Real-Time Oscilloscope	• Frequency bandwidth: 2 to 10 GHz. • Number of channels: 4. • Sampling rate: 40 GSa/s. • Input impedance: 50 Ω. • Vertical resolution: 8 bits,> 12 bits with averaging. • Maximum input voltage: ±5 V. • Trigger modes: Edge, glitch, line, state, and delay.
Tektronix DPO-71254C- Real-Time Oscilloscope	• Frequency bandwidth: 33 GHz. • Number of channels: 4 (analog), 16 (digital). • Sample rate: 50 GSa/s. • Record length (each channel): 31.25 M. • Time resolution: 10 ps. • Time resolution (ET/IT mode): 100 fs.
Southern Photonics HR 150- Optical Pulse Analyser (FROG)	• Input pulse temporal FWHM: 0.3 to 10 ps. • Temporal resolution: 15 fs. • Input centre wavelength: 1520 to 1610 nm. • Spectral resolution: 50 pm. • Input spectral width: 10 nm. • Input RF clock required: No. • Maximum input power (saturation): 3000 mW. • Minimum input power (sensitivity): 500 mW. • Fibre type= SMF-28 FC/APC.
Femtochrome Research FR-103MN- Autocorrelator	• Resolution: < 5 fs. • Wavelength range: 410-1800 nm. • Scan range: > 50 ps. • Minimum pulse width: < 5 fs. • Maximum pulse width: 20 ps. • Sensitivity: $(P_{av}P_{pk})_{min}$=0.3 $(10)^{-7}$ W. • Fibre Coupled/Free space.
PriTel OCM-16- Optical Clock Multiplier	• Multiplier factor: 16 X. • Insertion loss: < 20 dB. • Tunable delay: 70 ps. • Polarisation extinction ratio: > 20 dB. • Temperature stability: 10 ppm/°C.

CIP SOA-XN-OEC-1550 Semiconductor Optical Amplifier	• Small signal gain: 25 dB (typ.). • Saturated output power: 12 dB. • Gain peak: min=1550 nm, max=1570 nm. • 3 dB optical bandwidth: 35 nm. • Maximum DC current bias: 600 mA. • Maximum DC voltage forward bias: 5 V. • Maximum optical input power: +13 dBm. • Fibre type= SMF-28 FC/APC.
Calmar Laser PSL-40-TT-40 GHz Picosecond Fiber Laser	• Pulse width: 0.8 to ~5 ps (tunable). • Output wavelength: 1530 to ~1565 nm (tunable). • Repetition rate: 38 to 42 GHz (tunable). • Timing jitter: < 50 fs (carrier offset 100 Hz to 1 MHz). • Output power: > 20 mW. • Operating Temperature: 15 to ~30 °C.
LeCroy LW420- Arbitrary Waveform Generator	**Generator mode** • Square function: 1 Hz to 50 MHz. • Pulse (period): 20 ns*maximum memory DC. • Generate complex, phase synchronised signals on two channels. • Continuously variable sample clock from 6 MHz to 400 MHz with 1 Hz resolution. • Maximum output voltage: 10 V_{pp}. • Minimum output voltage: 10 mV_{pp}. • Vertical resolution: 8 bits. • Trigger modes: single, burst, gated.
OKI OM5642W-30B-Electro-Absorption Modulator (EAM)	**Optical & electrical parameters** • Insertion loss: 9 dB. • Extinction ratio: 20 dB. • TEC current: 1 A. • Thermistor resistance: 10 kΩ. • Applied voltage range: -5 to 1 dBm. • Input optical power: +13 dBm. • TEC voltage: 4 V.
EOspace PM-OK5-10-PFU-PFU- 10 Gb/s Phase Modulator	• Wavelength: 1550 nm. • Insertion loss with connector loss: < 3 dB. • V_{pi} @ 1 GHz: < 5 V. • Bandwidth: > 10 GHz. • Connector type: FC/UPC.
Calmar Optcom BRM-T-16-Bit Rate Multiplier	• Multiplication factor: 16. • Wavelength: 1530 to1565 nm. • Polarisation extinction ratio: > 20 dB. • Input data format: 2^7-1 to 2^{31}-1 PRBS. • Output data format: 2^7-1 PRBS. • Tunable delay: > 200 ps. • Insertion loss: 20 dB. • Temp. Stability: 10 (ppm/°C).

SHF 46210 C- Optical Transmitter	- Multi-format optical transmitter: ASK, DPSK, NRZ, RZ, and CS-RZ. **Optical parameters** - Wavelength range: C- and L-band. - Insertion loss: 11 dB. - DC extinction ratio: 20 dB. **Electrical and electro-optical parameters** - Electro-optical bandwidth of data modulator: Minimum 25 GHz. - Bit rate RZ data: maximum 44 and 50 GHz.
SHF 12100B- Bit Pattern Generator	Pattern Generator - Maximum data bit rate output: 50 Gb/s. - Output level: 400 mV. - Jitter (RMS): 500 fs. **Clock** - Clock input frequency: 50 GHz full clock mode. - Input level: Maximum 1V. - Output level: 600 mV. - Clock output frequency: 50 GHz. - Data patterns: multiple.
SHF 11100B- Bit Error Rate Tester (BERT)	- Number of channels: 8 @ 32 Gb/s or 4 @ 56 Gb/s. - Pattern lengths: 2^7-1 to 2^{31}-1 PRBS. - Aggregated data rate: > 200 Gb/s.
SHF 41210B Optical receiver	- Wavelength range: C and L band - High frequency 3 dB point: minimum 30 GHz - Low frequency 3 dB point: 30 kHz - Sensitivity: -9 dBm - Optical input power: 13 dBm
Highly nonlinear fibre (HNLF) for NOLM & Wavelength Converter	- Length: 500 m. - Dispersion: -0.41 ps/nm/km. - Dispersion slope: 0.005 ps/nm^2/km @ 1550 nm. - Nonlinear coefficient: 10.8 W^{-1} km^{-1}.
Centellax TG1P4A- 40 Gb/s Pulse Pattern Generator PRBS	**Data output** - Bit rate: 37 to 44 Gb/s. - RMS jitter: 400 fs. - Amplitude: 500 mV$_{pp.}$ - SNR: 18 dB. - Pattern lengths: 2^7-1 to 2^{31}-1 PRBS. **Clock output** - Offset: 0 V. - RMS jitter: 250 fs. - Amplitude: 2.8 to 4 dBm. - Frequency: 19.9 GHz.
Centellax Div/4 TD40MCA- 40 GHz Divider	- Frequency range: 0.2 to 40 GHz. - Divides 2/4/8 outputs. - RMS jitter output: Maximum 500 fs.

	• Maximum input power: +10 dBm.
ECL Agilent 81989A High Power Compact Tunable Laser	• Wavelength range: 1465 to 1575 nm. • Wavelength frequency resolution: 5 pm, 625 MHz at 1550 nm. • Tuning time: 3 sec for 100 nm. • Absolute wavelength accuracy: ± 100 pm. • Linewidth: 100 kHz. • Maximum optical power: > +13 dBm. • SMSR: > 50 dB. • RIN: -145 dB/Hz (0.1 to 6 GHz).
Stanford Research Systems CG635/2.05 GHz Synthesized Clock Generator	• Frequency range: DC to 2.05 GHz. • Random jitter: < 1 ps rms • 80 ps rise and fall times. • Outputs: Q, $\overline{Q}$ and Cmos.
HP E4437B ESG-DP Signal Generator	• Frequency range: 250 kHz to 4 GHz. • Resolution: 0.01 Hz. • Input& output impedance: 50 Ω. • Output power: > 1 to 3 GHz, +1 to-136 dBm. • Spectral purity (SSB phase noise): at 2 GHz < -123 dBc/Hz.
Lab Buddy PP DSC-R401HG-Discovery Semiconductors	• Linear PIN+ transimpedance amplifier. • RF bandwidth: 20 GHz. • Linear gain: > +3 dBm optical input. • Sensitivity: -15 dBm @ 10 Gb/s. • High responsivity at 1310 and 1550 nm. • K-connector.
U^2T XPDV2020R Photo-detector	• Bandwidth: 50 GHz. • Wavelength range: 1480-1620 nm. • DC Responsivity: 0.7 A/W. • Dark current: 5 nA. • Optical input power: max. 20 mW.
Rohde & Schwarz SMR 40-Signal Generator	• Frequency range: 1 GHz to 40 GHz. • Resolution: 1 kHz. • Impedance: 50 Ω. • Spurious signals Harmonics: for f> 20 GHz, < - 40 dBc. • Sub-harmonics: for f >20 GHz, < -30 dBc. • SSB Phase noise (f= 10 GHz, 10 kHz from carrier, 1 Hz bandwidth, CW, FM off): < -83 dBc.
HP 8168F Tunable Laser Source	• Wavelength range: 1480 nm to 1590 nm. • Wavelength accuracy: ±0.035 nm. • Wavelength resolution: 0.001 nm. • Wavelength stability: < ±100 MHz. • Output power: -7 to 7 dBm. • Sidemode suppression ratio: > 50 dB.

	• Linewidth: 100 kHz.
Yokogawa AP9945- Portable BERT	**Pattern generator** • Bit rate: 9.95 to 11.32 Gb/s. • Data format: NRZ. • Output level: 0.5 Vpp-2 $V_{pp.}$ **Clock** • Clock out (output level): 0.6 $V_{pp.}$ • Duty cycle: 50%. • Trigger frequency (clock trigger): 1/16 or 1/64. • Output pattern: 2^7-1, 2^{15}-1, 2^{23}-1, 2^{31}-1.
Alnair Labs BVF-200- Bandwidth Variable Tunable Filter	• Centre wavelength: 1515 to 1560 nm. • Bandwidth tunability: 0.1 to 13 nm. • Insertion loss: < 7 dB. • Return loss: > 40 dB. • Out-band suppression (OBS): > 40 dB. • In-band GVD: < ± 1ps/nm.
Santec OTF-950- Wavelength & Bandwidth Tunable Filter	• Wavelength range: 1525 to 1565 nm. • Accuracy: ≤ ± 0.04 nm. • Bandwidth @ - 3dB: 0.2 to 6 nm. • Maximum input power: +27 dBm. • Insertion loss: ≤ 3.5 dB (Typ.).
U^2T TMLL-1550 Tunable Mode-Locked Laser	• Centre wavelength: 1510 to 1550 nm. • Wavelength tuning range: 100 nm. • Repetition rate: 9.8 to 10.8 GHz. • Pulse width FHWM: < 1.5 ps. • Pulse shape: $Sech^2$. • Jitter@ 1550 nm: < 150 fs. • Laser current: < 120 mA. • Average output power: > -5 dBm (typ.). • RF input power: 25 to 30 dBm. • Operating temperature: 10 to 35 °C.

Appendix B

List of publications arising from this work

Refereed Journals

1. J. Luo, J. Parra-Cetina, P. Landais, H. J. S. Dorren, and N. Calabretta, "Performance assessment of 40 G burst optical clock recovery based on quantum dash laser," *IEEE Photonics Technology Letters*, vol. 25, no. 22, pp. 2221-2224, Nov. 2013.

2. J. Parra-Cetina, J. Luo, N. Calabretta, S. Latkowski, H. J. S. Dorren, and P. Landais, "Sub-harmonic all-optical clock recovery of up to 320 Gb/s signals using a quantum dash Fabry-Pérot mode-locked laser," *IEEE Journal of Lightwave Technology*, vol. 31, no. 19, pp. 3127-3134, Oct. 2013.

3. R. Maldonado-Basilio, J. Parra-Cetina, S. Latkowski, N. Calabretta, P. Landais, "Experimental investigation of the optical injection locking dynamics in single section quantum-dash Fabry-Perot laser diode for packet-based clock recovery applications," *IEEE Journal of Lightwave Technology*, vol. 31, no. 6, JTL-2012-2235820.pp. 860-865, Mar. 15, 2013.

4. S. G. Murdoch, R. T. Watts, Y. Q. Xu, R. Maldonado-Basilio, J. Parra-Cetina, S. Latkowski, P. Landais, and L. P. Barry," Spectral amplitude and phase measurement of a 40 GHz free-running quantum-dash modelocked laser Diode," *Optics Express*, vol. 19, no. 14, pp.13628-13635, Jun. 29, 2011.

5. J. Parra-Cetina, S. Latkowski, R. Maldonado-Basilio, and P. Landais, "Wavelength tunability of all-optical clock recovery based on quantum dash mode-locked laser diode under injection of a 40 Gb/s NRZ data stream," *IEEE, Photonics Technology Letters*, vol. 23, no. 9, PTL-22566-2010.pp. 531-533, May 1, 2011.

6. R. Maldonado-Basilio, <u>J. Parra-Cetina</u>, S. Latkowski, and P. Landais, "Timing-jitter, optical and mode-beating linewidths analysis on subpicosecond optical pulses generated by a quantum dash passively mode-locked semiconductor laser," *Optics Letters*, vol. 35 no. 8, pp.1184-1186, Apr. 2010.

Conferences papers

1. J. Luo, <u>J. Parra-Cetina</u>, and P. Landais, H. J. S. Dorren, and N. Calabretta, "40G Burst Mode Optical Clock Recovery after 52 km Transmission Enabled by a Dynamically Switched Quantum Dash Mode-Locked laser," *presented in The European Conference and Exhibition on Optical Communication, ECOC 2013*, London, UK, paper Th.2.A.2. Sep. 2013.

2. <u>J. Parra-Cetina</u>, J. Luo, N. Calabretta, H. J. S. Dorren, and P. Landais, "Phase noise and timing jitter analysis of an all-optical recovered clock at 40 Gb/s based on a QDash mode locked laser diode," *presented in Photonics Ireland 2013*, Belfast, Northern Ireland, Sep. 2013.

3. <u>J. Parra-Cetina</u>, J. Luo, N. Calabretta, H. J. S. Dorren, and P. Landais, " Fabry- Pérot QDash mode-locked laser for sub-harmonic all-optical clock recovery and demultiplexing of 160 and 320 Gb/s RZ coherent signals," *in International conference on transparent optical Networks (ICTON 2013)* Tu.A2.4,(invited paper) pp: 1-4, Cartagena, Spain, Jun. 2013.

4. <u>J. Parra-Cetina</u>, J. Luo, N. Calabretta, and P. Landais, "All optical clock recovery of 40 GHz quantum-dash mode-locked laser to return-to-zero 160 Gb/s data stream," *in The European Conference on Lasers and Electro Optics (CLEO/Europe) 2013*, CI-3.6, Munich, Germany, May 2013.

5. N. Calabretta, J. Luo, <u>J. Parra-Cetina</u>, S. Latkowski, R. Maldonado-Basilio, P. Landais, and H. Dorren, "320 Gb/s all-optical clock recovery and time demultiplexing enabled by a single quantum dash mode-locked laser Fabry-Perot optical clock pulse generator," *Optical Fiber Communications Conference*, *Technical Digest., OFC 2013*, paper OTh4D.5, Mar. 2013.

6. J. Luo, <u>J. Parra-Cetina</u>, S. Latkowski, R. Maldonado-Basilio, P. Landais, H. Dorren, and N. Calabretta, "Quantum Dash mode-locked laser open-loop optical clock recovery for 160 Gb/s transmission system," *in Optical Fiber Communications Conference*, *Technical Digest., OFC 2013*, paper OTh4D.6, Mar. 2013.

7. R. Maldonado-Basilio, <u>J. Parra-Cetina</u>, S. Latkowski, N. Calabretta, and P.Landais, "Characteristic switching-on and passive node-locking times in a quantum dash Fabry-Pérot laser diode," *in International conference on transparent optical Networks (ICTON 2012)* Mo.C4.4., 10.119/ICTON.2012.62544429, pp.1-4, Coventry, United Kingdom.

8. R. Maldonado-Basilio, <u>J. Parra-Cetina</u>, S. Latkowski, N. Calabretta, and P.Landais, "Mode-locking dynamics in a quantum dash Fabry-Pérot laser diode for packet based clock recovery," *in Optical Fiber Communications Conference*, *Technical Digest, OFC 2012*, paper JTh2A.14. Mar. 2012.

9. S. G. Murdoch, R.T Watts, Y.Q. Xu, R. Maldonado-Basilio, <u>J. Parra-Cetina</u>, S. Latkowski, P.Landais, and L.P. Barry, "Measurement of the spectral amplitude and phase of a free-running 40 GHz quantum-dash modelocked laser diode," *The European Conference on Lasers and Electro Optics (CLEO/Europe) 2011*, CB3.1 TUE10.119, pp. 1-3, May 22-26 Munich, Germany.

10. <u>J. Parra-Cetina</u>, R. Maldonado-Basilio, S. Latkowski, and P. Landais, "All-optical clock recovery based on a Quantum-dash Fabry-Perot semiconductor laser in a 3R regenerator with modulation format conversion at 40 Gb/s,*" Photonics Ireland 2011*, Malahide, Dublin, Ireland, Sep. 2011.

11. <u>J. Parra-Cetina</u>, S. Latkowski, R. Maldonado-Basilio, and P. Landais, "All-optical clock recovery based on a quantum-dash Fabry-Pérot semiconductor laser in a 3R regenerator with modulation format conversion at 40 Gb/s", *China-Ireland Intl. Conf. on Inf. and Comm. Technol., CIICT*, Wuhan, China, Oct. 2010.

12. <u>J. Parra-Cetina</u>, S. Latkowski, R. Maldonado-Basilio and P. Landais,"Non-return-to-zero 40 Gb/s all-ptical clock recovery and retiming, reshaping, and reamplification (3R) regenerator," *International Conference on Coherence and Nonlinear Optics*, *International Conference on Laser, Applications and Technologies, ICONO/LAT*, Kazan, Russia, Aug. 2010.

13. R. Maldonado-Basilio, S. Latkowski, , J. Parra-Cetina, and P. Landais, "All-optical 40 Gb/s 3R regeneration assisted by clock-extraction based on a passively mode-locked quantum-dash Fabry-Pérot laser," *European Conference and Exhibition on Optical Communication (ECOC) 2010*, 10.119, pp. 1-3, Torino, Italy.

14. J. Parra-Cetina, S. Latkowski, R. Maldonado-Basilio, and P. Landais, "Timing jitter and all-optical clock recovery based on a quantum-dash Fabry-Pérot semiconductor laser," *International conference on transparent optical Networks (ICTON 2010)*. We.D4.6, pp. 1-4, Munich, Germany, Jun-Jul. 2010.

15. J. Parra-Cetina, S. Latkowski, R. Maldonado-Basilio, and P. Landais, "Timing jitter and linewidth analysis based on a quantum dash Fabry-Pérot semiconductor laser with an all-optical clock recovery application," *Semiconductor and integrated optoelectronics SIOE 2010*. Cardiff, Wales, Mar. 2010.